

SPECTROSCOPIC STUDIES OF SOME IRON-SULFUR COMPLEXES

TO MY PARENTS

SPECTROSCOPIC STUDIES OF SOME IRON-SULFUR SYSTEMS

By

KHIN MAR TUN, B.Sc.

A Thesis

Submitted to the Faculty of Graduate Studies

in Partial Fulfilment of the Requirements

for the Degree

Doctor of Philosophy

McMaster University

November 1974

©

MAR TUN 1977

TITLE: Spectroscopic Studies of Some Iron-Sulfur Systems.

AUTHOR: Khin Mar Tun, B.Sc. (Rangoon Arts and Science University, Burma).

SUPERVISOR: Professor T. Birchall

NUMBER OF PAGES: ix, 135

SCOPE AND CONTENTS:

Transition metal complexes bonded to sulfur are of interest both from the theoretical standpoint of the bonding involved and from their chemical and biochemical properties. Iron is by far the most widespread and important transition metal with a functional role in living systems. Current interests in nonheme iron proteins containing iron-sulfur bonds and in complexes of nitric oxide with hemoglobin and related substances have received increasing attention and it was the purpose to investigate various aspects of the coordination chemistry of iron with sulfur ligands.

Mössbauer spectroscopy is a very useful probe with which to obtain information about the immediate iron environment. This technique gives information about the s-electron density at the Fe nucleus which is related to the oxidation state of the metal and in addition provides information about the symmetry of the electronic distribution around the nucleus. Electron spin resonance spectroscopy is also invaluable in providing structural information on paramagnetic transition metal complexes. In this work, some iron-sulfur complexes have been studied by means of these and other spectroscopic techniques.

Spectroscopic evidence has shown that the structures of iron-nitrosyl complexes with thioamide ligands should be formulated as $\text{Fe}(\text{NO})_2\text{LX}$ rather than $[\text{Fe}(\text{NO})_2\text{L}]^+\text{X}^-$. The crystal structure of

$\text{Fe}(\text{NO})_2(\text{thiobenzamide})\text{Br}$ shows that it is a covalent compound where bromine is coordinated to the iron atom and thioamide being attached as a monodentate ligand.

A series of iron-dithiooxalate complexes have been shown to be distorted from a cubic symmetry due to the effect of cations and/or solvent of crystallisation. The usefulness of Mössbauer spectroscopy to study the behaviour of complexes in solution has been demonstrated by a study of aqueous solutions of the thiooxalate and ferric (or ferrous) ions.

The orientation of $[\text{C}_5\text{H}_5\text{Fe}(\text{CO})_2]_2$ in liquid crystals was studied by Mössbauer spectroscopy. A similar study on the $\text{Fe}(\text{NO})_2\text{LX}$ complexes in liquid crystals was not successful.

ACKNOWLEDGEMENTS

I am grateful to my supervisor, Dr. T. Birchall, for his guidance and encouragement. I wish to thank Drs. D. R. Eaton and H. Howard-Lock for their advice. I also wish to thank Dr. C. Calvo who determined the single crystal X-ray structure.

Thanks are also due to the Governments of the Socialist Republic of the Union of Burma and Canada for the Colombo-Plan scholarship given to me under the auspices of the Canadian International Development Agency.

I am grateful to Mr. Jack Ballard for his valuable assistance. Much appreciation is also extended to Mrs. Jan Gallo who typed this thesis.

TABLE OF CONTENTS

<u>CHAPTER</u>		<u>Page</u>
I	INTRODUCTION	1
II	THEORY	14
	(A) The Mössbauer Effect	14
	(B) Isomer Shift	16
	(C) Quadrupole Splitting	17
	(i) The Electric Field Gradient Tensor	19
	(ii) Measurements of the Sign of the Quadrupole Interaction	23
	(D) Linewidth and Asymmetry	25
	(E) Magnetic Hyperfine Interactions	28
III	EXPERIMENTAL	31
	(A) Description of Apparatus Used	31
	(i) Mössbauer	31
	(ii) Infrared	36
	(iii) Electron Spin Resonance	36
	(iv) Magnetic Measurements	36
	(B) Materials	37
	(C) Preparation of the Iron-Nitrosyl Complexes	37
	(D) Preparation of the Iron-Dithiooxalate Complexes	39
	(E) Chemical Analyses	41
	(F) Liquid Crystals Experiments	41
IV	IRON-NITROSYL COMPLEXES	43
	(A) Introduction	43
	(B) Results and Discussion	44
	(i) Infrared	44
	(ii) Magnetic Measurements	53
	(iii) Electron Spin Resonance	56
	(iv) Mössbauer	63
	(v) Crystal Structure	76

<u>CHAPTER</u>	<u>Page</u>
V IRON-DITHIOOXALATE COMPLEXES	80
(A) Introduction	80
(B) Results and Discussion	80
(i) Iron-Dithiooxalate Complexes	80
(ii) Frozen Solution Studies	101
VI LIQUID CRYSTALS STUDIES	117
APPENDIX	121
REFERENCES	128

LIST OF TABLES

<u>Table</u>		<u>Page</u>
2.1	Magnitude of q for Various Atomic Orbitals.	22
4.1	Infrared Spectra of the Complexes in the Range 4000-400 cm^{-1} .	45
4.2	NO Stretching Frequencies for Iron-Nitrosyl Complexes.	47
4.3	Infrared Spectra of the Complexes in the Region 400-200 cm^{-1} .	49
4.4	Magnetic Moments for $\text{Fe}(\text{NO})_2\text{LX}$.	54
4.5	The Magnetic Susceptibilities for $[\text{Fe}(\text{NO})_2\text{I}]_2$.	55
4.6	E.s.r. Data for the $\text{Fe}(\text{NO})_2\text{LX}$ Complexes.	58
4.7	Mössbauer Data for Iron-Nitrosyl Complexes.	64
4.8	Mössbauer Data for Some Iron-Nitrosyls $\text{Fe}(\text{NO})_2\text{LX}$.	66
4.9	Point-Charge Predictions for Cases of Tetrahedral Symmetry.	72
5.1	Spectroscopic Data on the Iron-Dithiooxalate Complexes.	82
5.2	Magnetic Data for Iron-Dithiooxalates.	87
5.3	Mössbauer Parameters for Iron-Dithiooxalate Complexes.	90
5.4	A Comparison for Calculated and Experimental Data for Some Iron-Dithiooxalate Complexes.	97
5.5	Mössbauer Data for Frozen Aqueous Solutions of Mixtures of Ferric Nitrate and Potassium Dithiooxalate.	104
5.6	Mössbauer Data for Frozen Aqueous Solutions of Mixtures of Ferric Sulfate and Potassium Dithiooxalate.	107
5.7	Mössbauer Data for Frozen Aqueous Solutions of Mixtures of Ferrous Ammonium Sulfate and Potassium Dithiooxalate.	109
5.8	Mössbauer Data for Frozen Solutions of Mixtures of Ferric Nitrate (or Ferrous Ammonium Sulfate) and Potassium Dithiooxalate.	111

<u>Table</u>		<u>Page</u>
5.9	Mössbauer Data for Frozen Acidic Solutions (10% H ₂ SO ₄) of Mixtures of Ferric Nitrate and Potassium Dithiooxalate.	113
A.1	Mössbauer Data for Acid Solutions of a Mixture of Ferrous Ammonium Sulfate and Thionine.	124

LIST OF FIGURES

<u>Figure</u>		<u>Page</u>
1.1	Schematic Representation of the Region at which the Spin of the Ground Term of an Ion Changes, i.e., at the Cross-over Point Δ_x .	10
2.1	The Isomer Shift and Quadrupole Splitting for Nuclear Energy Levels $I_{gd} = \frac{1}{2}$, $I_{ex} = \frac{3}{2}$ and a Resultant Mössbauer Spectrum.	20
2.2	Magnetic and Quadrupole Splitting in ^{57}Fe .	29
3.1	A Block Diagram of the Mössbauer Spectrometer.	32
3.2	A Diagram of the Liquid Transfer Cryotip.	34
3.3	The Mössbauer Liquid-Cell.	35
4.1	The Far Infrared Spectra of (a) $[\text{Fe}(\text{NO})_2\text{I}]_2$ and (b) $[\text{Fe}(\text{NO})_2\text{Br}]_2$ in nujol.	51
4.2	The Far Infrared Spectra of (a) $\text{Fe}(\text{NO})_2(\text{tu})\text{I}$ and (b) $\text{Fe}(\text{NO})_2(\text{tu})\text{Br}$ in THF.	52
4.3	The E.s.r. Spectrum of $[\text{Fe}(\text{NO})_2\text{Br}]_2$ in THF.	57
4.4	The E.s.r. Spectrum of $\text{Fe}(\text{NO})_2(\text{tu})\text{Br}$ and $\text{Fe}(\text{NO})_2(\text{tu})\text{I}$.	61
4.5	Two Possible Structures for $\text{Fe}(\text{NO})_2(\text{o-atp})\text{Br}$.	68
4.6	The Mössbauer Spectrum of $\text{Fe}(\text{NO})_4$ at 77°K .	70
4.7	The Mössbauer Spectrum of $[\text{Fe}(\text{NO})_2\text{Br}]_2$ at 77°K .	71
4.8	The Mössbauer Spectrum of $\text{Fe}(\text{NO})_2(\text{tb})\text{Br}$ at 77°K .	74
4.9	The Molecular Configuration of $\text{Fe}(\text{NO})_2(\text{C}_6\text{H}_5\text{NH}_2\text{CS})\text{Br}$.	77
4.10	A Perspective Illustration of the Packing of the $\text{Fe}(\text{NO})_2(\text{C}_6\text{H}_5\text{NH}_2\text{CS})\text{Br}$ Molecules.	78
5.1	A Plot of $1/\chi_M$ Against T for $(\text{C}_6\text{H}_5\text{NH}_3)_2\text{Fe}(\text{S}_2\text{C}_2\text{O}_2)_3 \cdot \text{H}_2\text{O}$.	88
5.2	A Plot of $1/\chi_M^{\text{Corr}}$ Against T for $(\text{C}_6\text{H}_5\text{NH}_3)_2\text{Fe}(\text{S}_2\text{C}_2\text{O}_2)_3 \cdot \text{H}_2\text{O}$.	89

<u>Figure</u>		<u>Page</u>
5.3	The Mössbauer Spectra of $[(C_6H_5)_4As]_3Fe(S_2C_2O_2)_3 \cdot 3CH_3NO_2$ at (a) 298°K, (b) 77°K.	92
5.4	The Mössbauer Spectra of $(C_6H_5NH_3)_3Fe(S_2C_2O_2) \cdot H_2O$ at 298°K, 77°K and 4°K.	95
5.5	A Plot of Quadrupole Splitting vs. Temperature.	98
5.6	The Mössbauer Spectra of $[((C_6H_5)_3P)_2Cu]_3Fe(S_2C_2O_2)_3$ at 298°K and 77°K.	99
5.7	The Mössbauer Spectra of Frozen Aqueous Solutions of Ferric Nitrate and Potassium Dithiooxalate in the Ratios $Fe^{3+}:dto^{2-}$ of 1:0.4, 1:2.99; and 1:6.5.	103
5.8	The Mössbauer Spectra of Frozen Aqueous Solutions of Ferric Sulfate and Potassium Dithiooxalate in the Ratios $Fe^{3+}:dto^{2-}$ of 1:0.5; 1:3.0; and 1:6.0.	106
5.9	The Mössbauer Spectra of Frozen Aqueous Solutions of Ferrous Ammonium Sulfate and Potassium Dithiooxalate in the Ratios $Fe^{2+}:dto^{2-}$ of 1:0.49; 1:3.0; and 1:5.85.	108
5.10	E.s.r. Signals Obtained from a Solution of Ferric Nitrate and Potassium Dithiooxalate in 10% H_2SO_4 at 77°K.	114
6.1	The Mössbauer Spectra of $[CpFe(CO)_2]_2$ in the Liquid Crystal (N-(p-methoxybenzylidene)(p-butylaniline) at $\theta = 90^\circ$ and 45° .	119
A.1	The Mössbauer Spectra of Frozen Solution of Ferrous Ammonium Sulfate and Thionine in 0.1M H_2SO_4 (a) Before and (b) After Irradiation.	125
A.2	The Mössbauer Spectra of Frozen Solution of a Mixture of Fe^{2+} (Enriched in ^{57}Fe) and Thionine in 0.1M H_2SO_4 (a) Before Irradiation, (b) After Irradiation with a One Doublet Fit and (c) After Irradiation.	126

CHAPTER I

INTRODUCTION

During the last decade, interest in transition metal complexes containing the nitric oxide ligand has grown rapidly and the number of chemical studies in this area has increased correspondingly. These compounds are of interest both from the theoretical standpoint of the bonding involved and from their chemical and biochemical properties (1,2). The outstanding versatility of nitric oxide as a ligand arises from its unusual electronic structure and from its free-radical nature. There are four ways in which the nitric oxide molecule can form compounds with metals. It can function as NO^+ , NO , NO^- or act as a bridging group between two metals. The nitric oxide molecule has one electron in an antibonding molecular orbital, which is fairly easily lost (the ionization potential of NO is 9.4 eV) to give the nitrosonium ion. The process of coordination of a nitric oxide molecule to a transition metal atom involves the transfer of the antibonding electron from NO to the metal atom and coordination of the nitrosonium group to metal by an electron pair in an sp orbital of the nitrogen; thus, three electrons are involved in the metal nitrosyl bond. The precise nature of the three-electron bond remains a subject of some speculation, and recent work on the electronic and electron spin resonance spectra of nitrosyl pentacyano species makes it clear that a correct description of M-NO bonding can only be given by a full molecular orbital treatment which allows for considerable metal-ligand electron

delocalization (3-5).

The mode of coordination of the nitrosyl group in a complex is dependent on the relative energies of the π^* orbital of the NO and the d orbitals of the metal, the two limiting cases being NO^+ and NO^- (6). If there is an empty, low energy, d orbital on the metal, the pair of electrons forming the coordinate bond will be predominantly on the metal, and the ligand may be described as NO^+ . If not, the electrons will fill the π^* orbital of the nitrosyl, and the species may be written as NO^- . The majority of nitrosyl complexes are thought to involve σ donation from NO^+ to the transition metal and an appreciable amount of metal \rightarrow ligand π back bonding. This group of nitrosyl compounds is characterized by a linear, or nearly so, M-N-O group, a short M-N bond length, and an N-O infrared stretching frequency which is usually in the $1750\text{-}2000\text{ cm}^{-1}$ range (1,7,8).

However, examples (9-11) of complexes containing an NO^- group have recently been prepared. The N-O frequencies are in the region of $\sim 1500\text{-}1750\text{ cm}^{-1}$ and the electronic spectra and magnetic susceptibility indicate an oxidation state of the metal consistent with the presence of a formally coordinated NO^- group. The coordination of this species gives an M-N-O bond angle of ca. 120° and an M-N bond about $0.1 - 0.2\text{ \AA}$ longer than in an NO^+ complex. The X-ray data (12-16) suggest that there is less π bonding of the metal to ligand type for M- NO^- complexes than in metal complexes involving NO^+ .

Recently, complexes of iron with nitric oxide have also received increasing attention for their biological implications. Complexes of nitric oxide with hemoglobin and other heme-containing substances have

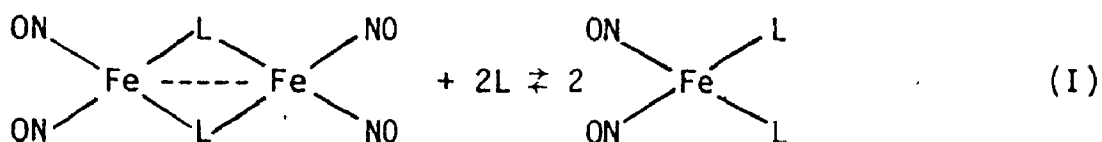
been reported by Azhipa et al. (17). The electron spin resonance signals, related to the Fe-NO group in carcinogen-induced rat liver tissue (18), with hemoglobin (19) and in several proteins (20) have been observed. Thus, electron spin resonance spectra have been employed to obtain information about the electronic structures of these biologically important molecules.

The simplest iron nitrosyl is the rather unstable iron tetra-nitrosyl, $\text{Fe}(\text{NO})_4$, for which various structures have been suggested. It has been suggested (21) that it is a nitrosonium salt $\text{NO}^+[\text{Fe}(\text{NO})_3]^-$. On the basis of an assignment of infrared absorption bands, it has been formulated as $\text{Fe}(\text{NO}')_3(\text{NO}'')$ (22) where NO' acts as NO^+ and NO'' as NO^- . An alternative structure $(\text{NO}')_3\text{Fe}-\text{ON}=\text{NO}-\text{Fe}-(\text{NO}')_3$ has also been proposed (1). Since the electron densities around the iron atom differ from one structure to another, it was thought that Mössbauer spectroscopy may be able to help in confirming the structure.

There are two different types of nitrosyl halide compounds, having empirical formulae $\text{Fe}(\text{NO})_3\text{X}$ and $\text{Fe}(\text{NO})_2\text{X}$ (23-26). Assuming that each NO donates three electrons, $\text{Fe}(\text{NO})_3\text{X}$ should be monomeric, and $\text{Fe}(\text{NO})_2\text{X}$ dimeric, with the odd electrons on each metal shared to form a metal-metal bond, analogous to that found for $[\text{Fe}(\text{NO})_2\text{SC}_2\text{H}_5]_2$ (27). $[\text{Fe}(\text{NO})_2\text{I}]_2$ has been shown by X-ray crystallography to be dimeric (28). It is formed by the fusion of two identical tetrahedral-like $\text{Fe}(\text{NO})_2\text{I}_2$ units along the common iodine-iodine edge such that the two iron and two bridging iodine atoms form a planar rhombus. Despite the unusually long Fe-Fe distance of 3.05 Å, an antiferromagnetic exchange interaction of the electron-pair in the Fe-Fe bond was suggested by Dahl et al. (28),

to account for the diamagnetism. These dimeric nitrosyl halides react with various ligands (L) to form complexes $\text{Fe}(\text{NO})_2\text{LX}$ which are paramagnetic.

Aqueous solutions containing Fe(II) salts, nitric oxide and a variety of inorganic and organic ligands are also paramagnetic. On the basis of e.s.r. spectra (29), it was proposed that these species were tetrahedral $\text{Fe}(\text{NO})_2\text{L}_2$ complexes. The observed e.s.r. spectra of the Fe complexes prepared in solution with NO in the presence of anions (e.g., phosphate, molybdate, thiourea, etc.) indicated that the complexes contain two equivalent nitrogen nuclei, one iron nucleus, and two anion ligands. The dependence of e.s.r. intensities on the complexing ligand concentrations suggest that the paramagnetic complex is in equilibrium (I) with a diamagnetic complex involving two iron atoms which are antiferromagnetically coupled.



It was also found by McDonald et al. (29) that it was not always possible to resolve the ^{14}N hyperfine splitting. Other workers (30-33) supported this evidence by e.s.r. studies of iron nitrosyl compounds in aqueous or in alcoholic solutions. Burlamacchi et al. (30), suggested that no hyperfine splitting from the nitrosyl group in iron nitrosyl halide compounds was observed because of the large line width, and they assumed that the unpaired electron was delocalized over the NO-Fe-NO unit with a predominant spin density over the iron atom.

Mössbauer investigations (34) indicated delocalization of

electrons from metal orbitals into vacant orbitals of NO^+ . Mössbauer studies on $\text{Fe}(\text{NO})_2\text{L}_2$, where L represents a unidentate ligand, such as CO, $(\text{C}_6\text{H}_5)_3\text{P}$, Br, etc. (32,35), or L_2 being a bidentate ligand, such as 2,2'-bipyridyl, 1,10-phenanthroline, etc. (33) have been reported. Iron nitrosyl bis-dithiolates (36) and bis-dithiocarbamates (37) have also been investigated by Mössbauer spectroscopy. These latter complexes have a square pyramidal geometry with the dithiolate and dithiocarbamate ligands forming five and four membered chelating rings, respectively, with the Fe. The coordination around the Fe atom is a square based pyramid formed from the four sulfur atoms, with the Fe atom on the pyramidal axis above the base and the nitrosyl group at the apex.

Recently, Heiber and Kaiser (38) reported that $[\text{Fe}(\text{NO})_2\text{Br}]_2$ reacted with thioamides and other ligands to form paramagnetic complexes which were formulated as $[(\text{ON})_2\text{FeL}]^+\text{Br}^-$, where L behaves as a bidentate ligand and completes the tetrahedral arrangement about the iron.

Thioamides are known to be coordinated to the metal, through the sulfur atom (39-41). In a few cases, however, it has been suggested that the coordination occurs through nitrogen in Pt(II), Pd(II), Cu(I) and TiCl_4 complexes, although the infrared spectral evidence (2-35 μ region) is not conclusive (42,43). Heiber and Kaiser's complexes (38) were apparently the first examples of a thioamide functioning in a bidentate fashion. In such complexes, delocalization of the metal electrons over the four membered $\text{Fe} \begin{array}{c} \text{S} \\ \diagup \quad \diagdown \\ \text{N} \quad \text{C} \end{array}$ ring is possible and it was of interest to see how such a delocalization would compete against the NO ligand which behaves as a very strong π -acceptor. Since Mössbauer spectroscopy is an extremely useful probe for obtaining

information about the immediate iron environment (44), and because e.s.r. has been invaluable in providing structural information on paramagnetic iron nitrosyl complexes (29,30,32), one of the purposes of this work was to reinvestigate Hieber and Kaiser's complexes (38) using these techniques. It was also hoped to further study the range of complexes formed with iron nitrosyls particularly those having tetrahedral structures.

The interest in transition metal complexes containing the sulfur ligand has closely paralleled that of metal nitrosyl complexes. Although most of the early investigations on these systems centred around the use of sulfur ligands as analytical reagents, there was and is considerable interest in metal sulfur bonding. Some sulfur ligands which may possibly form strong π -bonds with metal ions are the 1,2-dithiolenes (45), the dianions of malenitriledithiol, toluene 3,4-dithiol, etc. (46). The bonding in these complexes is complicated and is best represented by the delocalised form. The spectra and electronic structures of sulfur-containing ligands have recently been reviewed by Jørgensen (47). The electronic structures of the 1,2-dithiolene complexes have provoked a great deal of controversy (48,49). In molecular orbital terms the problem is one of the extent to which electrons reside in metal d orbitals or are delocalized over the ligand. Shupack et al. (46) and Davison et al. (50), in rationalizing their results obtained from electron spin resonance studies, concluded that the unpaired electron was localized in a molecular orbital predominantly of ligand character. Mössbauer studies on the dithiocarbamate complexes (51-53), the 1,2-dithiolate complexes

(36,54), etc., show that the extent of delocalization over the metal or ligand depends on the nature of the ligand.

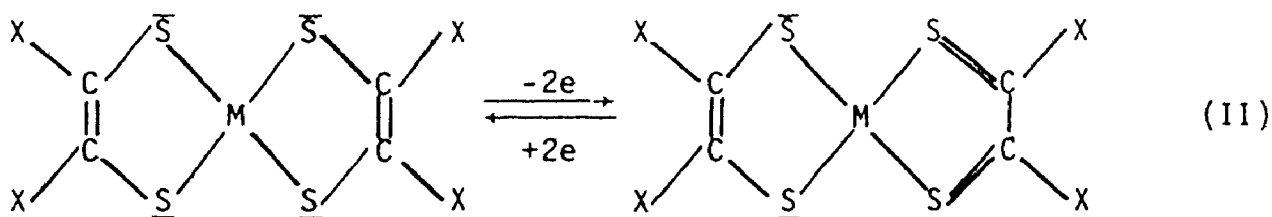
In the past few years, metal-sulfur complexes have received increasing attention because of their biological activity. The chemical behaviour of sulfur-rich iron complexes is of particular interest in view of the current studies of certain nonheme iron proteins (NHIP) which contain "acid-labile" or "inorganic" sulfur (55,56). The iron-sulfur coordination chemistry, related to this biological system, has been thoroughly studied (57-60).

In contrast with the trioxalato metal complexes, little investigation has been made of the analogous tris dithiooxalato complexes. The potassium salt of the dithiooxalic acid reacts with various metallic salts in the aqueous solutions and produces characteristic coloured solutions (61). The dithiooxalate ion generally binds to the metal via sulfur. X-ray studies (62) indicated that in potassium bis dithiooxalato nickelate(II), the nickel is in a planar environment surrounded by four sulfur atoms not unlike the arrangements found in the dithiolate systems.

Dwyer and Sargeson (63) first synthesized the $[\text{Fe}(\text{C}_2\text{O}_2\text{S}_2)_3]^{3-}$ ion and found μ_{eff} to be 2.95 B.M. This is very high for a low spin d^5 ion, and the authors ascribe part of this value to the presence of high spin impurities. Later workers (64) prepared samples of $\text{KBa}[\text{Fe}(\text{C}_2\text{O}_2\text{S}_2)_3] \cdot 6\text{H}_2\text{O}$ having a magnetic moment of 2.28 B.M. By studying the Co(III) and Cr(III) analogous, they showed that whilst dithiooxalate does not lead to exceptional Dq values, it does reduce the electron-electron repulsion on the central metal ion, making sulfur

ligands appear to be "strong" ligands in the nephelauxetic sense. Similar conclusions have been arrived at by earlier workers (65,66). From studies of the electronic structures of MS_4 complexes, the spectrochemical position of the dithiooxalate ligand was assigned as: $mnt^{2-} < (CF_3)_2C_2S_2^{2-} < dtp^- < exan^- < dtc^- < dmp^{2-} < dtm^- \sim dto^{2-}$ (67,68).

Recently, Coucouvanis (69-71) reported on the unique character of the dithiooxalate ligand. One of the characteristics is that dithiooxalate complexes in which the dithiooxalate ligands are sulfur bonded to the central metal ions, e.g., $M(dto)_2^{2-}$ where $M = Ni, Pd, Pt, Cu$ or Fe , can interact with coordinatively unsaturated metal complexes R_xSnCl_{4-x} ($x = 0, 1, 2$; $R = n$ -butyl), giving rise to polynuclear coordination compounds (69). This interaction stems from the ability of the free carbonyl groups of the dto^{2-} ligand to function as donors for Lewis acids. He also discovered that $M(dto)_2^{2-}$ complexes do not undergo reversible electron-transfer reactions (II) typical of the 1,2-dithiolate complexes, although they can be formally classified with the 1,2-dithiolate complexes (45).



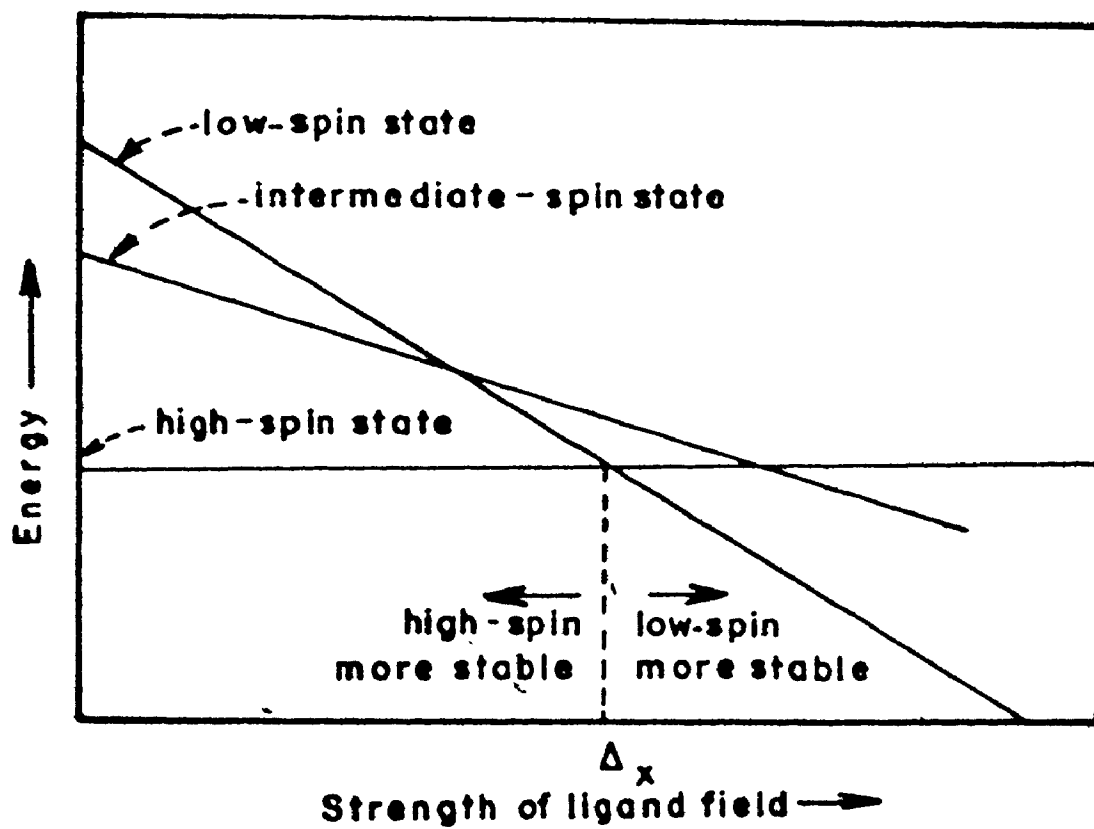
Coucouvanis suggested that this anomaly of the dithiooxalate complexes could be because the carbonyl groups do not allow the thiol-thione interconversion.

In a later study of the chemistry of the dithiooxalate complexes of Iron(III) (70), it was reported that both high spin (6A_1 ground state)

and low spin (2T_2 ground state) iron-sulfur complexes could be isolated by altering the charge distribution within the sulfur ligand. The Ph_4As^+ salt is low spin, but the $(\text{Ph}_3\text{P})_2\text{M}^+$ salts ($\text{M} = \text{Cu}, \text{Ag}$) are high spin; it was suggested that the metal M binds to two $\text{C}=\text{O}$ groups and reduces Dq sufficiently for the change in spin state.

If the energies of the two spin states are very similar, then both forms should be capable of coexistence. The transition between a high spin and a low spin is frequently depicted diagrammatically, as shown in Figure 1.1. A comprehensive discussion of the factors involved has been given by Martin and White (72). Mössbauer spectroscopy has proved extremely useful in the study of such systems. Several iron (II) complexes show the 5T_2 (high spin) - 1A_1 (low spin) crossover behaviour. The Mössbauer parameters of $\text{Fe}(\text{phen})_2(\text{NCS})_2$ at 293°K and 77°K are clearly those of 5T_2 and 1A_1 configurations (73). More extensive measurements over this temperature range show that the spectrum exhibits lines due to both spin states in the vicinity of the transition region. The tris(2-aminomethylpyridine)iron(II) halides also show a spin crossover (74). These salts give Mossbauer spectra indicating 5T_2 at room temperature, 1A_1 at 4.2°K , and both states coexistence at 77°K . Many of the dialkyldithiocarbamate complexes of iron (III) show an anomalous magnetic moment which is intermediate between the values $\mu = 2.0$ B.M. (2T_2 state of low spin iron (III)) and $\mu = 5.9$ B.M. (6A_1 state of high spin iron (III)) and which is temperature dependent. The consequence of the spin equilibrium exhibited by tris(dithiocarbamate)iron(III) on the Mössbauer effect has been studied independently by several groups of workers (51-53). Generally, good agreement is obtained and results can be interpreted

Figure 1.1. Schematic Representation of the Region at which the Spin of the Ground Term of an Ion Changes, i.e., at the Crossover Point Δ_x .



on the basis of 6A_1 and 2T_2 states in thermal equilibrium. The difference between iron(III) and iron(II) complexes in the spin crossover systems is that the Mössbauer spectra of iron(III) complexes only show evidence for one distinct iron environment in each case. The implication is that the interconversion is slow ($\gg 10^{-7}$ s, the Mössbauer excited-state lifetime) for iron(II) complexes, and fast ($\ll 10^{-7}$ s) for iron(III) complexes.

If there is a similarity between the iron-dithiooxalate complexes and the dithiocarbamates, particularly in the spin states, as stated by Coucouvanis (70), then Mössbauer spectroscopy should be able to provide valuable information about the nature of the crossover. It was the purpose of the present work to study the iron dithiooxalate complexes in order to obtain more structural information, and particularly to look for spin crossover.

The Mössbauer effect cannot be observed in a liquid, but Mössbauer spectra have been observed in glasses and smectic liquid crystals. Thus, it is possible to obtain information on the structure of a molecule in solution in such glasses and liquid crystals at low temperature.

The liquid crystal is characterized by long, rod-like molecules which possess particular degrees of translational and rotational freedom but still maintains a kind of crystalline order. It has more order in the arrangement of its molecules than the liquid state, but less than the solid state. Thus, the liquid crystalline state presents a completely different environment in which to study the Mössbauer effect. Liquid crystals are divided into two major groups -- thermotropic and lyotropic. There are three general types of thermotropic liquid

crystalline phases, namely, nematic, smectic and cholesteric. The thermotropic liquid crystals are a single component system, and the mesophases are obtained via temperature changes. Lyotropic liquid crystals constitute two or more components. In two-component systems involving water, the second component is generally an amphiphile. Lyotropic systems can be large in number and varied in composition (75).

Liquid crystals have long been used as solvents for probes for many experimental techniques such as n.m.r. and e.s.r., from which structural information can be obtained from ordered samples (76,77). Recently, observation of the Mössbauer effect in the liquid crystalline state (78) has been developed.

Mössbauer studies in liquid crystals can provide two different kinds of information:

(1) Properties of solute molecules: One can obtain the sign of the principal component of the electric field gradient tensor, the asymmetry parameter, and the molecular contribution to the nuclear vibrational asymmetry. Such information for triethyltin palmitate, trimethyltin benzylidene-4'-n-butylaniline and 1,1'-diacetyl ferrocene was obtained by using 4-n-hexoxybenzylidene-4'-n-propylene (HBPA) (78,79).

(2) Properties of the host liquid crystal: The Mössbauer isotope ^{129}I in the nematic liquid crystal 6-heptyloxy-5-iodo-2-naphthoic (HINA) (80) was shown to attain substantial alignment in the quenched sample.

In this thesis, Mössbauer spectroscopy is used to obtain structural information on ions and complexes in frozen solutions and in liquid crystals.

The purpose of the present work is to investigate the tetrahedral iron-nitrosyl complexes and the iron-dithiooxalate complexes. Structural information is obtained by spectroscopic investigations of the complexes in the solid state, in frozen solutions, and in liquid crystals.

CHAPTER II

THEORY

A THE MÖSSBAUER EFFECT

When a free unbound nucleus of mass M undergoes a nuclear transition from state E_e to state E_g by the emission of a gamma-ray of energy E_γ , the conservation of momentum requires that the momentum of the nucleus (P_n) recoiling in one direction, is equal and opposite to the momentum of the photon (P_γ) emitted in the other direction. The kinetic energy of the recoiling nucleus is E_r , so that for a nucleus of velocity v ,

$$E_r = \frac{1}{2} M v^2 = \frac{p_n^2}{2M} \quad [1]$$

The momentum of a photon of zero rest mass is related to the energy by

$$E_\gamma = P_\gamma c \quad [2]$$

where c is the velocity of light. Thus, P_γ^2 can be expressed as

$$P_\gamma^2 = \frac{E_\gamma^2}{c^2} \quad [3]$$

Since P_n and P_γ must be equal, it follows that

$$E_r = \frac{E_\gamma^2}{2Mc^2} \quad [4]$$

Conservation of energy for this system requires that

$$E_\gamma = E_t - E_r \quad [5]$$

where E_t is the energy difference between the excited and ground levels of the nucleus, $E_t = E_e - E_g$. A similar situation exists for a nucleus which absorbs a photon. As a result, a gamma-ray of energy, $E_\gamma = E_t + E_r$, is needed to both excite the nucleus and overcome the recoil energy.

The spectral linewidth Γ of a nucleus gamma-ray is typically much smaller than the recoil energy E_r of the nucleus. For example, the ^{57}Fe nucleus emits a 14.4 keV gamma-ray with a linewidth $\Gamma = 4.55 \times 10^{-9}$ eV and recoils with energy $E_r = 1.9 \times 10^{-3}$ eV. Under normal conditions there will be no overlap of emitted and absorbed lines, and resonance will not occur.

In 1957, R. L. Mössbauer (81,82), while investigating the nuclear resonance scattering of the 129 keV gamma-ray of Ir^{191} , found that upon cooling the source, an increase, instead of a decrease in scattering took place. Mössbauer theorized that the large resonance overlap implied by the observed increase in scattering was the result of a large fraction of the emission and absorption events occurring without any appreciable recoil energy loss. This explanation is reasonable if it is assumed that the effective recoiling mass has become the mass of the whole crystal lattice rather than the mass of an individual nucleus.

In terms of the Debye theory of solids (83), the fact that the lattice vibrations are quantized allows transitions to occur where the lattice remains in its initial state and the gamma-ray receives the full transition energy without recoil loss. Energy cannot be transferred to the lattice in an arbitrary fashion and a recoilless gamma emission occurs for those transitions which cannot excite phonons in the lattice. These recoilless emission and resonance absorption events are the basis of the Mössbauer effect.

B ISOMER SHIFT

The isomer shift is defined as the magnitude of the displacement of the centroid of the Mössbauer spectrum from zero velocity. This shift arises from the fact that the nucleus is surrounded and penetrated by electronic charge with which it interacts electrostatically. The electrostatic shift δE of a nuclear energy level (84,85) is given by the relation

$$\delta E = \frac{2\pi}{5} Ze^2 |\psi(0)|^2 R^2 \quad [6]$$

where $|\psi(0)|^2$ represents the total electron density at the nucleus, R is the radius, and Z is the atomic number of the nucleus.

In practice, only the s electrons have a finite density at the nucleus, and hence $|\psi(0)|^2$ may be approximated with the electron density of the s electrons, $|\psi_s(0)|^2$. Since a nuclear transition involves an excited and a ground state, the electrostatic change in the energy of a gamma transition is given by

$$\delta E_{\text{ex}} - \delta E_{\text{gd}} = \frac{2\pi}{5} Ze^2 |\psi(0)|^2 (R_{\text{ex}}^2 - R_{\text{gd}}^2) \quad [7]$$

In practice, $(\delta E_{\text{ex}} - \delta E_{\text{gd}})$ is not measurable by itself, but it can be evaluated only with respect to a given source-absorber pair. For such a pair of resonant atoms, the isomer-shift energy can be determined as

$$\text{Isomer Shift} = \frac{2\pi}{5} Ze^2 [|\psi(0)|_{\text{abs}}^2 - |\psi(0)|_{\text{source}}^2] (R_{\text{ex}}^2 - R_{\text{gd}}^2) \quad [8]$$

$$\text{Isomer Shift} = \frac{4\pi}{5} Ze^2 R^2 \left(\frac{\delta R}{R}\right) [|\psi(0)|_{\text{abs}}^2 - |\psi(0)|_{\text{source}}^2] \quad [9]$$

where $\delta R = R_{\text{ex}} - R_{\text{gd}}$. Thus, the isomer shift consists of two terms: the first contains only nuclear parameters; the second is basically a chemical parameter and is a measure of the electron density at the nucleus of an absorber relative to a given source.

The sign of $\delta R/R$ is negative (86) for ^{57}Fe since the nuclear radius decreases on excitation to the 3/2 spin state. Consequently, the isomer shift has a negative dependence on the s electron density in iron complexes. However, in the chemistry of iron, 3d and 4p orbitals play a dominant role in bonding: increasing the population of the 3d orbitals will shield the nucleus more effectively from the s electrons causing the s radial functions to expand. This will be observed as an increase in the isomer shift since $|\psi(0)_s|^2$ has decreased. The magnitude of the isomer shift is therefore influenced by two factors: the degree to which the s-orbitals are occupied and the extent to which electrons in s-orbitals are shielded from the nucleus by other electrons. Consequently, the isomer shift is a measure of the overall electronic environment of the Mössbauer nucleus.

The observed centre shift in a Mössbauer spectrum is a resultant of the isomer shift and the second order Doppler shift (87,88) which arises from the thermal motion of the Mössbauer atoms. Since the second order Doppler shift is usually much smaller than the isomer shift, it has usually been neglected. Therefore, in this thesis, the term centre shift will be used, and variations in the observed centre shift will be presumed to reflect only changes in $|\psi(0)_s|^2$, i.e., variations arising from the isomer shift only.

C QUADRUPOLE SPLITTING

The quadrupole splitting arises from the perturbation of those nuclear energy levels with spin $I > \frac{1}{2}$ by a non-spherical electric field; i.e., a finite electric field gradient (e.f.g.) arising from orbital imbalances or crystal field effects. The interaction of the nuclear

quadrupole Q and the electric field gradient lifts the $(2I + 1)$ - fold degeneracy of the nuclear state.

The electric field gradient (89) can be specified by the three components,

$$\delta^2 V / \delta x^2 = V_{xx}, \quad \delta^2 V / \delta y^2 = V_{yy} \quad \text{and} \quad \delta^2 V / \delta z^2 = V_{zz}.$$

These components are not independent, since they must obey the Laplace equation

$$V_{xx} + V_{yy} + V_{zz} = 0 \quad [10]$$

in a region where the charge density vanishes. There can be only two independent components which are conventionally chosen as V_{zz} and η , the asymmetry parameter, defined as:

$$\eta = \frac{V_{xx} - V_{yy}}{V_{zz}} \quad [11]$$

These components are usually chosen so that $|V_{zz}| \geq |V_{xx}| \geq V_{yy}$, making $0 \leq \eta \leq 1$.

The Hamiltonian describing the quadrupole coupling is defined as

$$H = \frac{e^2 q Q}{4I(2I-1)} \left[3I_z^2 - I(I+1) \right] + \eta (I_+^2 - I_-^2) \quad [12]$$

where I_+ and I_- are the raising and lowering operators.

The energy levels arising from the electric quadrupole interaction (81,90) are given by

$$E_Q(m_I) = \frac{e^2 q Q}{4I(2I-1)} \left[3m_I^2 - I(I+1) \right] (1 + \eta^2/3)^{1/2} \quad [13]$$

in which the magnetic quantum number m_I has the values $I, I-1, \dots, -I$.

If $I = 3/2$, m_I can have the values $3/2$ and $1/2$. The quadrupole splitting

E_Q is given by the difference in the eigenvalues of the above Hamiltonian for the two possible values of m_I , i.e.,

$$\begin{aligned} E_Q &= E_{Q(3/2)} - E_{Q(1/2)} \\ &= \frac{1}{2} e^2 q Q (1 + \eta^2/3)^{1/2} \end{aligned} \quad [14]$$

Since the selection rule $m_I = 0, \pm 1$ is obeyed, the observed Mössbauer spectrum for the $I = 3/2 \leftrightarrow I = 1/2$ nuclear spin transition will consist of two lines of equal intensity (Fig. 2.1):

$$I = 3/2, m_I = \pm 3/2 \rightarrow I = 1/2, m_I = \pm 1/2$$

$$I = 3/2, m_I = \pm 1/2 \rightarrow I = 1/2, m_I = \pm 1/2$$

sometimes referred to as the π and σ transitions, respectively.

(i) The Electric Field Gradient Tensor

The electric field gradient (89) is defined by the nine components,

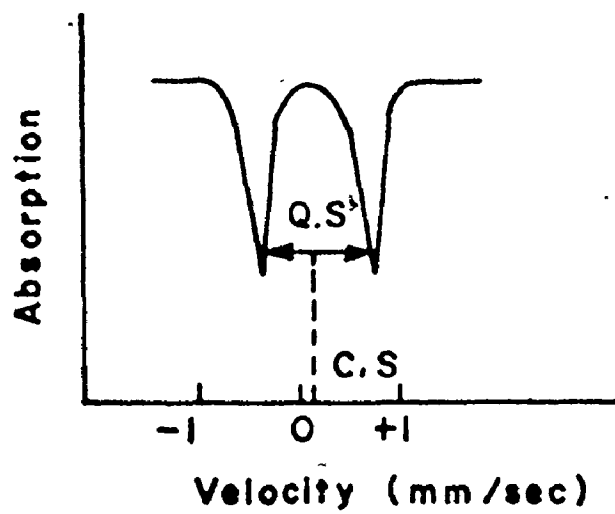
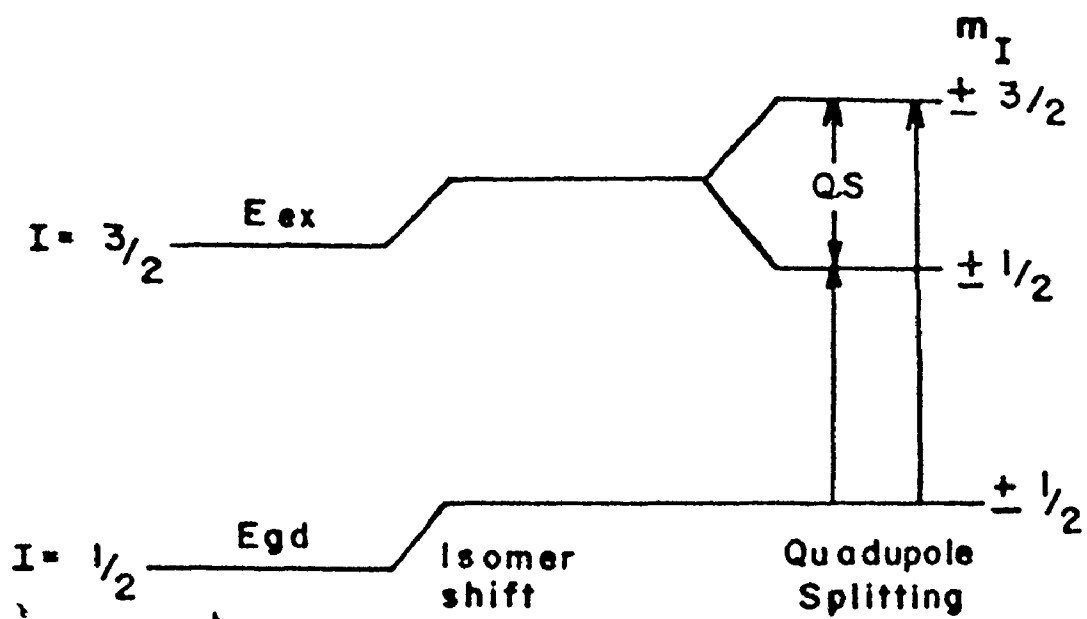
$V_{ij} = \frac{\partial^2 V}{\partial x_i \partial x_j}$, of the 3 x 3 tensor:

$$\text{efg} = - \begin{bmatrix} V_{xx} & V_{xy} & V_{xz} \\ V_{yz} & V_{yy} & V_{yz} \\ V_{zx} & V_{zy} & V_{zz} \end{bmatrix} \quad [15]$$

This tensor can be reduced to diagonal form if the coordinate axes are properly chosen, so that the electric field gradient can be completely specified by three non-zero components, V_{xx} , V_{yy} and V_{zz} , as has been described above.

The source of the electric field gradient tensor at the nuclear site is the charge-bearing environment of the nucleus. The two principal classifications of these external charges are:

Figure 2.1. The Isomer Shift and Quadrupole Splitting for Nuclear Energy Levels $I_{gd} = \frac{1}{2}$, $I_{ex} = \frac{3}{2}$ and a Resultant Mössbauer Spectrum.



- (1) the electrons directly associated with the nucleus in the atom or ion (valence contribution); and,
- (2) the charges on other ions in the lattice (lattice contribution) (91):

A simple point charge model is useful for rationalizing the electric field gradient. Such a model has proved quite successful in calculations on low-spin Fe(II) complexes (92), Sn(IV) compounds (93,94), and Fe(-II) complexes (35).

If the ligands around an atom are in a regular tetrahedral or octahedral arrangement, the electronic configuration has a cubic symmetry and the electric field gradient $q = 0$. The presence of quadrupole splitting in a Mössbauer spectrum, therefore, indicates a significant departure from the cubic symmetry and a finite value of the electric field gradient.

The value of the electric field gradient in the noncubic symmetry case may in general be expressed as:

$$q = q_{\text{valence}}(1-R) + q_{\text{lattice}}(1-\gamma_{\infty}) \quad [16]$$

where q_{valence} is the electric field gradient due to nonspherically symmetric distribution of the orbital electrons:

$$q_{\text{valence}} = - \sum_{\text{valence electrons}} \langle 3\cos^2\theta_i - 1 \rangle r_i^{-3} \quad [17]$$

and q_{lattice} is the electric field gradient due to noncubic symmetry of the distant charges on the ligand atoms in the crystal lattice:

$$q_{\text{lattice}} = \sum_i Z_i (3\cos^2\theta_i - 1) r_i^{-3} \quad [18]$$

Table 2.1 gives the contribution to q_{valence} from p and d electrons (44).

TABLE 2.1

Magnitude of q for various atomic orbitals

Orbital	q
p_z	$-\frac{4}{5}r^{-3}$
p_x	$+\frac{2}{5}r^{-3}$
p_y	$+\frac{2}{5}r^{-3}$
$d_{x^2-y^2}$	$+\frac{4}{7}r^{-3}$
d_z^2	$-\frac{4}{7}r^{-3}$
d_{xy}	$+\frac{4}{7}r^{-3}$
d_{xz}	$-\frac{2}{7}r^{-3}$
d_{yz}	$-\frac{2}{7}r^{-3}$

R and γ_{∞} are the Sternheimer antishielding factors (95-97), which correct for the polarization of the completely filled electron shells in the presence of q_{valence} and q_{lattice} , respectively. The antishielding factor may be quite large, with values such as $\gamma_{\infty} = -10.6$ for Fe^{2+} (95) and -9.14 for Fe^{3+} (98). q_{lattice} is zero for the octahedral or tetrahedral array of charges of equal magnitudes about a central iron but by compressing the axial and equatorial ligands a negative and positive q_{lattice} , respectively, can be obtained.

q_{valence} may be neglected in a spherically symmetric half-filled shell of compound such as in high spin Fe^{3+} ion; but for ionic compounds of Fe^{2+} ion, the major contribution to the efg would be from q_{valence} . q_{valence} can be considered to be made up of two contributions (99):

$$q_{\text{valence}} = q_{\text{C.F.}} + q_{\text{M.O.}} \quad [19]$$

where $q_{\text{C.F.}}$ is the valence contribution from a crystal field model with no overlap of ligand and metal orbitals, and $q_{\text{M.O.}}$ is the valence contribution from bonding between metal and ligands. Quadrupole splittings which arise from a $q_{\text{M.O.}}$ term vary little with temperature, while quadrupole splittings from a $q_{\text{C.F.}}$ term are temperature dependent. Although the separation of the contributions from $q_{\text{M.O.}}$ and $q_{\text{C.F.}}$ for Fe^{2+} high spin (96,99) and Fe(III) low spin (100,101) has been done, it is not possible to separate them for Fe^0 and $\text{Fe}(-1)$ without carrying out detailed molecular orbital calculations.

(ii) Measurements of the Sign of the Quadrupole Interaction

Any nucleus with a spin quantum number of greater than $I = \frac{1}{2}$ has a non-spherical charge distribution. The magnitude of the charge

deformation is described as the quadrupole moment Q . The sign of Q depends on the shape of the deformation. A negative quadrupole moment indicates that the nucleus is oblate or flattened along the spin axis, whereas for a positive moment, it is prolate or elongated. Thus, the sign of Q varies from one nucleus to another. For ^{57}Fe , Q is positive, whereas for ^{119}Sn , Q is negative. The quadrupole moment interacts with local electric fields to split the degeneracy of the nuclear levels. A transition between the two nuclear energy levels gives the quadrupole splitting. It is not possible to obtain the sign of the quadrupole splitting from the usual powder spectrum for the $e_q = \frac{1}{2}$, $e_e = \frac{3}{2}$ case since the two lines of the quadrupole split doublet are equal in intensity. Since the quadrupole splitting is proportional to the principal component of the electric field gradient tensor (V_{zz}) which interacts with the quadrupole moment of the nucleus, the sign of the quadrupole splitting is the same as the sign of the V_{zz} . There are two principle methods which are used to obtain the sign of the electric field gradient for ^{57}Fe or ^{119}Sn compounds. The first involves an angular dependence study of the quadrupole-split spectrum of a single crystal absorber (102). A single crystal absorber has angular properties, and the intensity of the hyperfine lines will vary according to orientation. A polycrystalline sample shows a 1:1 intensity ratio, while a single crystal with the gamma-ray axis perpendicular to and parallel to the principal axis of a symmetric electric field gradient tensor has intensity ratios of 5:3 and 1:3, respectively (see next section).

The second method involves perturbing the spectrum of polycrystalline sample by a large external magnetic field. Collins (103) shows that an applied field would cause the transition from the $\pm 3/2$ state of ^{57}Fe

to split into a doublet, and the transition from the + 1/2 component of the excited state to split into an apparent triplet (unresolved quartet), for a zero or small asymmetry parameter. The sign is indeterminate if the asymmetry parameter is substantially different from zero.

Recently, another method has been developed which enables the sign of the quadrupole splitting to be determined. Uhrich *et al.* (104) observed the quadrupole split ^{57}Fe spectrum of 1,1'-diacetyl ferrocene dissolved in 4,4'-di-n-heptyloxyazoxybenzene, a smectic liquid crystal. The ratio of the areas of each peak depends upon the angle (ν) between the molecular long axes as determined by an external magnetic field and the direction of the gamma ray beam. This method is applicable to both a smectic liquid crystal with complete planar alignment and to a nematic system frozen so as to preserve the molecular alignment of the mesophase.

Mössbauer studies in liquid crystals can thus enable the sign of the quadrupole splitting to be determined without the necessity of growing a single crystal, without the use of superconducting magnets, and without supplementary data from other sources, such as X-ray measurements.

D LINE WIDTH AND ASYMMETRY

The natural line width of a Mössbauer line is determined by the half-life of the excited nuclear state and the Heisenberg uncertainty principle as:

$$\Gamma_{\text{nat}} = h/2\pi\tau$$

where τ is the mean lifetime of the excited state. In practice, however, it is seldom possible to observe resonance lines as narrow as $2\Gamma_{\text{nat}}$, due to broadening effects such as nonhomogeneity of chemical environments of the resonant atoms in source and/or absorber, finite absorber thickness, geometric effects, thermal effects and the presence of hyperfine structure due to extranuclear field effects.

Quadrupole split doublets arising from polycrystalline samples should have both lines of equal intensity as has been demonstrated above. But, quadrupole split doublets are sometimes asymmetric. Three factors can cause this asymmetry.

- (1) Quadrupole splitting coupled with partial orientation of the crystallites: the occurrence of a preferential orientation of the absorber crystallites in the sample holder can produce non-random orientations of some crystal axis with respect to the source-detector axis. This effect has been observed in $\text{Fe}_2(\text{CO})_9$ by Gibb et al. (105). The origin of the non-equivalence of the intensity for resonance lines lies in the angular dependence of this intensity which can be expressed as:

Transition	Angular Dependence	$\theta = 90^\circ$	$\theta = 0^\circ$
$+ 1/2 \rightarrow \pm 1/2$	$2 + 3\sin^2\theta$	5	2
$+ 3/2 \rightarrow \pm 1/2$	$3(1 + \cos^2\theta)$	3	6

- (2) Anisotropy of the recoil-free fraction: this possibility arises if the Mössbauer atom is not in a site of cubic symmetry, and the asymmetry in the intensity should increase as the temperature is raised. This is commonly referred to as the Goldanskii-Karyagin effect (106,107), but was originally given mathematical formulation

by Karyagin (108). Karyagin (108) has derived an expression for the ratio of the two lines as a function of the difference of the mean-square vibrational amplitudes of the nucleus along and perpendicular to the V_{zz} axis. Since the recoilless fraction is related to the mean-square vibrational amplitude in the direction of the incident gamma ray, the contribution of each microcrystal in the sample is dependent upon its orientation, yielding a "preferential intensity", having an effect similar to preferential orientation. In cases where there is a large asymmetry in the chemical bonding, this line asymmetry is especially pronounced and this asymmetry persists even when there is random orientation of the crystal axes with respect to the optical axes.

(3) Fluctuation of the environment about the paramagnetic ions:

Asymmetric quadrupole split lines can also arise as a result of the fluctuating electric and magnetic fields produced by relaxation of paramagnetic ions, or by fluctuation of the environment around the nucleus (109). If a paramagnetic solid contains ions with $S = 1/2$, then there are two orientations of S_z , namely $+ 1/2$ and $- 1/2$. These form a degenerate Kramers' doublet. Both configurations generate a field H at the nucleus but with opposite sign. If the fluctuation rate is very slow compared to the precession frequency of the nucleus in the field H , the six-line hyperfine pattern is observed. If the fluctuation rate is extremely rapid, the nucleus will see only the time-averaged field which is zero on a symmetric quadrupole pattern will be seen. At intermediate frequencies, the spectra reflect the fact that the $\pm 3/2 \rightarrow \pm 1/2$

transitions relax at higher frequencies than do the $\pm 1/2 \rightarrow \pm 1/2$ and $\pm 1/2 \rightarrow \mp 1/2$ transitions because of their differing Zeeman precession frequencies. In the presence of magnetic interactions, the $\pm 3/2$ component of a quadrupole doublet broadens considerably before the other, and this is a potential cause of apparent asymmetry in quadrupole spectra.

If the fluctuations in internal magnetic field are due to electronic spin-lattice relaxation, one would expect the relaxation times and also the asymmetry to decrease with increased temperature. But, if fluctuations are due to electronic spin-spin relaxation, asymmetry will depend on concentration of paramagnetic ions and will be essentially independent of temperature.

E MAGNETIC HYPERFINE INTERACTIONS

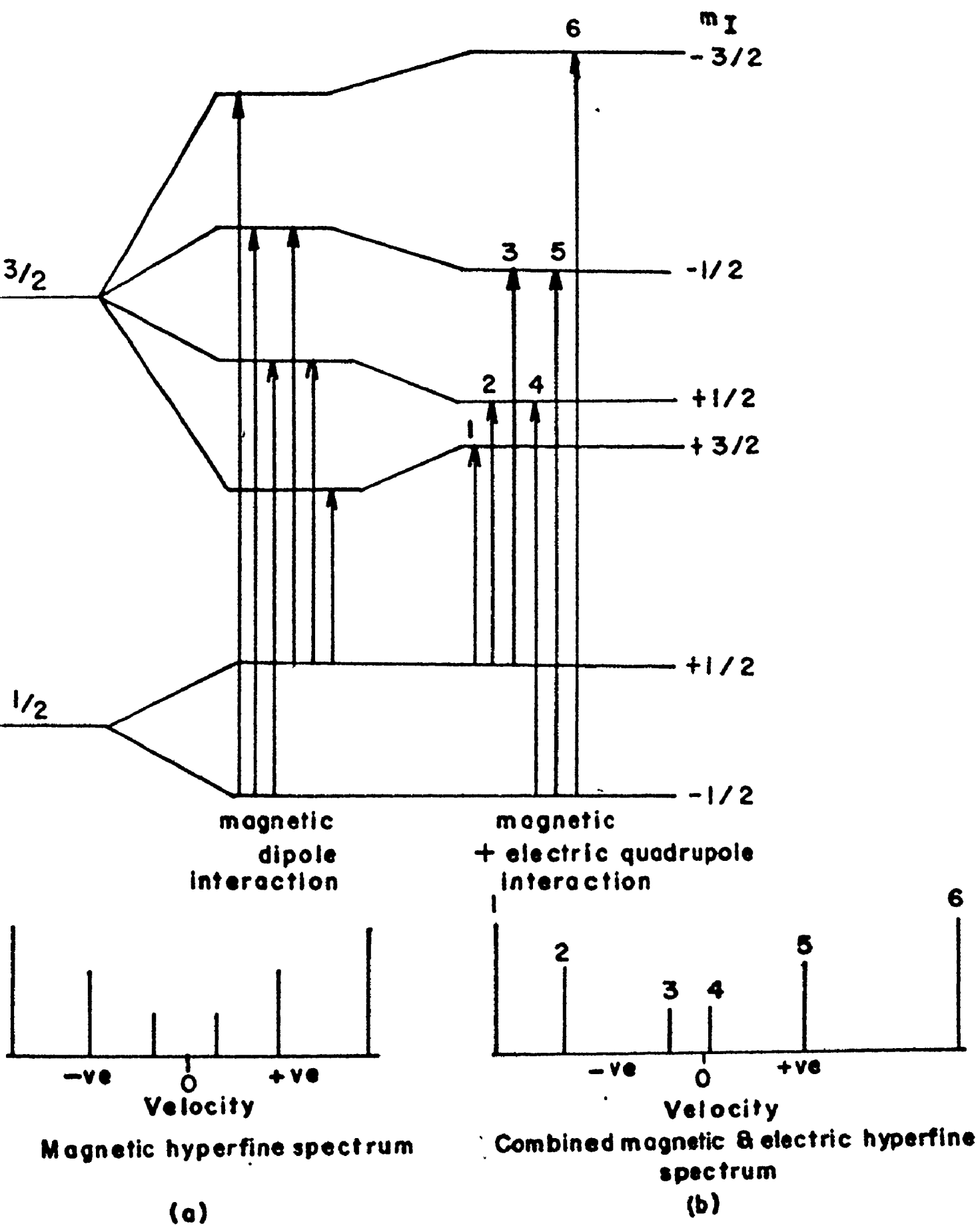
A nucleus having a spin I has a magnetic dipole moment U_N ,

$$U_N = g_N \beta_N I \quad [20]$$

This magnetic dipole moment interacts with local or applied magnetic fields at the nucleus, and the degeneracy of the nuclear energy level is removed as shown in Fig. 2.2a. Under such conditions, a nuclear Zeeman effect is observed in which each nuclear energy is split into its $2I + 1$ components. For ^{57}Fe , the g_N values of ground and excited states have different signs, and a six-line hyperfine structure spectrum will be observed by the selection rules $\Delta m_1 = 0, \pm 1$.

Magnetic hyperfine splittings are usually of the same order of magnitude as quadrupole splittings. The line widths of the six peaks are in general equal, but the intensities are very different. For a

Figure 2.2. Magnetic and Quadrupole Splitting in ^{57}Fe .



sample in which the magnetic domains are randomly oriented, the area ratio of the six lines is 3:2:1:1:2:3.

In the presence of both a magnetic field and an electric field, the $\pm 1/2$ levels are moved in one direction and the $\pm 3/2$ levels in the other. If the electric field gradient tensor is axially symmetric and its principal axis make an angle θ with the magnetic axis, the spectrum shown in Fig. 2.2b exists providing that $e^2qQ \ll \mu H$. The importance of this complicated combined hyperfine splitting is that they allow a determination of the sign of the electric field gradient. If the $\pm 3/2$ states are perturbed to higher energy levels and $\pm 1/2$ to lower energy levels (as shown in Fig. 2.2b), the resultant spectrum consists of $\pm 3/2 \rightarrow \pm 1/2$ transitions in positive velocities and $\pm 1/2 \rightarrow \pm 1/2$ transitions in negative velocities. The sign of the quadrupole splitting is indeterminate unless the angle between the principal axis of the electric field gradient and the axis of the magnetic field is known.

CHAPTER III

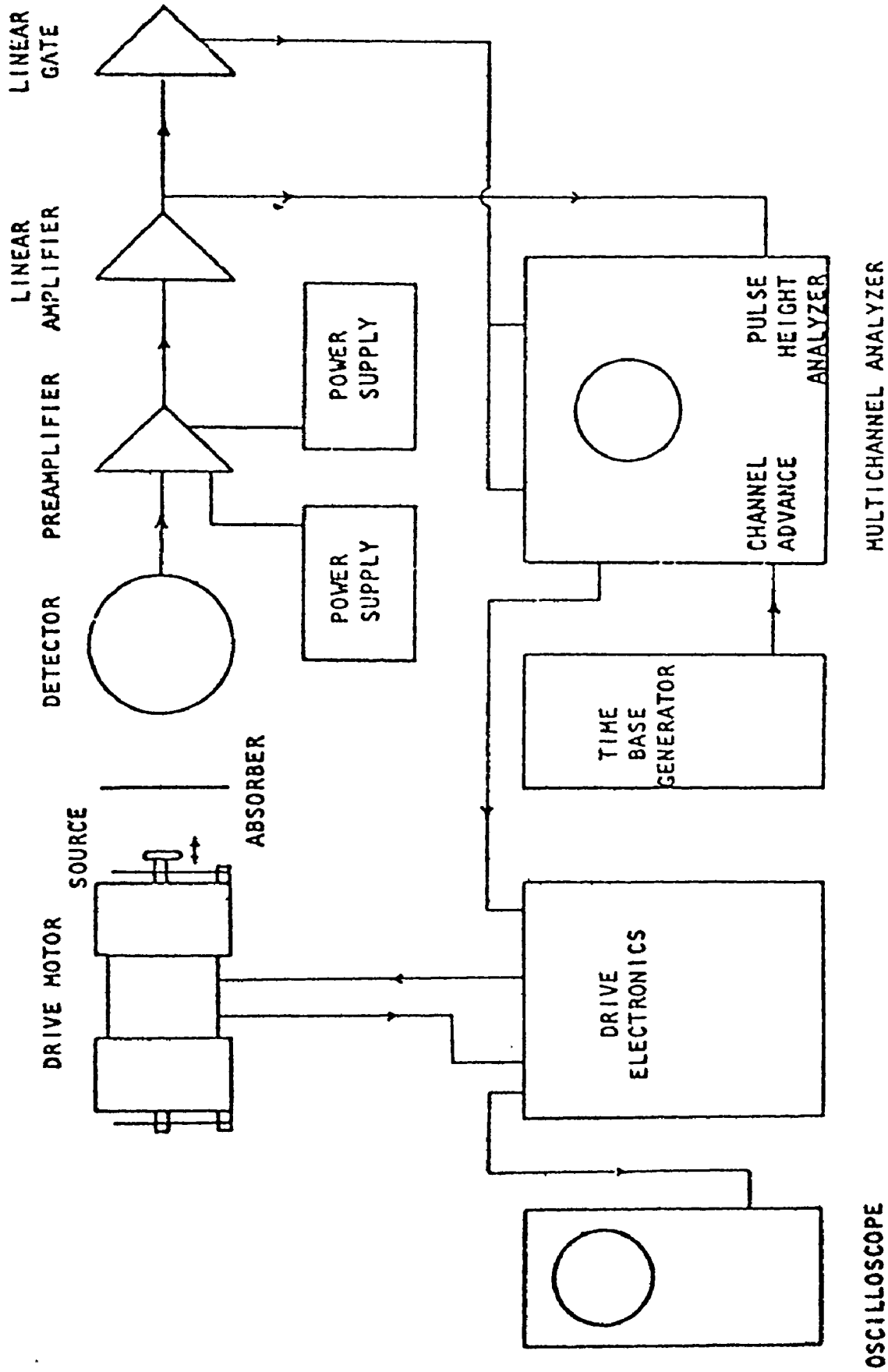
EXPERIMENTAL

A DESCRIPTION OF APPARATUS USED

(i) Mössbauer

The Mössbauer spectra were recorded with an Austin Science Associates model S3 drive system, used in conjunction with a Victoreen PIP 400A multichannel analyzer operating in the multiscalar mode. The block diagram, Fig. 3.1, illustrates the elements of the Mössbauer spectrometer. The gamma ray source was a nominally 10 mC ^{57}Co in Pd obtained from New England Nuclear Corp. The 14.4 keV gamma rays were detected by a Xe-CO₂ (1 atm.) gas-filled proportional counter, model CSP-400, obtained from Austin Science Associates, and operated at 2000 volts. This detector unit included a close coupled field effect transistor preamplifier. Power for the detector unit was supplied by a DC regulated power supply, model 2K-10, from Power Designs Pacific, Inc. The power supply for the timing unit was an ORTEC 401A Modular System Bin. The drive motor was of the constant acceleration type. The velocity, and hence the gamma ray energy varies linearly with time in a triangular waveform which was monitored continuously on an oscilloscope. The Mössbauer spectrum consisted of a plot of count rate vs velocity. The 400 channel multiscaling M.C.A. controlled the constant acceleration motion which has opposite sign in alternate halves of the memory. As a result, mirror image spectra appear in the memory

Figure 3.1. A Block Diagram of the Mössbauer Spectrometer.



OSCILLOSCOPE

MULTICHANNEL ANALYZER

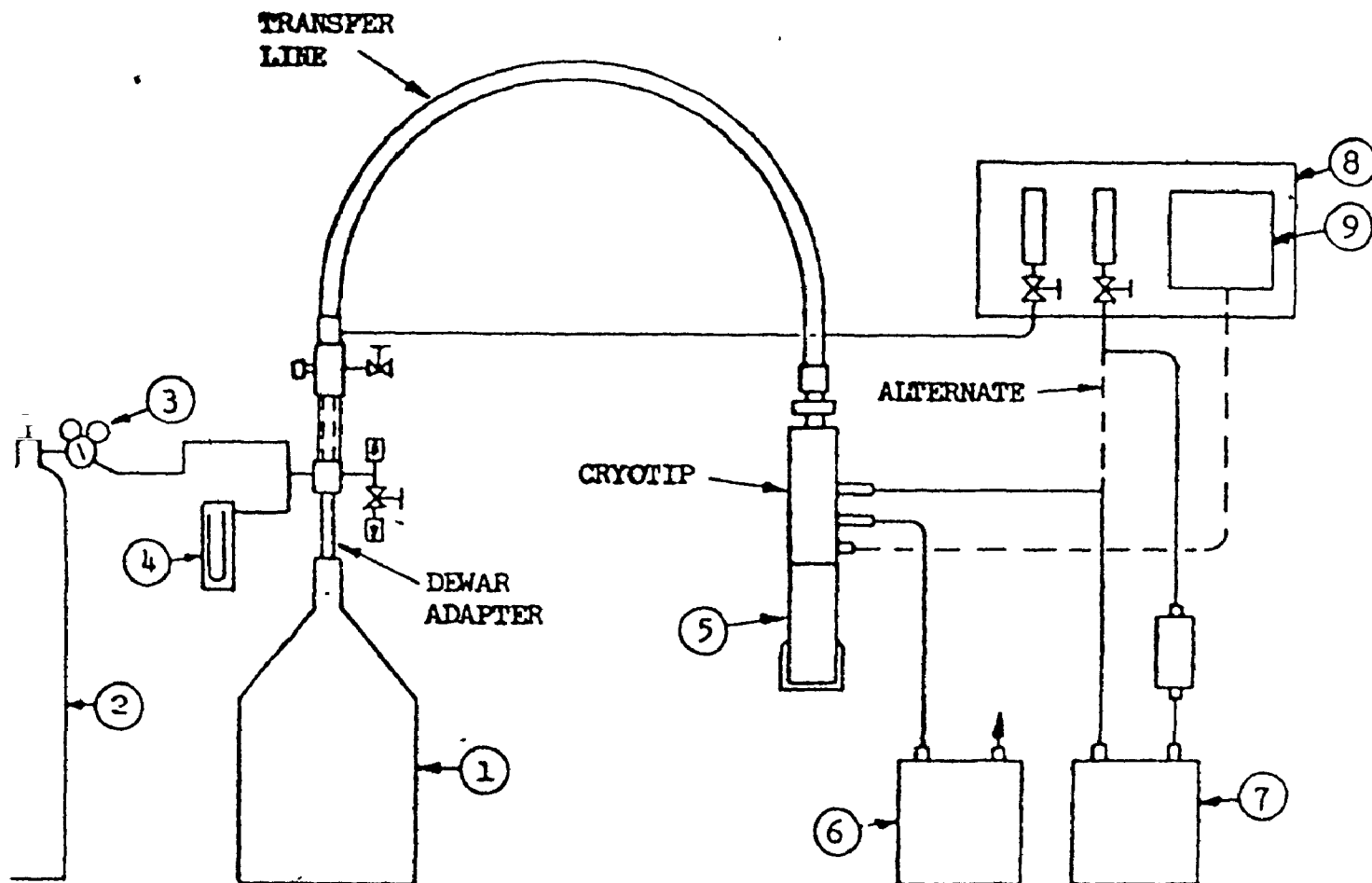
halves, with one spectrum being counted during intervals of increasing velocity and the other during intervals of decreasing velocity. Since there are other radiations emitted by the source, it is essential that an energy selective device be used, so that only the gamma ray of desired energy will be counted. The preamplifier and a linear amplifier amplify and shape the resulting pulses. The voltage levels in the single channel analyzer can be set to select only the 14.4 keV gamma ray. The signal from single channel is counted and stored as information in the memory bank of source velocity. A crystal controlled time base generator provides the signals for the address advance and the velocity drive is controlled by a signal from the multichannel analyzer.

Spectra were recorded at various temperatures. A model LT-3-110 liquid transfer cryo-tip, shown in Fig. 3.2, from Air Products and Chemicals, Inc., was used for recording spectra at liquid helium temperature.

Spectra were printed out as counts per channel on a Teletype paper punch. The information was transferred to computer cards, and peaks were fitted to Lorentzian line shapes using an iterative least squares method (110). The drive velocity was calibrated using a standard iron foil and all parameters are quoted with respect to this standard. The standard deviations were less than $\pm 0.02 \text{ mm s}^{-1}$.

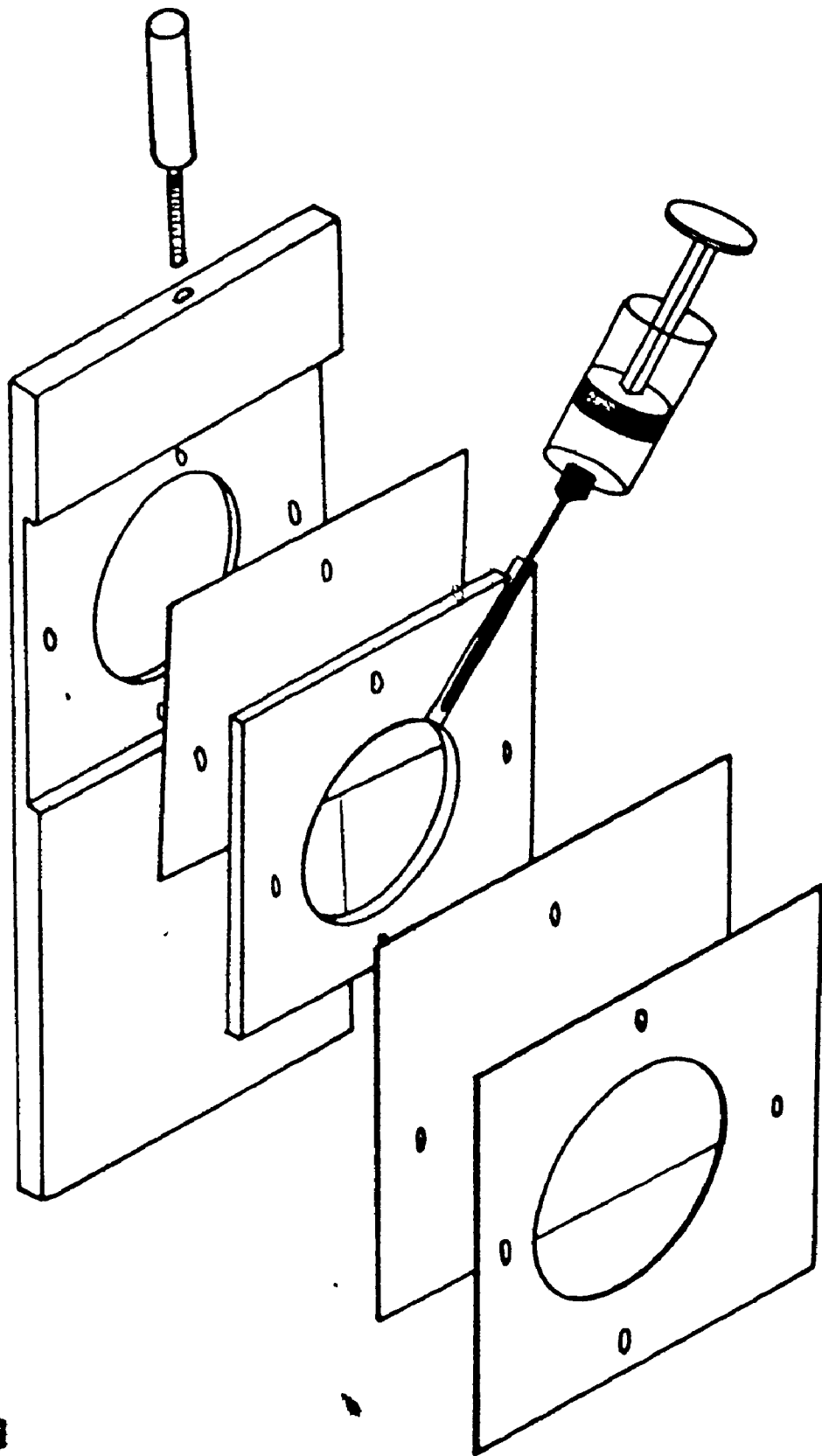
Samples generally contained 10 mg/cm^2 of iron and were held in sample holders either as a compressed powder or mixed with apiezon grease. For frozen solution spectra, the samples were syringed into the cell, shown in Fig. 3.3 and the samples were quenched rapidly, to prevent crystallization. The samples dissolved in liquid crystals,

Figure 3.2. A Diagram of the Liquid Transfer Cryotip.



1. HELIUM DEWAR
2. HELIUM CYLINDER
3. PRESSURE REGULATOR
4. MERCURY MANOMETER, 0 TO 20" Hg
5. VACUUM SHROUD
6. VACUUM SHROUD PUMP
7. VACUUM PUMP FOR OPERATION BELOW 4.2°K
8. ACCESSORY FLOW CONTROL PANEL
9. ACCESSORY TEMPERATURE CONTROLLER, MANUAL OR AUTOMATIC

Figure 3.3. The Mössbauer Liquid-Cell.



contained less than 7% of iron, and were poured into the cell described above.

(ii) Infrared

Infrared spectra in the 400-4000 cm^{-1} range were recorded using either a Perkin-Elmer 337 or Beckman IR5. Spectra in the 200-400 cm^{-1} range were recorded using a Beckman IR12. Samples were prepared as mulls or as solutions in tetrahydrofuran. KBr windows were used for the near infrared spectra and polyethylene windows were used for far infrared spectra.

(iii) Electron Spin Resonance

Electron spin resonance spectra were recorded using a JES-3B5-X spectrometer at X-band frequency with 100 kHz/sec field modulation. The spectra were calibrated using an external standard of Mn^{2+} in MgO .

(iv) Magnetic Measurements

Magnetic susceptibilities of the solid samples were measured by the Gouy balance method on equipment already described (110), using $\text{HgCo}(\text{CNS})_4$ as a calibration standard.

The magnetic susceptibilities of the solution samples were measured by the nuclear magnetic resonance method, following the Evans' procedure (112). The solution under investigation, along with 1-2% of the standard proton containing substance, was placed in a normal NMR tube. A capillary tube containing the same solvent with the same concentration of the standard substance, was also placed in the above NMR tube. *t*-Butyl alcohol was a standard for aqueous solutions, while for non-aqueous solutions the solvent used to prepare the solutions was used as a standard. A Varian A-60 NMR spectrometer was used.

B MATERIALS

All solvents were reagent grade and were dried and deoxygenated before use.

Anhydrous ferrous bromide and ferrous iodide were obtained from Alfa Inorganics, Inc., and were used without further purification. All ligands were reagent grade and were used without further purification. Thiourea was obtained from Fisher Scientific Company; thiobenzamide, thiourea and orthoaminothiophenol from Eastman Chemical Corporation; diphenylthiourea from Aldrich Chemical Company; and Nitric oxide gas from Matheson of Canada, Ltd., Ethanethiol, oxalyl chloride, tetraethylammonium chloride, tetrabutylammonium bromide were obtained from Eastman Organic Chemicals; BaCl_2 from Fisher Scientific Company; and trisethylenediamine cobalt(III)chloride from Alfa Inorganics, Inc.

C PREPARATION OF THE IRON-NITROSYL COMPLEXES

The complexes were prepared according to the procedures of Hieber and Kaiser (38). All compounds were prepared and manipulated in an atmosphere of pure nitrogen. The starting materials, i.e., the dimeric iron nitrosyl halides $[\text{Fe}(\text{NO})_2\text{X}]_2$ where $\text{X} = \text{Br}$ and I , were prepared by literature methods (24,113).

$\text{Fe}(\text{NO})_4$: 10 ml iron pentacarbonyl was placed in a 120 ml stainless steel bomb. Nitric oxide which has been condensed into a 2 litre flask from a cylinder, was introduced at about 5.3 atmospheres and the bomb was then closed and held at room temperature for three days. The product was washed with sodium-dried ether.

$[\text{Fe}(\text{NO})_2\text{X}]_2$: Anhydrous FeX_2 and an excess of iron powder were ground together to fine powder. NO gas which was purified by passing through solid KOH, to remove NO_2 , and P_2O_5 , to remove moisture, was reacted with FeX_2 initially at room temperature, and then at 50°C until the reaction was complete. The crude product was sublimed at 110°C for the bromide complex and 90°C for the iodide complex. This sublimation was repeated several times in order to obtain pure product.

$\text{Fe}(\text{NO})_2\text{LX}$: A solution of 5 mmole of the thioamide (L) in 30 ml THF was slowly added to a solution of 2.5 mmole (1 g) $[\text{Fe}(\text{NO})_2\text{X}]_2$ in 20 ml THF. The solution mixture was shaken for one hour after which the THF was removed at reduced pressure. Petrol ether (b.p. $30^\circ\text{--}60^\circ\text{C}$) was added to the concentrated solution. An oily black air-sensitive liquid was shaken with (1:1) petrol ether/ether several times until crystals were obtained. L = thiourea (tu), thioacetamide (ta), thiobenzamide (tb); o-aminothiophenol (o-atp) and diphenylthiourea (dptu).

$[\text{Fe}(\text{NO})_2(\text{tu})\text{Br}]$: calc.: Fe, 20.53; S, 11.53.

found: Fe, 20.48; S, 11.78.

$\text{Fe}(\text{NO})_2(\text{ta})\text{Br}$: calc.: Fe, 21.57; S, 12.35.

found: Fe, 21.94; S, 12.21.

$\text{Fe}(\text{NO})_2(\text{tb})\text{Br}$: calc.: C, 25.23; H, 2.10; N, 12.62; Br, 24.01; S, 9.63;
Fe, 16.78.

found: C, 24.31; H, 1.98; N, 12.00; Br, 26.60; S, 8.86;
Fe, 17.13.

$\text{Fe}(\text{NO})_2(\text{dptu})\text{Br}$: calc.: Fe, 13.16.

found: Fe, 12.83.

$\text{Fe}(\text{NO})_2(\text{o-atp})\text{Br}$: calc.: Fe, 17.39; S, 9.96.

found: Fe, 18.35; S, 8.83.]

$\text{Fe}(\text{NO})_2\text{L}_2\text{X}$: The same procedure mentioned above, was performed, except 10 mmole of ligand and 2.5 mmole of iron nitrosyl halide were used.

$[\text{Fe}(\text{NO})_2(\text{o-atp})_2\text{Br}]$: calc.: C, 32.30; H, 3.17; N, 12.58.
found: C, 32.09; H, 2.65; N, 11.71.]

D PREPARATION OF THE IRON-DITHIOOXALATE COMPLEXES

KHS: 6.8 g of potassium was refluxed in 40 ml absolute ethanol until the ethoxide began to separate. A fast stream of H_2S was bubbled through the solution. It was filtered, and absolute ether was added to the filtrate. A dense, pure white precipitate of KHS was recrystallized from absolute ethanol/ether.

$(\text{C}_2\text{H}_5)_2\text{C}_2\text{O}_2\text{S}_2$: Ethyl dithiooxalate was prepared by mixing one gram-molecule of oxalyl chloride with two of ethyl mercaptan in the cold. The mixture was heated to expel any excess of either of the reactants and, on cooling, yellow needle-like crystals were obtained which were then recrystallized from ether.

$\text{K}_2\text{C}_2\text{O}_2\text{S}_2$: The reaction of an equivalent quantity of alcoholic potassium hydrosulphide and ethyl dithiooxalate in alcoholic solution yielded potassium dithiooxalate. It was washed free from potassium hydrosulphide with alcohol.

$\text{KBa}[\text{Fe}(\text{C}_2\text{O}_2\text{S}_2)_3] \cdot 6\text{H}_2\text{O}$: Ferric nitrate dodecahydrate (~ 0.4 g) dissolved in cold water was treated with solid potassium dithiooxalate (~ 0.6 g). The mixture was filtered, and barium chloride (~ 0.24 g) was added to the filtrate. The dark potassium barium salt was precipitated from the deep

purple solution. It was recrystallized from a minimum volume of water at 60°C. [calc.: Fe, 7.97; found: Fe, 7.81.]

The same procedure was used for $\text{KSr}[\text{Fe}(\text{C}_2\text{O}_2\text{S}_2)_3] \cdot \text{H}_2\text{O}$ and $[\text{Coen}_3][\text{Fe}(\text{C}_2\text{O}_2\text{S}_2)_3] \cdot 3\text{H}_2\text{O}$ using anhydrous strontium nitrate and tris ethylenediamine cobalt(III)chloride, respectively.

$[\text{C}_6\text{H}_5\text{NH}_3]_3[\text{Fe}(\text{C}_2\text{O}_2\text{S}_2)_3] \cdot \text{H}_2\text{O}$: The stoichiometric amount of anilinium hydrochloride was added to an aqueous solution of $[\text{Fe}(\text{C}_2\text{O}_2\text{S}_2)_3]^{3-}$, produced from ferric nitrate dodeca-hydrate and potassium dithiooxalate in cold water. Black needle-like crystals were obtained. [calc.: C, 40.23; H, 3.62; N, 5.86; S, 26.85; found: C, 40.28; H, 3.85; N, 6.07; S, 26.94.]

Attempts to make the ferrous complex by using ferrous ammonium sulfate resulted in the ferric complex only. [Found: C, 40.30; H, 3.58; N, 6.23; S, 26.34.]

$[(\text{C}_6\text{H}_5)_4\text{As}]_3[\text{Fe}(\text{C}_2\text{O}_2\text{S}_2)_3] \cdot 3\text{CH}_3\text{NO}_2$: About 0.6 g of potassium dithiooxalate was added to a cold solution of ~ 0.4 g ferric nitrate in water. The solution was filtered. The aqueous solution of $[\text{Fe}(\text{C}_2\text{O}_2\text{S}_2)_3]^{3-}$, was extracted with a dichloromethane solution of tetraphenyl arsonium chloride. The crude product isolated from dichloromethane solution was recrystallized from nitromethane.

A similar procedure was used to prepare $[(\text{C}_6\text{H}_5)_3\text{P}]_2\text{M}[\text{Fe}(\text{C}_2\text{O}_2\text{S}_2)_3]$, where M = Cu or Ag.

$[(\text{C}_5\text{H}_5)_4\text{N}]_2[\text{Fe}(\text{C}_2\text{O}_2\text{S}_2)_2(\text{NO})]$: The dark purple solution of the $[\text{Fe}(\text{C}_2\text{O}_2\text{S}_2)_3]^{3-}$ anion in aqueous NaNO_2 was heated to 70°C. The colour changed to green,

as the $[\text{Fe}(\text{C}_2\text{O}_2\text{S}_2)_2(\text{NO})]^{2-}$ ion was formed. An aqueous solution of tetraethyl ammonium chloride was added to the green solution and the product was recrystallized from 1:1 acetone solution. [Calc.: Fe, 9.53; S, 21.84; Found: Fe, 9.28; S, 21.46.]

Tetrabutyl ammonium bromide was used to obtain the tetrabutyl ammonium salt.

E CHEMICAL ANALYSES

Iron was determined gravimetrically as ferric oxide after precipitation as hydrated ferric hydroxide. Sulfur was determined as barium sulfate after precipitation with barium chloride (114). Carbon, hydrogen, nitrogen and halogen analyses were done by Chemalytics, Inc., Arizona, and/or A. B. Gygil, Microanalysis Laboratories Limited, Toronto.

F LIQUID CRYSTALS EXPERIMENTS

The liquid crystals used in this work were N-(p-methoxybenzylidene)-p-butylaniline (Aldrich Chemical Company), p-(p-ethoxyphenylazo)-phenyl hexanoate and p-(p-ethoxyphenylazo)-phenyl heptanoate (Eastman Organic Chemicals). The nematic temperature of the first one is room temperature, while that of a 40:60 mixture of the latter two is 45°C.

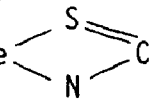
All of the absorber samples were prepared by heating weighed amounts of the complex and the liquid crystal to the isotropic phase, and the mixture then poured into the cell shown in Fig. 3.3. The liquid crystal and hence the dissolved sample may be oriented in a magnetic field by cooling from the isotropic phase to room temperature, passing through the nematic phase. The sample can be ordered such that the preferred molecular direction is parallel to the external magnetic field

if the material possesses a mematic phase. This arrangement is preserved in the nematic state, hence the sample can be removed from the magnetic field without disturbing the alignment. A magnetic field of 9000 gauss was used. The samples could also be oriented in the cell by stroking with tissue. The aligned sample was then cooled to liquid nitrogen temperature, and the Mössbauer spectrum was recorded. The absorber holder could be rotated, so that the gamma ray beam was incident to the plane of the absorber at any desired angle.

CHAPTER IV

IRON-NITROSYL COMPLEXES

A. INTRODUCTION

A number of iron-nitrosyl complexes formed in aqueous solution with a variety of organic and inorganic ligands have been reported by McDonald et al. (29), Wollum et al. (18) and by Burlamacchi et al. (30). The structures of the complexes formed in solution were inferred, from electron-nuclear hyperfine interactions, to have the formulation $\text{Fe}(\text{NO})_2\text{L}_2$, where L represents a monodentate ligand. Recently, Hieber and Kaiser (38) have shown that the reaction of $[\text{Fe}(\text{NO})_2\text{X}]_2$ with sulfur containing ligands, such as thioacetamide, thiourea, etc., yields complexes having the general formula $\text{Fe}(\text{NO})_2\text{LX}$, where X = Br or I, and L = ligand. From a comparison of the i.r. bands in the 400-4000 cm^{-1} region of the spectrum for the free and complexed ligand, it was proposed that these complexes should be formulated as $[\text{Fe}(\text{NO})_2\text{L}]^+\text{X}^-$ with the ligand L behaving in a bidentate fashion by coordination through both S and N. These complexes were apparently the first examples of a thioamide functioning as a chelating ligand. It was, therefore, of considerable interest to investigate how the four membered ring  would compete against the very strong π -acceptor NO ligand in these tetrahedral iron-nitrosyl complexes for the available metal electrons.

The results of studies of these iron-nitrosyl complexes are reported in this chapter.

B. RESULTS AND DISCUSSION

The spectroscopic and analytical data confirm that the complexes $\text{Fe}(\text{NO})_2\text{LX}$ obtained are identical to those previously reported (38). $\text{Fe}(\text{NO})_2(\text{tu})\text{I}$ and $\text{Fe}(\text{NO})_2(\text{dptu})\text{Br}$ are reported for the first time. The physical properties and spectroscopic data for these two complexes suggest that they have the same structure as the other thioamide complexes.

(i) Infrared

Infrared spectra of these compounds are complex and a complete analysis has not been attempted. However, it is possible to identify some of the characteristic vibrations of the thiobenzamide and thioacetamide ligands from a comparison of the spectra of free ligand and when complexed. According to the proposed structure (38), both the $\nu_{\text{C}=\text{S}}$ and $\nu_{\text{N}-\text{H}}$ or δ_{NH_2} vibrations are expected to be shifted in frequency as a result of coordination through sulfur and nitrogen to the metal. Hieber and Kaiser (38) found significant shifts in N-H, C=S and C-N regions, on going from the free ligand to the complex. In this study, the C=S and C-N stretching bands are shifted significantly on complexation, but there is no change in the N-H frequency (Table 4.1). A similar observation has been reported by Flint and Goodgame (41) for $\text{CoX}_2(\text{ta})_2$ complexes, and by Birchall and Morris (115) for $\text{FeX}_2(\text{ta})_2$ complexes. These workers suggest that the thioamide is coordinated through sulfur to the metal atom. Hence, infrared evidence suggests that the coordination of ligand to metal is through sulfur, but not nitrogen, and that the thioamide ligands probably function in a monodentate fashion towards iron in these complexes. However, it should be pointed out that, the data shown in

TABLE 4.1

I.R. Spectra of the Complexes in the Range 4000-400 cm^{-1}

Complex	ν_{NH}	ν_{NH_2}	ν_{CS}	$\nu_{\text{CN}} + \nu_{\text{CS}}$
Thiourea	3364	1618	1409	730
$\text{Fe}(\text{NO})_2(\text{tu})\text{Br}$	3362	1620	1365	708
Thioacetamide	3400	1640		725
$\text{Fe}(\text{NO})_2(\text{ta})\text{Br}$	3400	1648		690
Thiobenzamide	3300	1635	1400	770
$\text{Fe}(\text{NO})_2(\text{tb})\text{Br}$	3300	1640	1360	710

Table 4.1, were recorded in solution rather than in the solid state and the structures of the complexes could be different in solution, with a solvent molecule occupying the site formerly taken by the NH_2 group in the solid state.

Infrared data, in the NO stretching frequency region, for the iron-nitrosyl complexes are shown in Table 4.2. For iron-tetranitrosyl, Griffith et al. (22) have found three infrared bands, two in the NO^+ region and one in the NO^- region. In this study, the two bands at 1810 cm^{-1} and 1730 cm^{-1} were found, in agreement with the previous workers, but the band at 1150 cm^{-1} , reported by Griffith et al. (22) was not detected. Since this compound is very unstable, it is possible that some decomposition occurred while the spectrum was being recorded and therefore these data are rather inconclusive.

There is a decrease in N-O stretching frequency on going from $\text{Fe}(\text{NO})_4$ to the $\text{Fe}(\text{NO})_2\text{LX}$ complexes. This indicates that both L and X are poorer π -acceptors than the NO group. The NO groups in the $\text{Fe}(\text{NO})_2\text{LX}$ complexes must accept $d\pi$ electrons from the metal to a greater extent in order to prevent the accumulation of negative charge on the metal atom. Thus, an increase in the M-N bond strength must cause an equal decrease in the N-O bond strength; this, in turn, will cause a drop in the NO frequency. Two N-O stretching absorptions are observed in the $1600\text{-}1800\text{ cm}^{-1}$ region for $\text{Fe}(\text{NO})_2\text{LX}$ complexes, but they vary little upon changing the ligand L (Table 4.2). A shift in NO frequencies for the dinitrosyl iron bromide dimer in various solvents, as shown below, reveals the polarising influence of the solvent.

TABLE 4.2

NO Stretching Frequencies* for Iron-Nitrosyl Complexes

Complex	$\nu_{\text{NO}} \text{ cm}^{-1}$
+ Fe(NO) ₄	1826, 1763
[Fe(NO) ₂ Br] ₂	1774, 1709
[Fe(NO) ₂ I] ₂	1752, 1688
Fe(NO) ₂ (tu)Br	1788, 1725
Fe(NO) ₂ (tu)I	1785, 1723
Fe(NO) ₂ (ta)Br	1793, 1720
Fe(NO) ₂ (tb)Br	1794, 1730
Fe(NO) ₂ (dptu)Br	1773, 1725
Fe(NO) ₂ (o-atp)Br	1784, 1752
Fe(NO) ₂ (o-atp) ₂ Br	1780, 1719

* In THF solution.

+ mull

(tu = thiourea; ta = thioacetamide; tb = thiobenzamide;
dptu = diphenylthiourea; o-atp = o-aminothiophenol).

Solvent	$\nu_{\text{NO}} \text{ cm}^{-1}$
Nujol	1818, 1768
CCl_4	1816, 1762
CH_2Cl_2	1826, 1762
THF	1774, 1709

These data are supported by the e.s.r. evidence which will be discussed in a later section.

Far infrared spectra were recorded in an attempt to obtain information about the metal-ligand linkages. The spectra of these complexes, together with those of $[\text{Fe}(\text{NO})_2\text{Br}]_2$ and $[\text{Fe}(\text{NO})_2\text{I}]_2$ are listed in Table 4.3. Bands, attributed to Fe-NO vibrations, are generally weak and broad, and are observed in both the mull and solution spectra. This assignment of $\nu_{\text{Fe-N}}$ agrees with the infrared assignments made for nitrosyl complexes of Co and Fe, by Jahn (26). However, the $[\text{Fe}(\text{NO})_2\text{I}]_2$ mull spectrum showed no bands in this region, and no explanation is apparent.

Terminal M-X stretching bands appear in the region at $400\text{-}200 \text{ cm}^{-1}$ for M-Cl, $300\text{-}200 \text{ cm}^{-1}$ for M-Br, and $200\text{-}100 \text{ cm}^{-1}$ for M-I (116). The far infrared spectra of tetrahedral MCl_2py_2 , (M = Co, Zn and py = pyridine) show two bands in the 300 cm^{-1} region which are assigned as $\nu_{\text{M-X}}$ (117). Clark and Williams (117) reported that a series of polymeric halogen bridged complexes MCl_2py_2 (M = Mn, Fe, Co, Ni) gives $\nu_{\text{M-Cl}}$ bands in the $200\text{-}260 \text{ cm}^{-1}$ region. In general, bridging M-X stretching frequencies are lower than terminal M-X stretching frequencies. However, the infrared spectra of $\text{Fe}(\text{NO})_2\text{LX}$ and $[\text{Fe}(\text{NO})_2\text{X}]_2$ are quite complex, making it dif-

TABLE 4.3

I.R. Spectra of the Complexes in the Region 400-200 cm^{-1}

Complex		$\nu_{\text{Fe-N}}$	$\nu_{\text{Fe-S}}$	$\nu_{\text{Fe-X}}$	Other Bands
$[\text{Fe}(\text{NO})_2\text{Br}]_2$	THF mul1	283w 304sh, 292m		(235vs.b.) (235vs.b.)	400m
$[\text{Fe}(\text{NO})_2\text{I}]_2$	THF mul1	200w	250m 229s		395m
$\text{Fe}(\text{NO})_2(\text{tu})\text{Br}$	THF mul1	305w, 292m 275m, 262		(240w, 220w) (238m, 224m)	413s
$\text{Fe}(\text{NO})_2(\text{tu})\text{I}$	THF mul1	288vb. 314w, 270bm.	212w 240w, 220w		423s
$\text{Fe}(\text{NO})_2(\text{ta})\text{Br}$	THF mul1	313w, 272m 337m, 265m		(240m, 222m) (243m, 222m)	413m
$\text{Fe}(\text{NO})_2(\text{tb})\text{Br}$	THF	290vb.	(255m, 230m, 210m)		417m
$\text{Fe}(\text{NO})_2(\text{o-atp})\text{Br}$	THF mul1	288vb. 395w, 373m	(254w, 247w, 227sh) (240w)		
$\text{Fe}(\text{NO})_2(\text{o-atp})_2\text{Br}$	mul1	463s, 393m, 370s 299w, 288s	(234m, 211m)		

difficult to differentiate between terminal and bridging ν_{M-X} .

Bands in the 200-250 cm^{-1} region, are not so well resolved and are not readily assignable. It has been suggested that the bands in this region are strongly coupled ν_{Fe-Br} and ν_{Fe-S} vibrations (41,115). The Fe-I stretch should occur at much lower frequency than 200 cm^{-1} as mentioned earlier. As a result, less interaction might be expected with the Fe-S vibrations in the 200-250 cm^{-1} region and simpler spectra should result. This is observed for $[Fe(NO)_2Br]_2$ and $[Fe(NO)_2I]_2$, and for $Fe(NO)_2(tu)Br$ and $Fe(NO)_2(tu)I$ with the iodo complexes having less complex spectra in the 200-250 cm^{-1} region than the bromo complex (Figs. 4.1-4.2).

All of the complexes except those involving ortho-aminothiophenol have a band at ca. 400 cm^{-1} in their solution spectra, which is not present in the mull spectra. This band could well arise from an interaction between the complex and the solvent and indeed such an interaction in the case of $[Fe(NO)_2X]_2$ compounds is supported by the e.s.r. evidence (32). Since M-O stretching vibrations generally occur in the 400 cm^{-1} region (116), it is suggested that the band at 400 cm^{-1} is from an Fe-O band, which arises because of interaction between the solvent tetrahydrofuran and the metal complex.

On the basis of the data in Table 4.3, it is not possible to ascertain with certainty if the amide ligands are coordinated to iron through both the sulfur and nitrogen centres. However, the data do seem to suggest that the halogen may be coordinated to the metal. If this is so, then, this throws considerable doubt on the structures proposed for these complexes by Hieber and Kaiser (38).

Figure 4.1. The Far Infrared Spectra of

(A) $\cdot[\text{Fe}(\text{NO})_2\text{I}]_2$ and

(B) $\cdot[\text{Fe}(\text{NO})_2\text{Br}]_2$ in nujol.

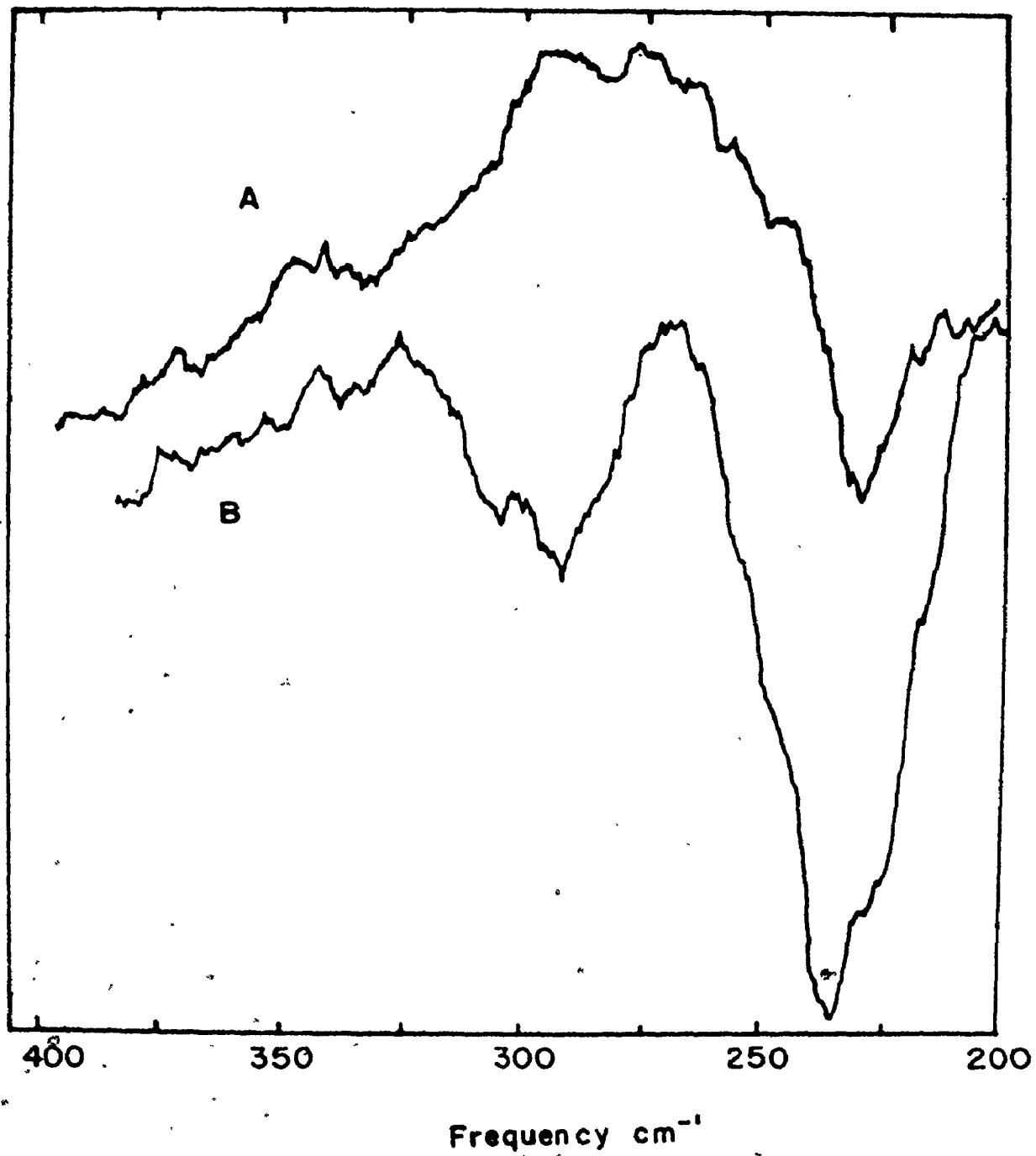
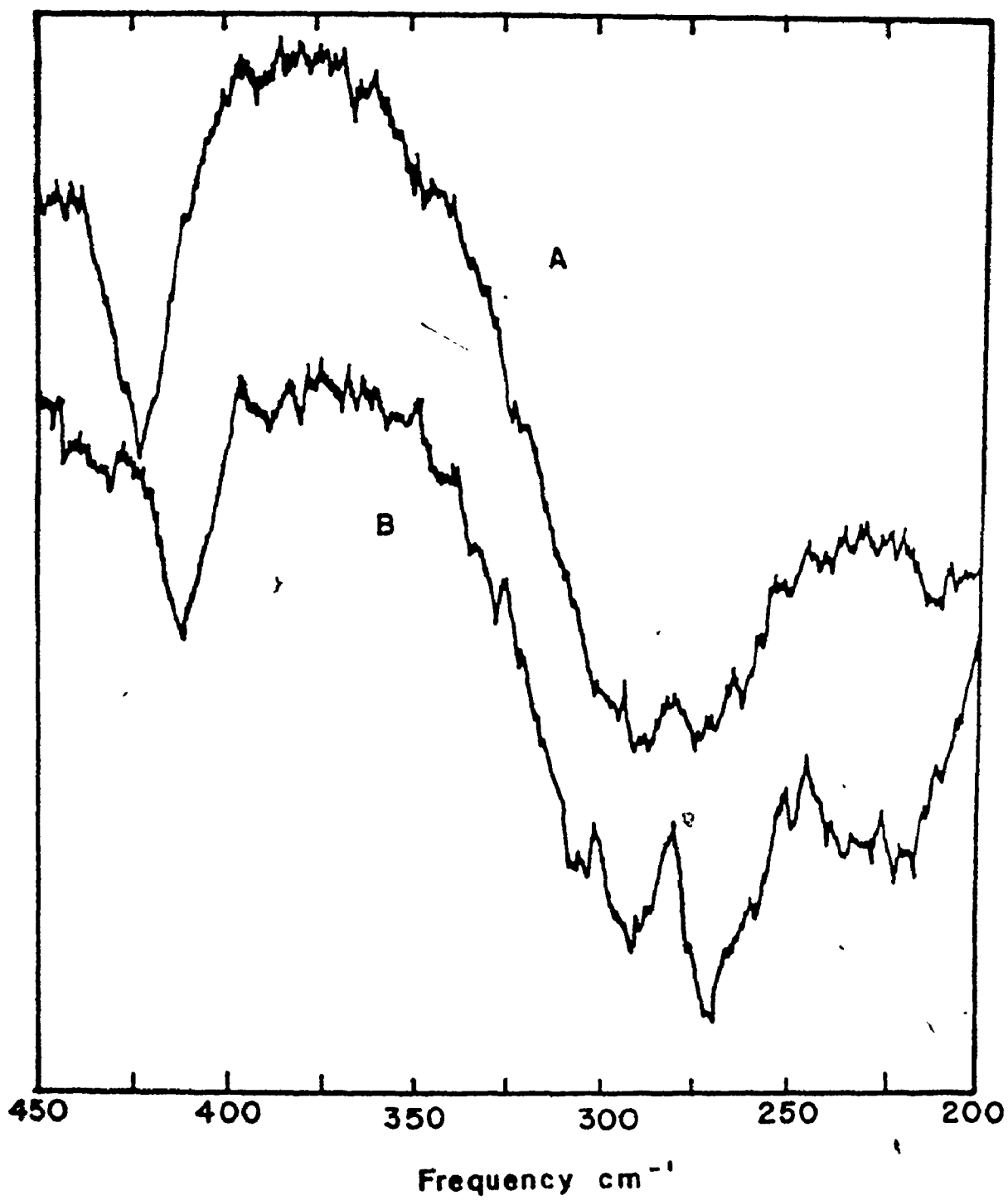


Figure 4.2. The Far Infrared Spectra of

(A) $\text{Fe}(\text{NO})_2(\text{tu})\text{I}$ and

(B) $\text{Fe}(\text{NO})_2(\text{tu})\text{Br}$ in THF.



(ii) Magnetic Measurements

All of the complexes studied, except the dinitrosyl iron halide dimers are paramagnetic in the solid state (Table 4.4). Careful purification of these dimer complexes, by repeated sublimation, resulted in materials which were, based on careful Gouy measurements, diamagnetic. Table 4.5 illustrates a temperature series of magnetic susceptibilities for $[\text{Fe}(\text{NO})_2\text{I}]_2$. The apparent increased diamagnetism at lower temperatures is not considered significant. The experimental error is usually large when such small susceptibilities are being measured as is the case here. Irreproducible results were obtained for the dinitrosyl iron bromide dimer. Soling and Asmussen (118) also had difficulty in obtaining reproducible results for this complex. Since it is improbable that the magnetic properties of the bromine analogue would be different from that of the iodide, it is concluded that $[\text{Fe}(\text{NO})_2\text{Br}]_2$ is diamagnetic when chemically pure. The monomeric form $\text{Fe}(\text{NO})_2\text{X}$ contains an uneven number of electrons and will be paramagnetic. A binuclear structure leaves one unpaired electron on each iron atom which could interact to form a metal-metal bond in order to satisfy the diamagnetism. This is in agreement with the proposal of Dahl et al. (28) who suggested that a metal-metal bond existed in $[\text{Fe}(\text{NO})_2\text{I}]_2$ despite the very long Fe-Fe distance of 3.05 Å. The corresponding bromide complex would be expected to be similar.

In the $\text{Fe}(\text{NO})_2\text{LX}$ complexes, paramagnetism arises from a single hole in the iron 3d shell which leaves an unpaired electron in the t_2 level. These complexes are, therefore, classified as $d^9 \text{Fe}(-1)$ complexes.

TABLE 4.4
Magnetic Moments for $\text{Fe}(\text{NO})_2\text{LX}$

Complex	μ_{eff} (B.M.)
$\text{Fe}(\text{NO})_2(\text{tu})\text{Br}$	1.80
$\text{Fe}(\text{NO})_2(\text{tu})\text{I}$	†
$\text{Fe}(\text{NO})_2(\text{ta})\text{Br}$	2.00
$\text{Fe}(\text{NO})_2(\text{tb})\text{Br}$	1.81
$\text{Fe}(\text{NO})_2(\text{dptu})\text{Br}$	1.90
$\text{Fe}(\text{NO})_2(\text{o-atp})\text{Br}$	1.92
$\text{Fe}(\text{NO})_2(\text{o-atp})_2\text{Br}$	1.82

† This compound was not sufficiently stable at room temperature to enable the magnetic moment to be measured.

TABLE 4.5

The Magnetic Susceptibilities for $[\text{Fe}(\text{NO})_2\text{I}]_2$

Temperature	$\times 10^{-6}$
$^{\circ}\text{K}$	c.g.s.
202	-0.575
234	-0.503
271	-0.479
279	-0.479
295	-0.479

(iii) Electron Spin Resonance

Crow and coworkers reported (32) that solutions of $[\text{Fe}(\text{NO})_2\text{Br}]_2$ in CCl_4 are paramagnetic and give a very weak seven line e.s.r. spectrum. It was suggested (32) that such a spectrum would arise if the dimer unit remained intact while electrons in the Fe-Fe bond were not completely coupled. The possibility that the septet arose from two equivalent chlorine atoms ($I = 3/2$) which had been incorporated into the molecule via halogen exchange between the solvent and the complex, was also suggested. Addition of acetone or dimethylsulphoxide to the solution resulted in the collapse of this multiplet to a single broad line which was attributed to a complex of the form $\text{Fe}(\text{NO})_2\text{Br}(\text{solvent})$ with a reduced spin density on the halogen (32). The present investigation also shows that solutions of $[\text{Fe}(\text{NO})_2\text{Br}]_2$ in CCl_4 give rise to a seven line pattern (Fig. 4.3), but with slightly different parameters (Table 4.6) to those reported previously (32). Addition of acetone to this solution does give a broad singlet but upon dilution a four line pattern was resolved. Spectra were recorded in a variety of solvents but only solutions in CCl_4 gave the seven line pattern, all others gave a quartet pattern for dilute solutions or a single broad line for concentrated solutions. These data are summarised in Table 4.6. The origin of the septet spectrum is not clear. If the two electrons in the Fe-Fe bond are exchange coupled, no e.s.r. signal is expected because the molecule could be diamagnetic. If they are not exchange coupled, a complex spectrum is expected, due to an anisotropic dipolar mechanism. However, no signals other than the apparent septet were observed even in the frozen state. Although the origin of the e.s.r.

Figure 4.3. The E.s.r. Spectrum of $[\text{Fe}(\text{NO})_2\text{Br}]_2$ in THF.

5

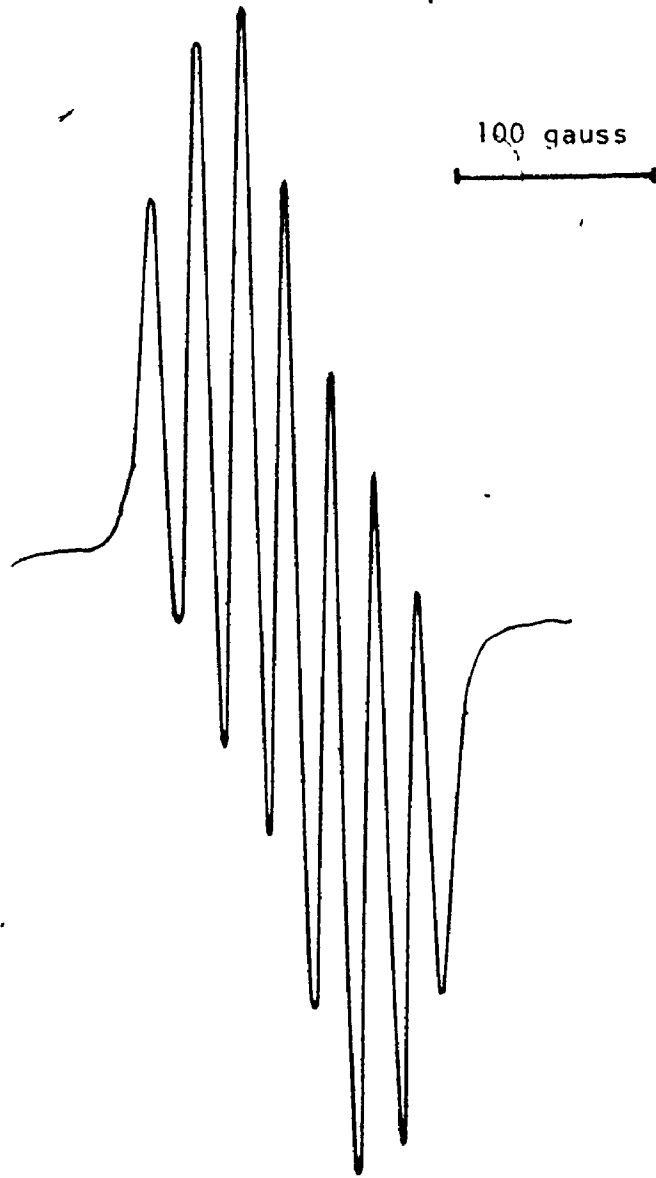


TABLE 4.6

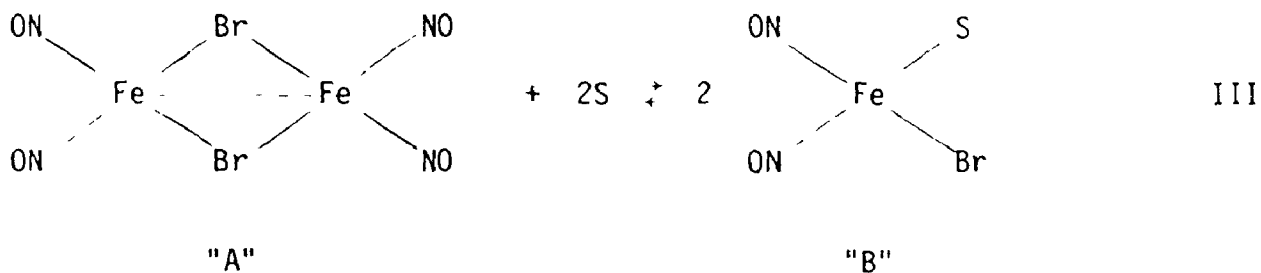
E.s.r. Data for the $\text{Fe}(\text{NO})_2\text{LX}$ Complexes

Complex	Solvent	g. value	a_{χ} gauss [†]	Γ^* gauss
$[\text{Fe}(\text{NO})_2\text{Br}]_2$	CCl_4	2.053	23.1(7)	12.2
	$\text{CCl}_4 + (\text{CH}_3)_2\text{CO}$	2.048	15.3(4)	7.8
	CH_2Cl_2	2.048	16.1(4)	5.6
	CHCl_3	2.047	16.0(4)	7.8
	$(\text{CH}_3)_2\text{CO}$	2.048	--- (1)	38.0
	$\text{C}_4\text{H}_8\text{O}$	2.046	--- (1)	39.8
	$\text{C}_4\text{H}_8\text{O}$	2.047	16.7(4)	8.9
$[\text{Fe}(\text{NO})_2\text{I}]_2$	CCl_4	2.062	15.5(6)	7.8
	$\text{CCl}_4 + (\text{CH}_3)_2\text{CO}$	2.063	--- (1)	42.7
	$\text{C}_4\text{H}_8\text{O}$	2.062	--- (1)	42.7
	$\text{C}_4\text{H}_8\text{O}$	2.062	19.4(6)	7.8
$\text{Fe}(\text{NO})_2(\text{tu})\text{Br}$	$\text{C}_4\text{H}_8\text{O}$	2.044	16.4(4)	7.7
$\text{Fe}(\text{NO})_2(\text{tu})\text{I}$	$\text{C}_4\text{H}_8\text{O}$	2.061	19.0(6)	9.0
$\text{Fe}(\text{NO})_2(\text{ta})\text{Br}$	$\text{C}_4\text{H}_8\text{O}$	2.048	16.8(4)	7.9
$\text{Fe}(\text{NO})_2(\text{tb})\text{Br}$	$\text{C}_4\text{H}_8\text{O}$	2.045	15.3(4)	7.7
$\text{Fe}(\text{NO})_2(\text{tb})\text{I}$	$\text{C}_4\text{H}_8\text{O}$	2.056	16.0(6)	6.0
$\text{Fe}(\text{NO})_2(\text{dptu})\text{Br}$	$\text{C}_4\text{H}_8\text{O}$	2.042	16.4(4)	8.8
$\text{Fe}(\text{NO})_2(\text{o-atp})\text{Br}$	$\text{C}_4\text{H}_8\text{O}$	2.046	15.3(4)	7.7
$\text{Fe}(\text{NO})_2(\text{o-atp})_2\text{Br}$	$\text{C}_4\text{H}_8\text{O}$	2.041	20.8(4)	10.9

[†] ^{79}Br and ^{81}Br isotropic coupling was not resolved.

* linewidth.

spectrum of the bromide dimer in CCl_4 is not clear, it appears that strong polar solvents can cleave the dimer, and coordinate to the metal to give the four coordinate species "B", in equilibrium III, in which the electron is coupled to one bromine ($I = 3/2$).



Such an interaction with the solvent is supported by the far i.r. data in Section IV. B. (i).

It should be pointed out that the intensities of the e.s.r. signals arising from $[\text{Fe}(\text{NO})_2\text{Br}]_2$ in solution were comparatively weaker than those from the solution of the paramagnetic species. Since e.s.r. spectroscopy is very sensitive to paramagnetic ions, a very small amount of impurity could produce the observed seven line e.s.r. signal. Hence, it is concluded that the unusual behaviour of this dimer in CCl_4 solution probably arises from the presence of a small amount of paramagnetic impurity in the system.

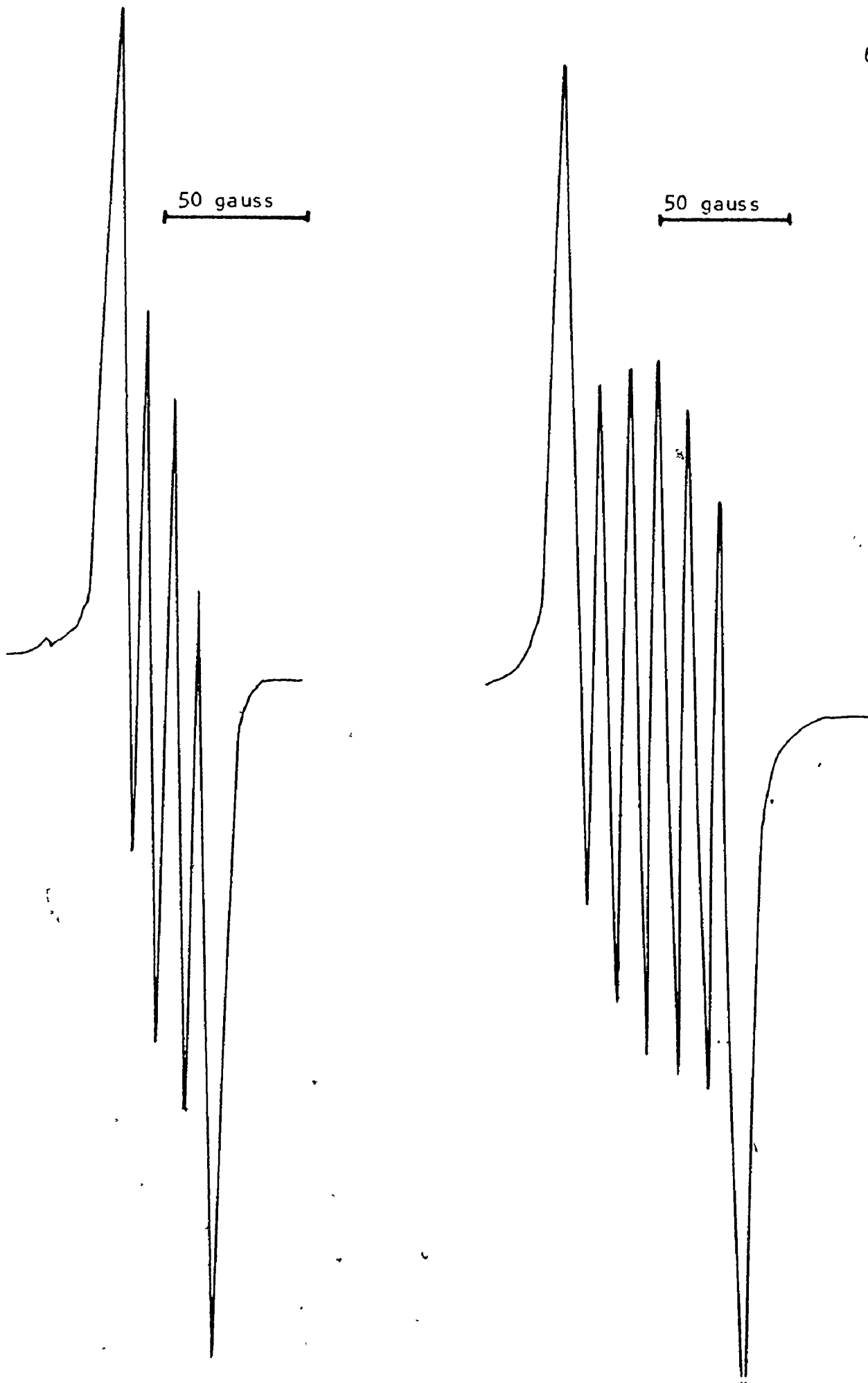
In contrast, solutions of $[\text{Fe}(\text{NO})_2\text{I}]_2$ in all solvents gave only a one or a six line e.s.r. spectrum indicating that the dimer unit, even in CCl_4 was completely dissociated. The six line spectrum would arise from coupling to a single iodine atom which has $I = 5/2$. This evidence excludes the possibility of halogen exchange between the solvent and the complex. The iodine bridge bonds are sufficiently

weak compared to bromine bridge bonds that even a solvent as weakly coordinating as carbon tetrachloride appears to effect cleavage of the dimer.

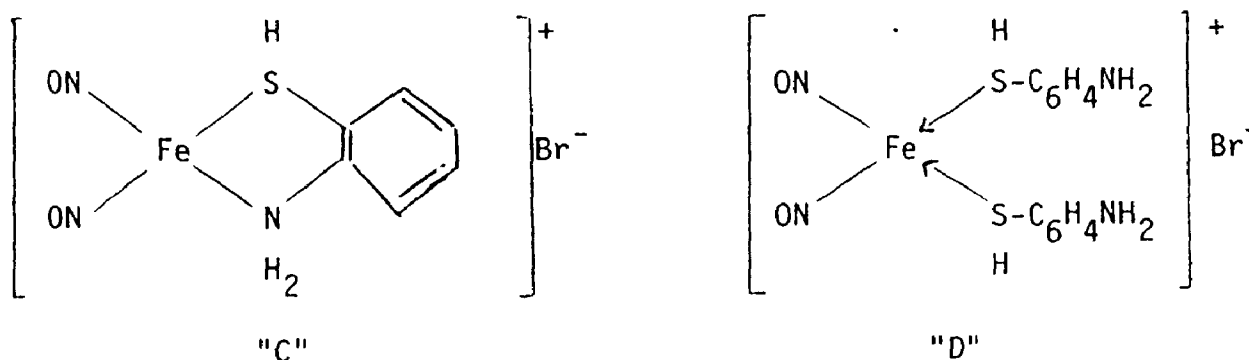
Coordinating ligands such as thioamides do effect cleavage of both dimers and the complexes reported in this thesis were produced in this manner. All of the complexes give strong e.s.r. signals with coupling to the halogen: four lines for the bromo complexes and six lines for the iodo complexes. The e.s.r. data for all of the complexes are reported in Table 4.6 and some typical spectra are shown in Fig. 4.4. The g values for the bromo complexes are ~ 2.045 while the iodo complexes are somewhat higher at 2.060. There is no apparent trend in the hyperfine splittings. The isotropic splittings of two bromine nuclei ($I_{Br79} = I_{Br81} = 3/2$) are not resolved.

It is clear that the unpaired electron in these complexes is strongly coupled to the halogen indicating that the halogen is covalently bound to the metal. These complexes cannot, therefore, be formulated as ionic species as Hieber and Kaiser have suggested (38). This also supports the suggestion made earlier from a consideration of the i.r. data that the amide ligand is not acting in a chelating fashion but is only coordinated to the iron through the sulfur. Further resolution of the spectra to reveal coupling to ^{14}N (2 N's from two nitrosyl groups or 3 N's from two nitrosyl groups and one thioamide group) could solve this problem but, unfortunately, the rather large line widths did not allow any additional hyperfine structure to be seen. In this respect, the spectra are similar to those reported by Burlamacchi et al. (30) and Crow et al. (32), neither group reporting any hyperfine

Figure 4.4. The E.s.r. Spectra of $\text{Fe}(\text{NO})_2(\text{tu})\text{Br}$ and $\text{Fe}(\text{NO})_2(\text{tu})\text{I}$.



coupling to ^{14}N in dinitrosyl iron complexes. Hyperfine coupling to ^{14}N has been observed in some $\text{Fe}(\text{NO})_2\text{L}_2$ complexes by McDonald *et al.* (29), with splitting constants being generally about 2 gauss. In contrast, $\text{Fe}(\text{NO})(\text{dithiol})_2$ complexes (dithiol = maleonitriledithiol, benzene-1,2-dithiol; 1,1-dicyanoethylene 2,2-dithiol (29); and N,N-dimethyldithiocarbamate (119)) showed coupling to ^{14}N ranging from 12.7 - 15.5 gauss, indicating that considerable electron spin delocalised onto the NO ligands. The axial position of the NO in these five coordinate complexes is favourable for back donation from the metal d orbitals to the vacant NO antibonding π -orbitals. It seems reasonable to suppose that the thioamide complexes have tetrahedral structures in view of the similarity of e.s.r. spectra reported here to those of other workers (29,30,32). However, in solution, a five or six coordinate structure with solvent molecules occupying the other sites cannot be ruled out. The structures of $\text{Fe}(\text{NO})_2(\text{o-atp})\text{Br}$ and $\text{Fe}(\text{NO})_2(\text{o-atp})_2\text{Br}$ are much less certain but in the light of the e.s.r. evidence presented above, they certainly cannot be formulated as "C" and "D" (38).



It is tempting to suggest that $\text{Fe}(\text{NO})_2(\text{o-atp})\text{Br}$ has a similar structure to the thioamide complexes with a monodentate o-atp ligand bonded through sulfur and a coordinated halogen, but the Mössbauer

data in Section IV. B. (iv) suggest that this may not be so. The structure of the $\text{Fe}(\text{NO})_2(\text{o-atp})_2\text{Br}$ is even less clear but this molecule also clearly has a bromine atom covalently bound to iron.

(iv) Mössbauer

The Mössbauer data obtained for the iron-nitrosyl complexes are given in Table 4.7. The data for $[\text{Fe}(\text{NO})_2\text{X}]_2$ in this study are in reasonable agreement with those reported previously (32).

In a tetrahedral crystal field, the iron 3d shell is split into a doubly degenerate e level lying below a triply degenerate t_2 level. A high spin arrangement of the electrons is favourable for this small splitting. In the $\text{Fe}(\text{NO})_2\text{LX}$ compounds, paramagnetism arises from an unpaired electron in the t_2 level and the compounds are described as $d^9 \text{Fe}(-1)$.

The magnitude of the centre shift is influenced by the extent of both ligand to metal σ bonding and metal to ligand π back bonding (120). As the σ -donor strength of the ligands increases, an increase in 4s-participation in the bonding by σ -donation will decrease the centre shift, or an increase in the effective 3d-population by σ -donation from the ligands will increase the centre shift by increased shielding effects. However, these are synergetically related to the π -bonding effect. If the ligands have empty low-lying antibonding π orbitals available, then back bonding from the filled iron 3d orbitals to these π^* orbitals will result in less shielding of the metal s electrons from the nucleus. This will result in an increase in s electron density and hence a decrease in the centre shift.

TABLE 4.7
Mössbauer Data for Iron-Nitrosyl Complexes

Complex	Temperature °K	Centre Shift (mm/sec)	Quadrupole Splitting (mm/sec)
Fe(NO)_4	77	0.44	0.93
$[\text{Fe(NO)}_2\text{Br}]_2$	77	0.43	1.85
$[\text{Fe(NO)}_2\text{I}]_2$	77	0.34	1.62
$\text{Fe(NO)}_2(\text{tu})\text{Br}$	77	0.33	1.31
	298	0.25	1.18
$\text{Fe(NO)}_2(\text{tu})\text{I}$	77	0.32	1.22
	298	0.22	1.18
$\text{Fe(NO)}_2(\text{ta})\text{Br}$	77	0.32	1.25
	298	0.24	1.17
$\text{Fe(NO)}_2(\text{tb})\text{Br}$	77	0.32	1.21
	298	0.27	1.13
$\text{Fe(NO)}_2(\text{dptu})\text{Br}$	77	0.33	1.31
	298	0.39	0.78
$\text{Fe(NO)}_2(\text{o-atp})\text{Br}$	77	0.20	1.20
	298	0.12	1.17
$\text{Fe(NO)}_2(\text{o-atp})_2\text{Br}$	77	0.23	1.25
	298	0.12	1.15

The thioamide and thiourea complexes have less positive centre shifts compared to the iron tetranitrosyl or the nitrosyl halide dimers, indicating a higher s electron density at the iron. Since the $\text{Fe}(\text{NO})_2\text{LX}$ complexes are d^9 systems, as opposed to d^{10} for $[\text{Fe}(\text{NO})_2\text{X}]_2$, this shift is not unexpected. One fewer d electron results in less shielding of the s electrons from the nucleus and hence a higher s electron density. Crow et al. (32) have reported data for similar d^9 complexes involving ligands of group V elements, their centre shifts are somewhat lower than those reported here. Their reported Mössbauer data are given in Table 4.8 for comparison. The generalisation of this observation is that the complexes with sulfur ligands have higher positive centre shifts than that of the complexes with phosphorus or arsenic ligands. The higher isomer shifts for complexes containing sulfur ligands could be caused by either a decrease in the 4s population or an increase in the effective 3d shielding of the s levels. The former would require the sulfur to be a less efficient σ -electrons donor. The latter implies an increase in the sulfur-to-metal π -donation or a decrease in the metal-to-ligand back π -bonding. It seems likely that an increase in σ -donation would cause a more negative isomer shift; a forward π -donation would cause a positive shift and the corresponding back donation would give a negative shift. Greenwood and coworkers (121) have observed the same effect in iron carbonyl compounds and concluded that σ -donation properties of these ligands are more important than that of π -donation properties. By analogy, it seems reasonable to conclude that the sulfur is a less effective σ -donor than phosphorus or arsenic. The parameters reported here for the thioamide and thiourea complexes are independent of the

TABLE 4.8

Mössbauer Data for Some Iron-Nitrosyls $\text{Fe}(\text{NO})_2\text{LY}^a$

Complex	Centre Shift ^b (mm/sec)	Quadrupole Splitting ^b (mm/sec)
$[\text{Fe}(\text{NO})_2\text{Br}]_2$	0.41	1.76
$[\text{Fe}(\text{NO})_2\text{I}]_2$	0.34	1.68
$\text{Fe}(\text{NO})_2(\text{C}_5\text{H}_{11}\text{N})\text{Br}$	0.34	1.12
$\text{Fe}(\text{NO})_2((\text{C}_6\text{H}_5)_3\text{P})\text{Br}$	0.24	1.02
$\text{Fe}(\text{NO})_2((\text{C}_6\text{H}_5)_3\text{As})\text{Br}$	0.26	1.28
$\text{Fe}(\text{NO})_2((\text{C}_6\text{H}_5)_3\text{Sb})\text{Br}$	0.25	1.49
$\text{Fe}(\text{NO})_2((\text{C}_6\text{H}_5)_3\text{P})\text{I}$	0.23	1.09
$\text{Fe}(\text{NO})_2((\text{C}_6\text{H}_5)_3\text{As})\text{I}$	0.24	1.28

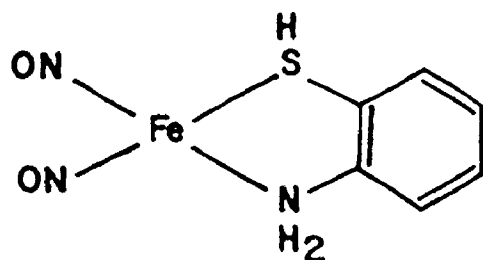
^a Taken from Ref. 32.

^b Measured at 77°K.

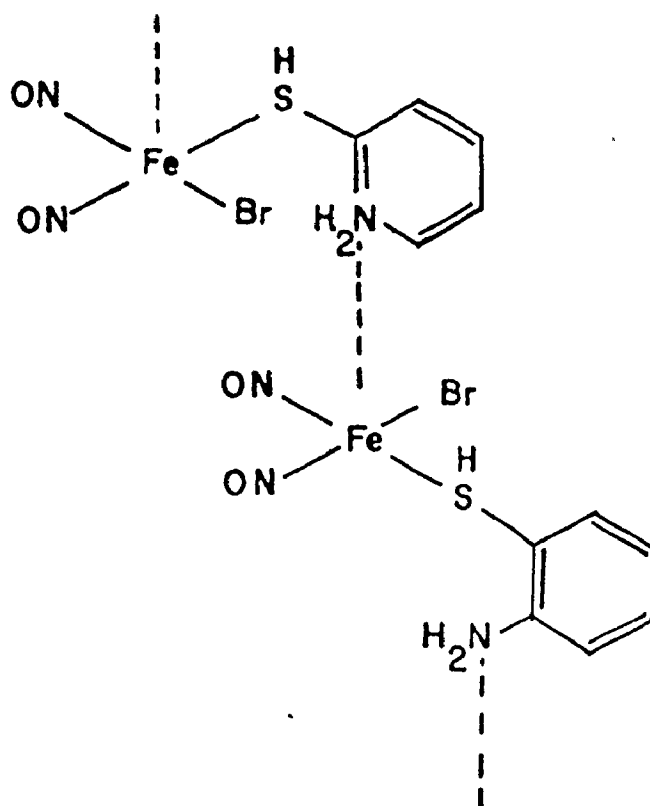
nature of the ligand L, or the halogen, and suggest that it is the NO ligand which is the dominant factor in determining the Mössbauer parameters. A similar behaviour is observed for carbonyl complexes of iron. Both of the o-atp complexes have significantly lower centre shifts than the thioamide complexes. In the case of $\text{Fe}(\text{NO})_2(\text{o-atp})\text{Br}$ this increased s electron density means either, that the o-atp ligand is a much better π -acceptor than the thioamides, which does not seem very likely, or that this complex has quite a different structure! Both o-atp complexes have similar Mössbauer parameters and therefore probably have structures which are closely related. $\text{Fe}(\text{NO})_2(\text{o-atp})_2\text{Br}$ contains five ligands, assuming o-atp to be monodentate, and can clearly not contain four coordinate iron. By inference, the $\text{Fe}(\text{NO})_2(\text{o-atp})\text{Br}$ is suggested to have at least five coordinate iron. Thus, the coordination of the o-atp through both sulfur and nitrogen cannot be ruled out in this case. Two possible structures for this complex are shown in Fig. 4.5; an o-atp acts as a chelate in Fig. 4.5(a) or the complex has a polymeric structure as shown in Fig. 4.5(b). It is obvious that the much more definitive structural information is necessary, and crystallographic analyses will be necessary in order to solve this problem.

The centre shift of iron tetranitrosyl is 0.44 mm/sec at 77°K. The structure proposed by Griffith et al. (22), $\text{Fe}(\text{NO}')_3(\text{NO}'')$ where NO' acts as NO^+ , and NO'' as NO^- , would have a distorted tetrahedral structure and exhibit a moderate quadrupole splitting. It is an iron (-II) d^{10} system. The structure suggested by Sidgwick (21) $\text{NO}^+[\text{Fe}(\text{NO})_3]^-$, having the anion isoelectronic with well-established $\text{Co}(\text{NO})_3$ complex (122), would have a pyramidal arrangement around the iron atom and its quad-

Figure 4.5. Two Possible Structures for $\text{Fe}(\text{NO})_2(\text{o-atp})\text{Br}$.



(a)



(b)

quadrupole splitting would be expected to be very large. However, the observed quadrupole splitting of $\text{Fe}(\text{NO})_4$ is about the same as the other distorted tetrahedral iron-nitrosyl complexes and the observed centre shift is the same as that of other d^{10} iron complexes, i.e., the dinitrosyl iron halide dimers (Table 4.7). In view of this it seems likely that the first structure would be the most reasonable. It is not unexpected that the quadrupole splitting of $\text{Fe}(\text{NO})_4$ is smaller than $[\text{Fe}(\text{NO})_2\text{X}]_2$ since the dinitrosyl halide dimer has a five coordinate arrangement around the iron atom (Figs. 4.6-4.7).

Recently, Mazak and Collins (35) have computed the electric field gradient tensor components for tetrahedral Fe(-II) molecules of the types FeA_2B_2 , FeA_3B and FeA_2BC . Some of their results are shown in Table 4.9. As mentioned in equation (16), $V_{zz} = eq$ will depend both on noncubic distributions of the iron valence electrons and on external charges (91). In general, only q_{lattice} is considered in the point-charge model. However, it has recently been shown (91) that q_{valence} also follows the predictions of the point charge model. This term was approximated (122) as

$$q_{\text{valence}} = q_l (3\cos^2\theta_l - 1)r_l^{-3} \quad [21]$$

where q is an effective charge on the M-L bond axis representing the "electron hole" density in the appropriate orbital. The V_{zz} becomes

$$V_{zz} = \sum_L [L] (3\cos^2\theta_L - 1) \quad [22]$$

where

Figure 4.6. The Mössbauer Spectrum of $\text{Fe}(\text{NO})_4$ at 77°K .

PERCENT ABSORPTION

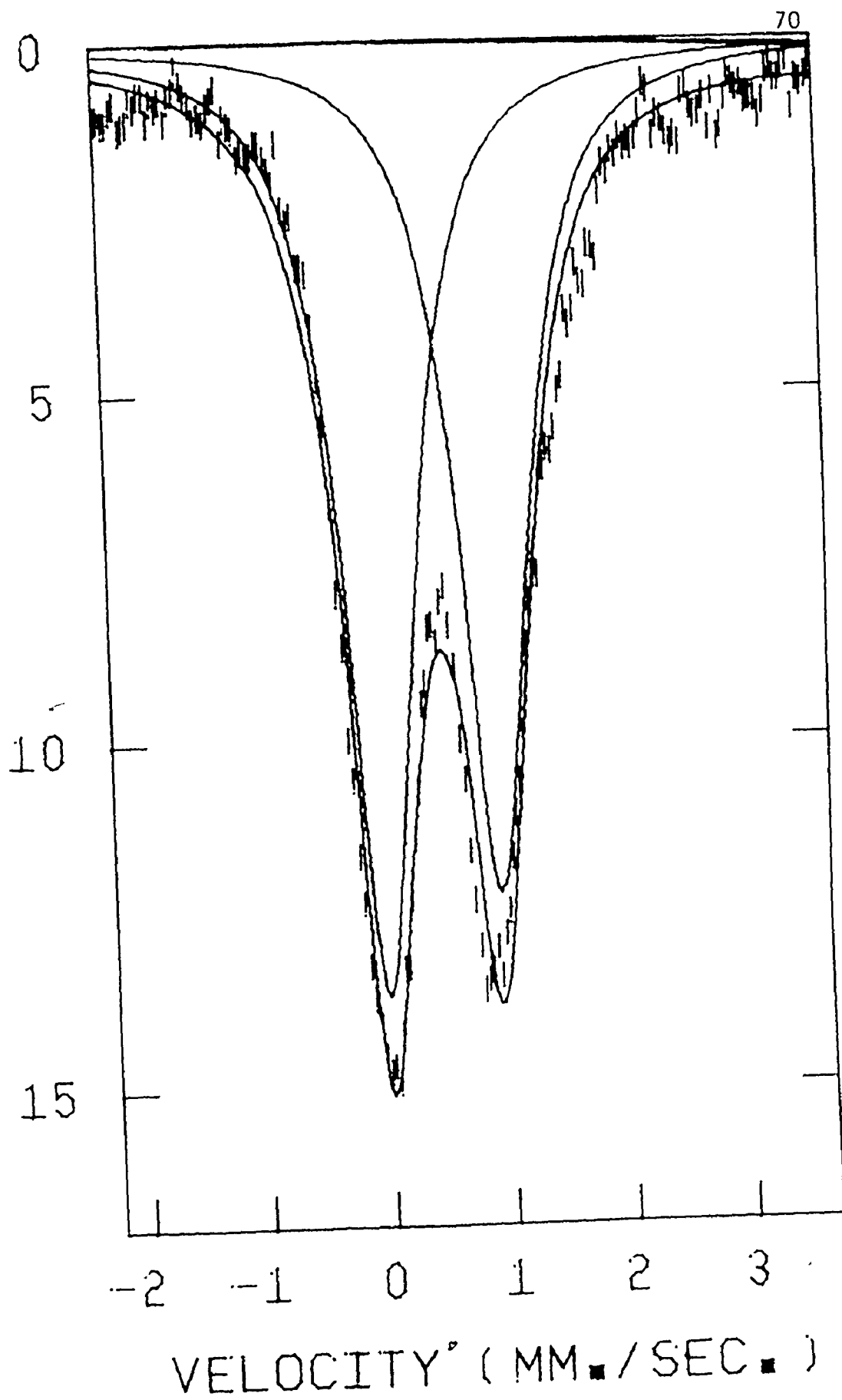
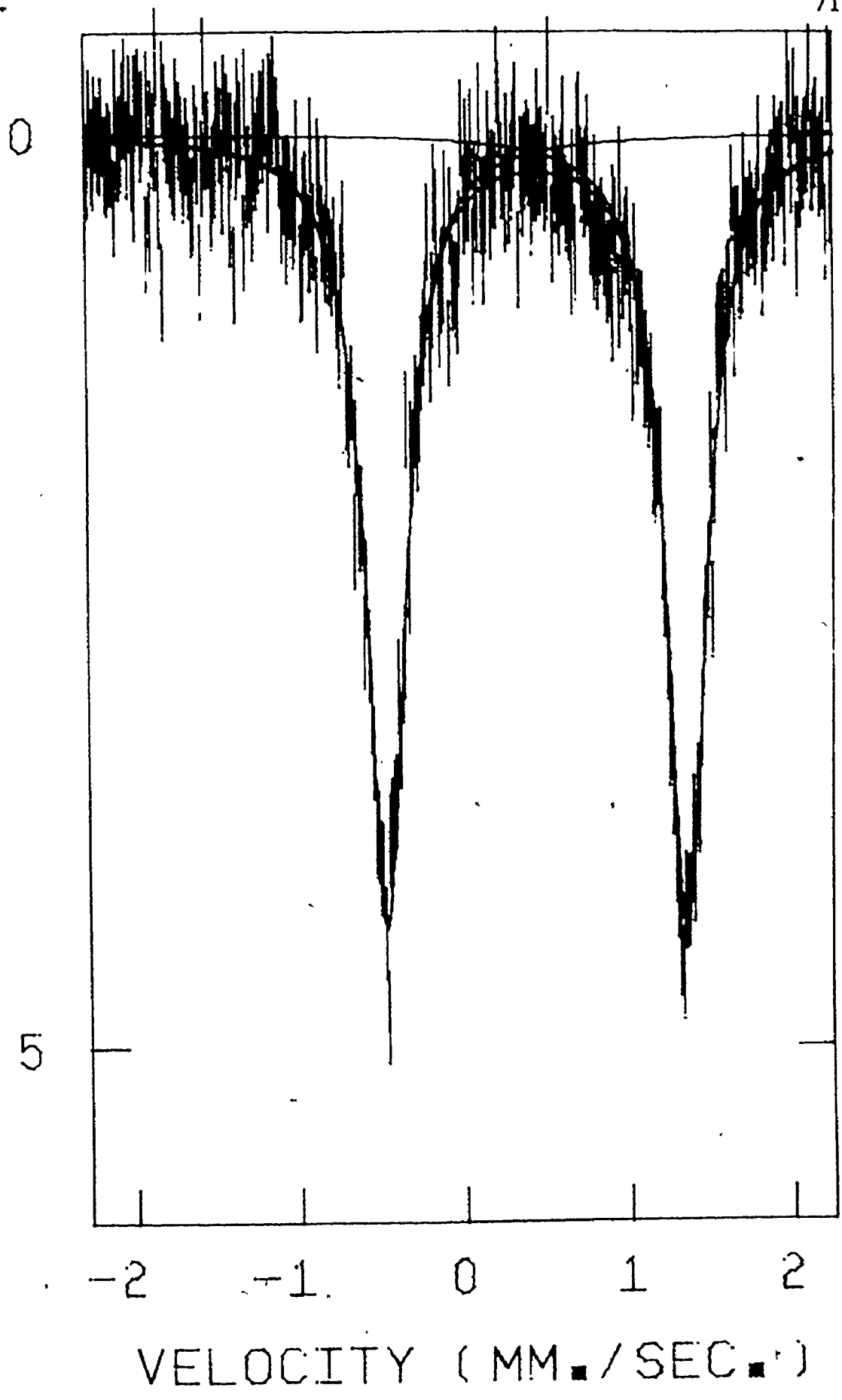


Figure 4.7. The Mössbauer Spectrum of $[\text{Fe}(\text{NO})_2\text{Br}]_2$ at 77°K.

PERCENT ABSORPTION



VELOCITY (MM./SEC.)

TABLE 4.9

Point-Charge Predictions for Cases of Tetrahedral Symmetry ^a

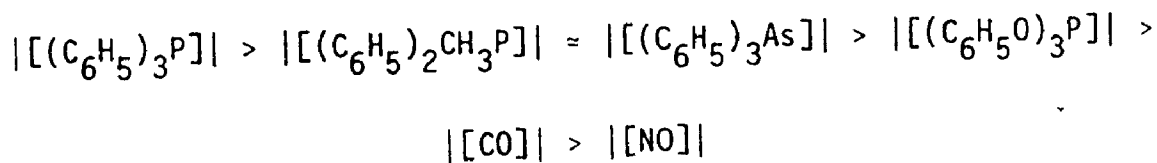
Case	Order of [L] ^b	V_{zz}	Γ
FeA_2B_2		$2(A-B)$	1
FeA_2B	$[B] < [A] < 0$	$2(B-A) > 0$	0
FeA_3B	$[A] < [B] < 0$	$2(B-A) < 0$	0
FeA_2BC	$[A] < [C] < [B] < 0$	> 0	< 1
FeA_2BC	$[C] < [B] < [A] < 0$	< 0	< 1

^a Taken from Ref. 35.

^b The contribution of ligand L to e.f.g.

$$[L] = e[(1 - R)q_1 r_1^{-3} + (1 - \gamma_\infty)q_L r_L^{-3}] \quad [23]$$

In this case, the contribution of ligand L to the electric field gradient tensor components, $|[L]|$, determines the magnitude of the quadrupole splitting. In Fe(-II) d^{10} compounds, therefore, the quadrupole splitting obtained will be mainly dependent upon the ligands involved. Thus, the q_{M-0} term dominates the q_{valence} contribution, given in equation (19). It is expected that a strong π -acceptor will reduce the effective iron d orbital population and also tend to delocalize the d orbital charge density (32). Both effects reduce q_{lattice} (equation (17)), and therefore the best π -acceptor ligand is expected to show the smallest $|[L]|$. Crow et al. (32) have ranked the ligands according to their $|[L]|$ values as:

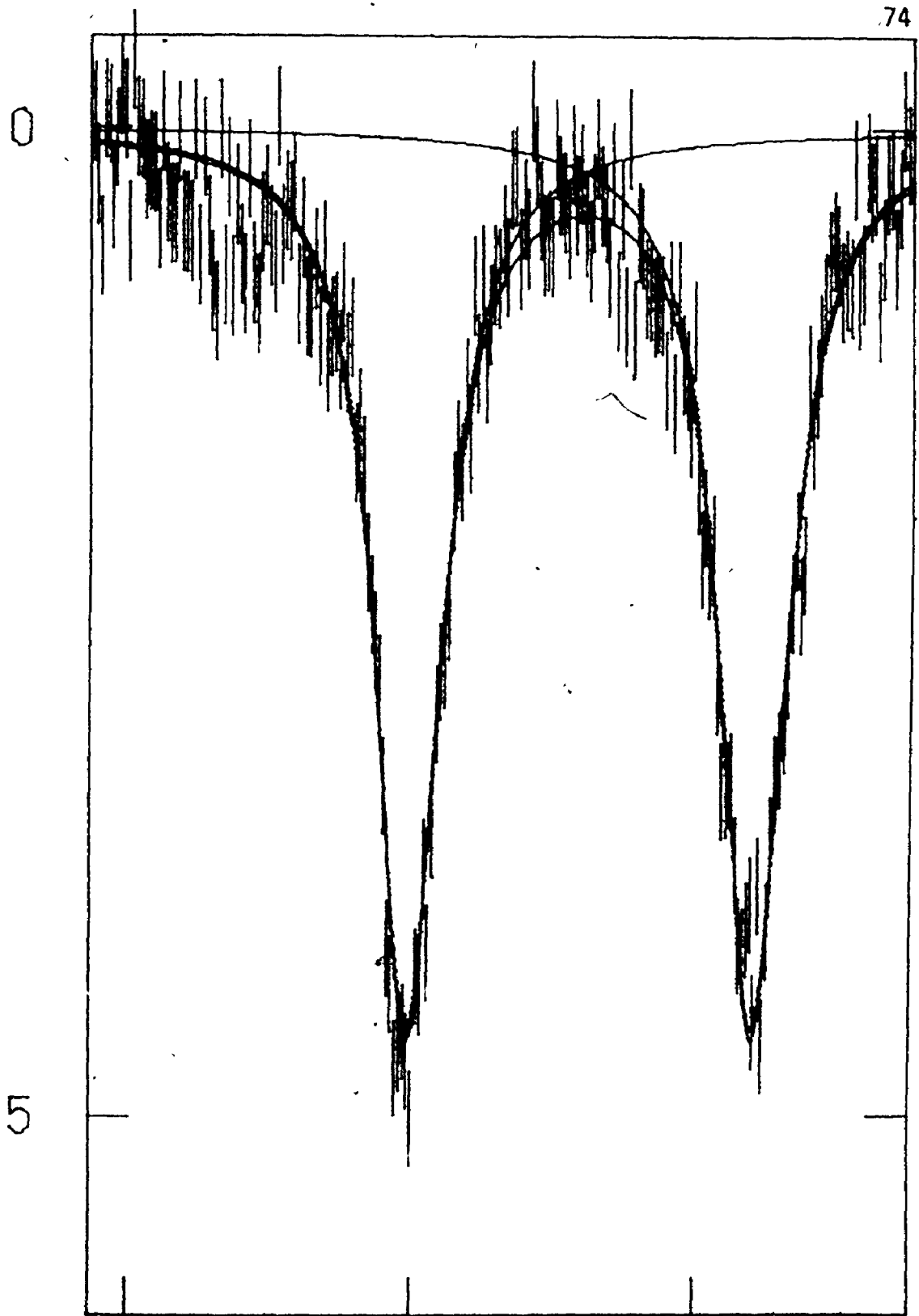


Mazak and Collins (35) have used the magnetic perturbation technique (124) and determined the signs of V_{zz} and magnitudes of n for $KFe(CO)_3(NO)$ [$V_{zz} > 0$, $n \approx 0$], $Fe(CO)_2(NO)_2$ [$V_{zz} < 0$, $n \approx 0.85$], and $Fe((C_6H_5)_3P)_2(NO)_2$ [$V_{zz} < 0$, $n \approx 0.76$]. On the basis of these results, Crow et al. (32) have assumed that V_{zz} will be negative for the $L_2Fe(NO)_2$ complexes.

In this study, the quadrupole splittings for d^9 Fe(-I) complexes arise not only from differences in strength and disposition of the ligands but also from the hole in the iron 3d shell (Fig. 4.8). According to equation (16), this will lead to a larger q_{valence} term,

Figure 4.8. The Mössbauer Spectrum of $\text{Fe}(\text{NO})_2(\text{tb})\text{Br}$ at 77°K .

PERCENT ABSORPTION



-1 0 1

VELOCITY (MM./SEC.)

but there seems no way to separate the two contributions to the quadrupole splitting or to predict the signs of V_{zz} . However, if the effect of the valence contribution is assumed to be negligible and the contribution to the quadrupole splitting is solely from the ligands, the sign of V_{zz} of $\text{Fe}(\text{NO})_2\text{LX}$ complexes can be predicted to be negative, from Table 4.9. In fact, the electron hole has to be taken into account and this valence contribution to the electric field gradient will be either the same or of opposite sign to that of the ligand contribution. A hole in the d_{xy} orbital has an opposite (negative) contribution to a hole in the d_{xz}, d_{yz} subset (positive) and since valence contributions usually dominate ligand contributions to the electric field gradient tensor, the actual sign of the e.f.g. would allow a determination of which d orbital lies lowest in these compounds. In Chapter VI, an attempt to obtain the sign of the electric field gradient by making use of the properties of liquid crystals will be discussed.

(v) Crystal Structure

The compound $\text{Fe}(\text{NO})_2(\text{C}_6\text{H}_5\text{NH}_2\text{CS})\text{Br}$ crystallizes in the monoclinic space group $\text{P}2_1/c$ with lattice parameters $\underline{a} = 6.930(2)$, $\underline{b} = 16.272(5)$, and $\underline{c} = 21.030(4)$ Å, $\beta = 90.14(2)^\circ$. The unit cell contains eight molecules; all are chemically identical although they form two groups which are crystallographically distinct molecules. The molecules are hydrogen bonded through N-H...Br units connecting the pair of crystallographically distinct molecules. These hydrogen bonded molecules form chains along \underline{a} . The phenyl groups lie in (010) planes at $y = 0$, and $\frac{1}{2}$. This aromatic layer apparently contains dissolved solvent. The Br ions lie in (001) planes separated by $z = \frac{1}{2}$. The crystallographic distinct molecules are nearly related by glide planes at $z = \pm \frac{1}{4}$ and are separated by $3.44 \pm .08$ Å of O...O and 3.36 ± 0.06 Å of O...S van der Waals contacts. The pseudo space group is Pbcu but the structure deviates substantially from the requirements of this space group.

The structure has been refined by least-squares methods to the present R of 0.137 using 1039 reflections taken from two crystals. The refinement is incomplete, possibly due to the presence of crystallographic disorder and/or solvent. However, a qualitative description of the structure is available and reported in this thesis, and a better refinement will probably be obtained.

Fig. 4.9 shows the molecular configuration of $\text{Fe}(\text{NO})_2(\text{C}_6\text{H}_5\text{NH}_2\text{CS})\text{Br}$. The packing of the molecules is illustrated in Fig. 4.10.

The short metal-nitrogen bond length 1.66 ± 0.06 Å which is indicative of strong multiple bonding between the NO groups and the metal

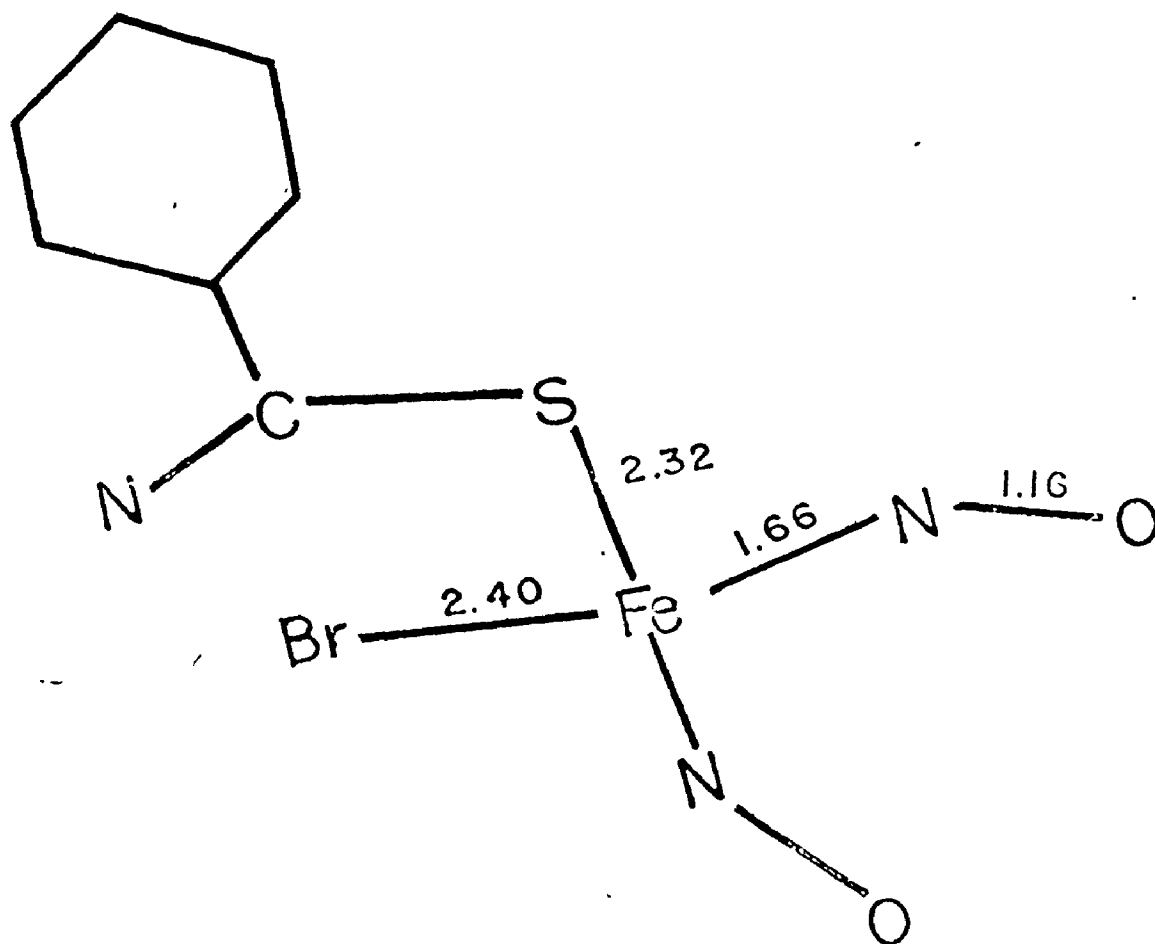


Figure 4.9. The Molecular Configuration of $\text{Fe}(\text{NO})_2(\text{C}_6\text{H}_5\text{NH}_2\text{CS})\text{Br}$.

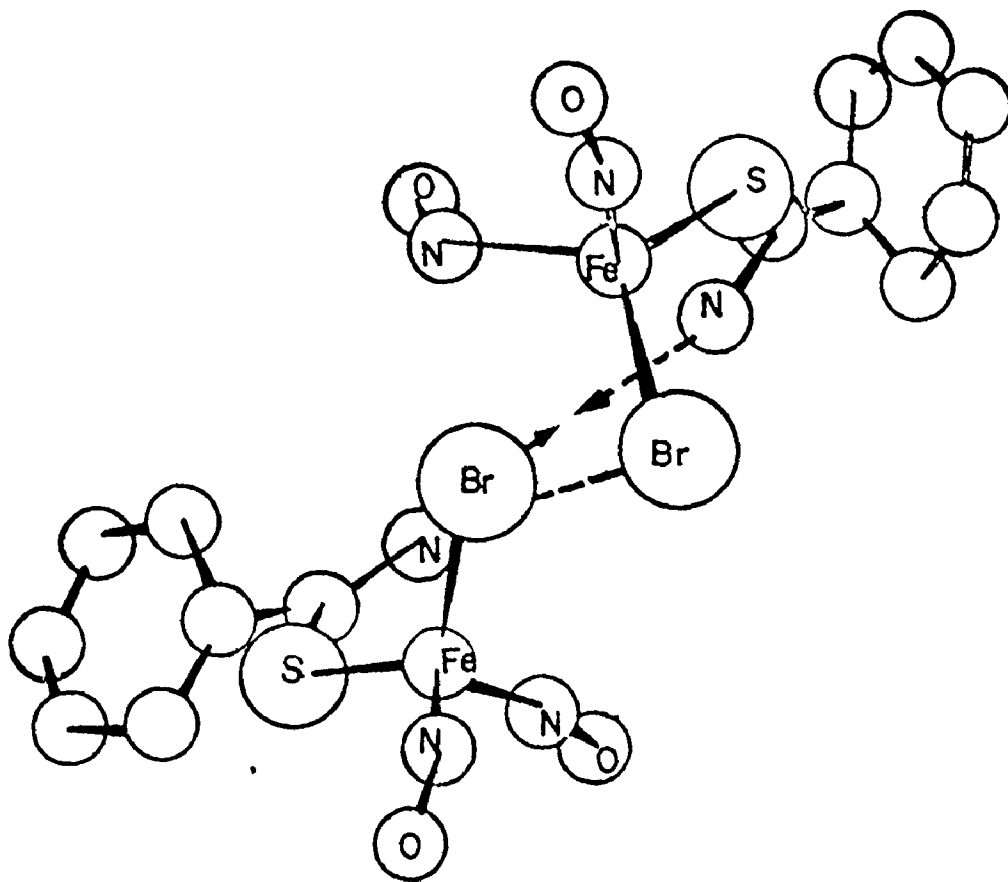


Figure 4.10. A Perspective Illustration of the Packing of the $\text{Fe}(\text{NO})_2(\text{C}_6\text{H}_5\text{NH}_2\text{CS})\text{Br}$ Molecules.

atom, is consistent with the mean Fe-NO bond distances in $\text{Na}_2\text{Fe}(\text{CN})_2(\text{NO})\cdot 2\text{H}_2\text{O}$ ($1.63 \pm 0.02 \text{ \AA}$) (125) and $[\text{Fe}(\text{NO})_2\text{I}]_2$ ($1.67 \pm 0.02 \text{ \AA}$) (28). The average N-O bond length of $1.16 \pm 0.08 \text{ \AA}$ in the present compound also compares favourably with those in $\text{Na}_2\text{Fe}(\text{CN})_5(\text{NO})\cdot 2\text{H}_2\text{O}$ ($1.13 \pm 0.02 \text{ \AA}$) (125), $[\text{Fe}(\text{NO})_2\text{SC}_2\text{H}_5]_2$ ($1.17 \pm 0.02 \text{ \AA}$) (27) and $[\text{Fe}(\text{NO})_2\text{I}]_2$ ($1.15 \pm 0.03 \text{ \AA}$) (28). The Fe-Br bond length of $2.40 \pm 0.01 \text{ \AA}$ indicates that the bromine atom is coordinated to the metal. The distance between the Fe atom and the N atom of thiobenzamide group is a nonbonding value of $3.34 \pm 0.05 \text{ \AA}$. This shows that the thiobenzamide ligand acts as a monodentate but not a bidentate. The angles around the Fe atom are close to those expected for tetrahedral geometry. Thus, the arrangement around the Fe atom is a distorted tetrahedron.

This crystal data confirms the evidence obtained by other spectroscopic methods as discussed in earlier sections, namely that $\text{Fe}(\text{NO})_2\text{LX}$ are covalent molecules with a distorted tetrahedral arrangement around the iron atom, Br being coordinated to Fe and thioamide acting as a monodentate ligand.

CHAPTER V

IRON-DITHIOOXALATE COMPLEXES

A. INTRODUCTION

Many complexes are known between transition metals and sulfur containing ligands such as dithiocarbamate, 1,2-dithiolato, thioxanthate, etc., and their chemistries have been reviewed (45,57,126). Recently, Coucouvanis and coworkers (69-71,127) have studied the chemistry of dithiooxalate complexes and reported on the unique properties of the dithiooxalate ligand. Reversible electron transfer reactions which are typical of the 1,2-dithiolate systems (45), are not observed in these dithiooxalate complexes. Many of the iron(III) dithiocarbamate complexes have magnetic moments intermediate between the high and low spin values and which are temperature dependent. The data are consistent with an equilibrium between these extremes and one technique that has proved invaluable in studying such systems is ^{57}Fe Mössbauer spectroscopy (44). Since the iron-dithiooxalate complexes apparently can be prepared in both high and low spin configurations, it was of interest to examine these complexes by means of the Mössbauer technique.

The results obtained from a study of the solid complexes are reported and discussed in the first part of this Chapter. In the second part of the Chapter, some solution studies are discussed.

B. RESULTS AND DISCUSSION

(i) Iron-Dithiooxalate Complexes

The potassium salt of dithiooxalic acid reacts with various

metallic salts in aqueous solutions to produce solutions of characteristic colour (61). The anilinium salt of tris(dithiooxalato)iron(III) was first reported by Robinson and Jones (128), but was incorrectly formulated as an iron(II) complex. Dwyer and Sargeson (63) isolated a compound containing the $[\text{Fe}(\text{C}_2\text{O}_2\text{S}_2)_3]^{3-}$ ion and found the magnetic moment to be close to that for a low spin iron(III) complex. Recently, Coucouvanis and co-workers (70) have studied the chemistry of these tris(dithiooxalato)iron(III) complexes and found that both high spin and low spin complexes can be isolated. In order to obtain more structural information, these complexes were prepared and studied in this work. The complexes prepared here were identified by a comparison of their physical and spectroscopic properties with the reported values (70).

All of the dithiooxalato complexes decomposed slowly in the dark and quite rapidly in light. The Fe(III) complex isolated as the dark purplish brown potassium barium salt decomposed especially easily in the light.

Infrared and the magnetic moment data are given in Table 5.1. In the dithiooxalate dianion, the presence of four donor atoms and the possibilities of charge delocalization over the molecule results in a versatile ligand with unique coordination properties. The resonance forms of the $\text{S}_2\text{C}_2\text{O}_2^{2-}$ ligand can be written, as:

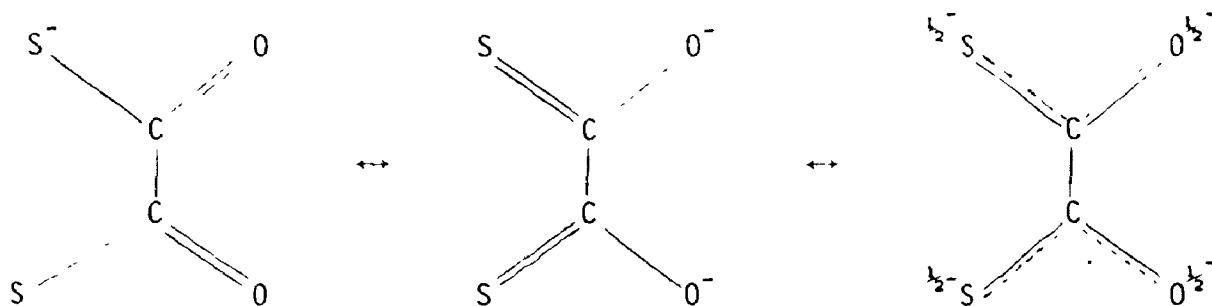


TABLE 5.1

Spectroscopic Data on the Iron-Dithiooxalate Complexes

Complex	$\nu_{C=O}$, cm^{-1} ^a	μ_{eff} , BM ^b
$\text{KBeFe(dto)}_3 \cdot 6\text{H}_2\text{O}$	1553, 1518	2.36
$\text{KSrFe(dto)}_3 \cdot \text{H}_2\text{O}$	1562, 1520	2.21
$(\text{Coen}_3)\text{Fe(dto)}_3 \cdot 3\text{H}_2\text{O}$	1575, 1518	2.34
$(\text{C}_6\text{H}_5\text{NH}_3)_3\text{Fe(dto)}_3 \cdot \text{H}_2\text{O}$	1580, 1510	2.61
$((\text{C}_6\text{H}_5)_4\text{As})_3\text{Fe(dto)}_3 \cdot 3\text{CH}_3\text{NO}_2$	1630, 1560	2.93
$[(\text{C}_2\text{H}_5)_4\text{N}]_2\text{Fe(dto)}_2(\text{NO})$ ^c	1558	2.24
$[(\text{C}_4\text{H}_9)_4\text{N}]_2\text{Fe(dto)}_2(\text{NO})$ ^c	1590	2.30
$[((\text{C}_6\text{H}_5)_3\text{P})_2\text{Ag}]_3\text{Fe(dto)}_3$	1380	5.81
$[((\text{C}_6\text{H}_5)_3\text{P})_2\text{Cu}]_3\text{Fe(dto)}_3$	1385	5.93

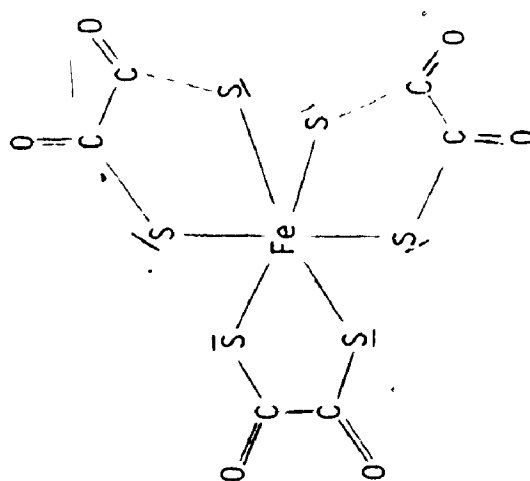
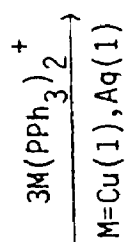
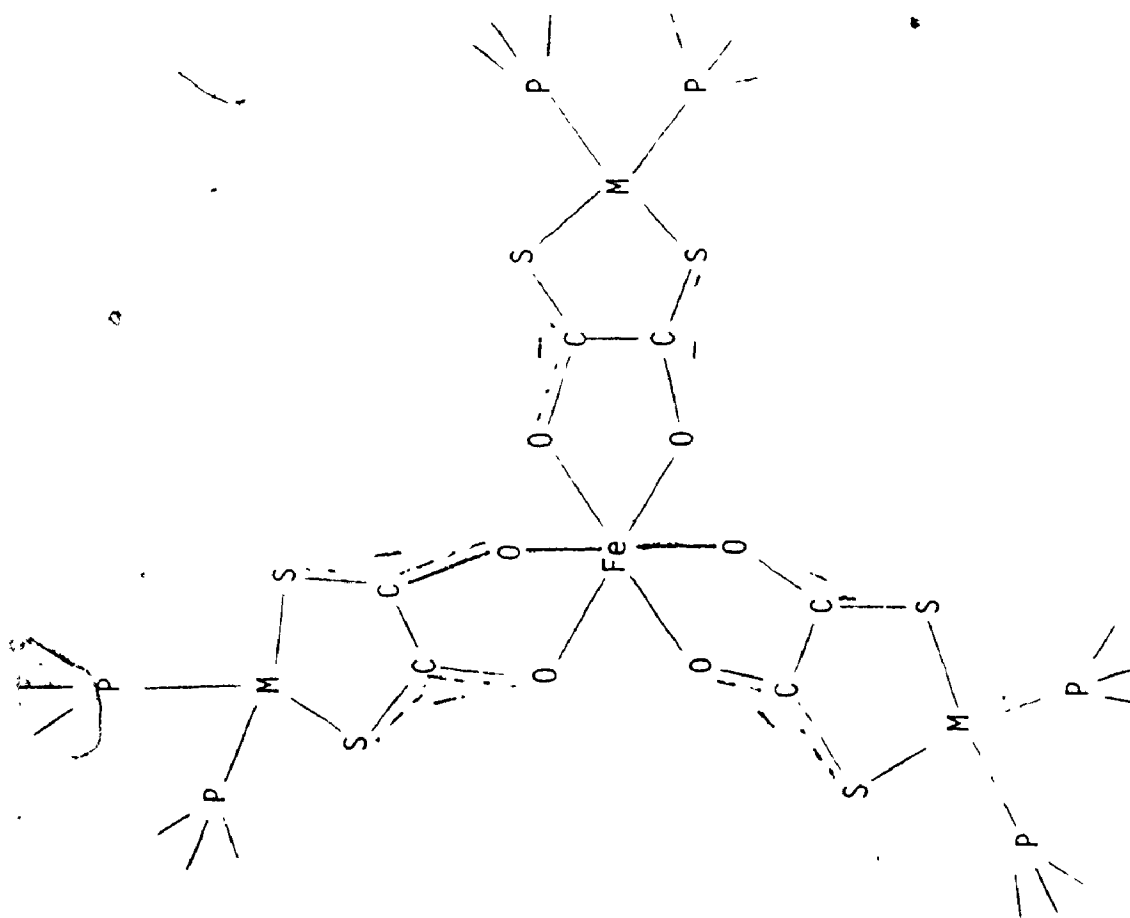
^a mull spectra

^b room temperature

^c $\nu_{\text{NO}} = 1688 \text{ cm}^{-1}$

X-ray structures of the planar $\text{Ni}(\text{S}_2\text{C}_2\text{O}_2)_2^{2-}$ (62) and octahedral $\text{Co}(\text{S}_2\text{C}_2\text{O}_2)_3^{3-}$ complexes (129) show that the ligands are coordinated through their sulfur atoms. Their C-O stretching vibrations are 1570 cm^{-1} for the Co(III) complex and 1600 cm^{-1} for the Ni(II) complex. Similar C-O absorptions for the low spin Fe(III) complexes (Table 5.1) suggest that these are also sulfur chelated complexes. The low frequency of the C-O vibrations in the high spin $\text{Fe}(\text{S}_2\text{C}_2\text{O}_2)_3^{3-}$ complexes (1380 cm^{-1}) is similar to that found in the oxalate complex (130). Such a decrease in the C-O stretching frequency is expected to occur if the ligand is O,O-bonded to the metal. Stannic chloride was found to interact with the sulfur bonded $\text{Fe}(\text{S}_2\text{C}_2\text{O}_2)_3^{3-}$ complex anion, and the isolated $[\text{Fe}(\text{S}_2\text{C}_2\text{O}_2)_3(\text{SnCl}_4)_2]^{3-}$ salt has C-O absorptions at 1380 cm^{-1} (70). The crystal structures of $[\text{M}(\text{S}_2\text{C}_2\text{O}_2)_2(\text{SnCl}_4)_2]^{2-}$ where M is Ni(II) or Pd(II) (131) show that both sulfur and oxygen atoms are involved in the bonding; sulfur is bonded to Ni(II) (or Pd(II)) and oxygen is bonded to SnCl_4 . Recently, the crystal structure determination of tris(bis(triphenylphosphine)silver(I))tris(dithiooxalato)iron(III) was reported (132). The central metal atom was found to be octahedrally coordinated by the O,O "bites" of three dithiooxalate ligands, and the $\text{Ag}(\text{PPh}_3)_2^+$ cations interact at the S,S "bite" of each ligand. This then explains the low $\nu_{\text{C-O}}$ vibration observed for this complex. Coucouvanis et al. (132) have suggested that the ligand "flips" from S,S chelation to O,O chelation as a result of the $(\text{PPh}_3)_2\text{M}^+$ interaction.

When the violet solutions of the $[\text{Fe}(\text{S}_2\text{C}_2\text{O}_2)_3]^{3-}$ anion in either aqueous NaNO_2 or nitroparaffins were heated, the green $[\text{Fe}(\text{S}_2\text{C}_2\text{O}_2)_2\text{NO}]^{2-}$ complex was formed. For a five coordinate system there are two possible stereochemical formulations for a dsp^3 hybridized central



metal ion; namely a trigonal bipyramid and a square pyramid. A square pyramidal structure has been found for $\text{Fe}(\text{Me}_2\text{dtc})_2(\text{NO})$ (133) and $\text{Fe}(\text{Et}_2\text{dtc})_2(\text{NO})$ (134), in which the NO group occupies the apex of a pyramid with a square base defined by the iron and the four coordinated sulfur atoms. It has been suggested that the $[\text{Fe}(\text{S}_2\text{C}_2\text{O}_2)_2\text{NO}]^{2-}$ ion has a structure similar to these (133,134) rather than being trigonal pyramidal.

The magnetic moments of the low spin iron(III) complexes fit those expected for a spin-paired complex (Table 5.1). Figgis (135) has studied the various factors which influence the magnetic susceptibility of a transition metal ion with a ${}^2\text{T}_2$ ground state. He discussed the way in which the magnetic moment arising from the ${}^2\text{T}_2$ term in a cubic ligand field is expected to vary with temperature in the presence of an axial ligand field component, spin-orbit coupling, and with delocalization of the t_{2g} electrons. Carlin and Caziani (64) have studied the temperature dependence of the magnetic moment of $\text{KBaFe}(\text{S}_2\text{C}_2\text{O}_2)_3 \cdot 6\text{H}_2\text{O}$. Their results have been analyzed by the empirical methods of Figgis (135) and evaluated as:

$$k = 0.8 \quad \Delta = 270 \text{ cm}^{-1} \quad \lambda = -270 \text{ cm}^{-1}$$

where k is the parameter, introduced originally by Stevens (136), which measures orbital delocalization, λ is the spin-orbit coupling constant, and Δ measures the axial field. By comparison of these results with those for $\text{Fe}(\text{CN})_6^{3-}$ ($k = 0.8$, $\Delta = 0$, and $\lambda = -400 \text{ cm}^{-1}$), $\text{Fe}(\text{o-phen})_3^{3+}$ and $\text{Fe}(\text{bipy})_3^{3+}$ ($k = 1.0$, $\Delta = 600 \text{ cm}^{-1}$) (7), it was concluded that dithiooxalate is as efficient as cyanide in causing t_{2g} electron delocalization (usually called π bonding) (64). The Weiss constants

are abnormally large for the low-spin tris(dithiooxalato)iron(III) complexes. The θ value of -33°K for $(\text{C}_6\text{H}_5\text{NH}_3)\text{Fe}(\text{S}_2\text{C}_2\text{O}_2)_3 \cdot \text{H}_2\text{O}$ (Fig. 5.1) is similar to that obtained for $\text{KBaFe}(\text{S}_2\text{C}_2\text{O}_2)_3 \cdot 6\text{H}_2\text{O}$ ($\theta = -42^\circ\text{K}$) (64). In general, a negative Curie-Weiss associates with antiferromagnetism. However, no break for a Curie point in the plot of susceptibility χ versus temperature (Fig. 5.2) was observed, suggesting that these complexes do not exhibit antiferromagnetism. The tris(ethylthioxanthate)iron(III) complex has been reported (137) to have a magnetic moment of 2.57 BM at 300°K and a Weiss constant of -85°K . At room temperature, this complex exists mainly in $^2\text{T}_2$ (low spin) state although $^6\text{A}_1$ (high spin) state is also populated to a small degree (137). If a spin-equilibrium exists in the dithiooxalate system, as in the thioxanthate, then Mössbauer spectroscopy may be able to prove its existence.

The Mössbauer data for the iron-dithiooxalate complexes are given in Table 5.3. The centre shifts fall in the region expected for iron(III) compounds. Typical values for high spin Fe(III) complexes are about $0.5 \text{ mm} \cdot \text{sec}^{-1}$ and for low spin complexes are about $0.0 \text{ mm} \cdot \text{sec}^{-1}$ (138). A high value of the centre shift implies a low s electron density at the nucleus which results from electron donation from the ligand σ -orbitals into the metal d orbitals. The resultant increase in screening of the metal s electrons from the nucleus causes the increase in centre shift. This is to be expected as the sulfur atoms of the ligands are highly polarizable. If dithiooxalate is as efficient as cyanide in causing electron delocalization, as stated in reference (64), then the centre shift values for these two series of complexes should be in the same region. However, the centre shifts for ferricyanides (44) are

TABLE 5.2

Magnetic Data for Iron-Dithiooxalates

87

Temperature	$\chi_M^{\text{corr}} 10^{-6}$	$1/(\chi_M^{\text{corr}})$	μ_{eff}
$^{\circ}\text{K}$	cgs	cgs	B.M.
(a) $(\text{C}_6\text{H}_5\text{NH}_2)_3\text{Fe}(\text{dto})_3 \cdot \text{H}_2\text{O}$			
77	9001	111	2.36
105	6608	151	2.36
120	6230	160	2.36
154	4970	201	2.45
182	4214	237	2.48
202	3836	260	2.48
239	3396	294	2.50
261	3018	331	2.52
293	2892	345	2.61
(b) $(\text{Coen})_3\text{Fe}(\text{dto})_3 \cdot 3\text{H}_2\text{O}$			
85	7079	141	2.20
100	6173	162	2.23
125	5128	195	2.27
164	4000	250	2.30
205	3268	306	2.32
240	2816	355	2.33
297	2297	435	2.34
(c) $(\text{Ph}_4\text{As})_3\text{Fe}(\text{dto})_3 \cdot 3\text{CH}_3\text{NO}_2$			
90	10526	95	2.76
120	8333	120	2.84
166	6098	164	2.86
220	4545	220	2.84
245	4348	230	2.93
298	3585	279	2.93
(d) $[(\text{C}_2\text{H}_5)_2\text{N}]_2\text{Fe}(\text{dto})_2(\text{NO})$			
84	6850	146	2.15
105	5714	175	2.19
132	4545	220	2.20
170	3636	275	2.23
206	2994	334	2.23
242	2597	385	2.24
297	2103	475	2.24

Figure 5.1. A Plot of $\frac{1}{\chi_M}$ Against T for $(C_6H_5NH_3)_2Fe(S_2C_2O_2)_3 \cdot H_2O$.

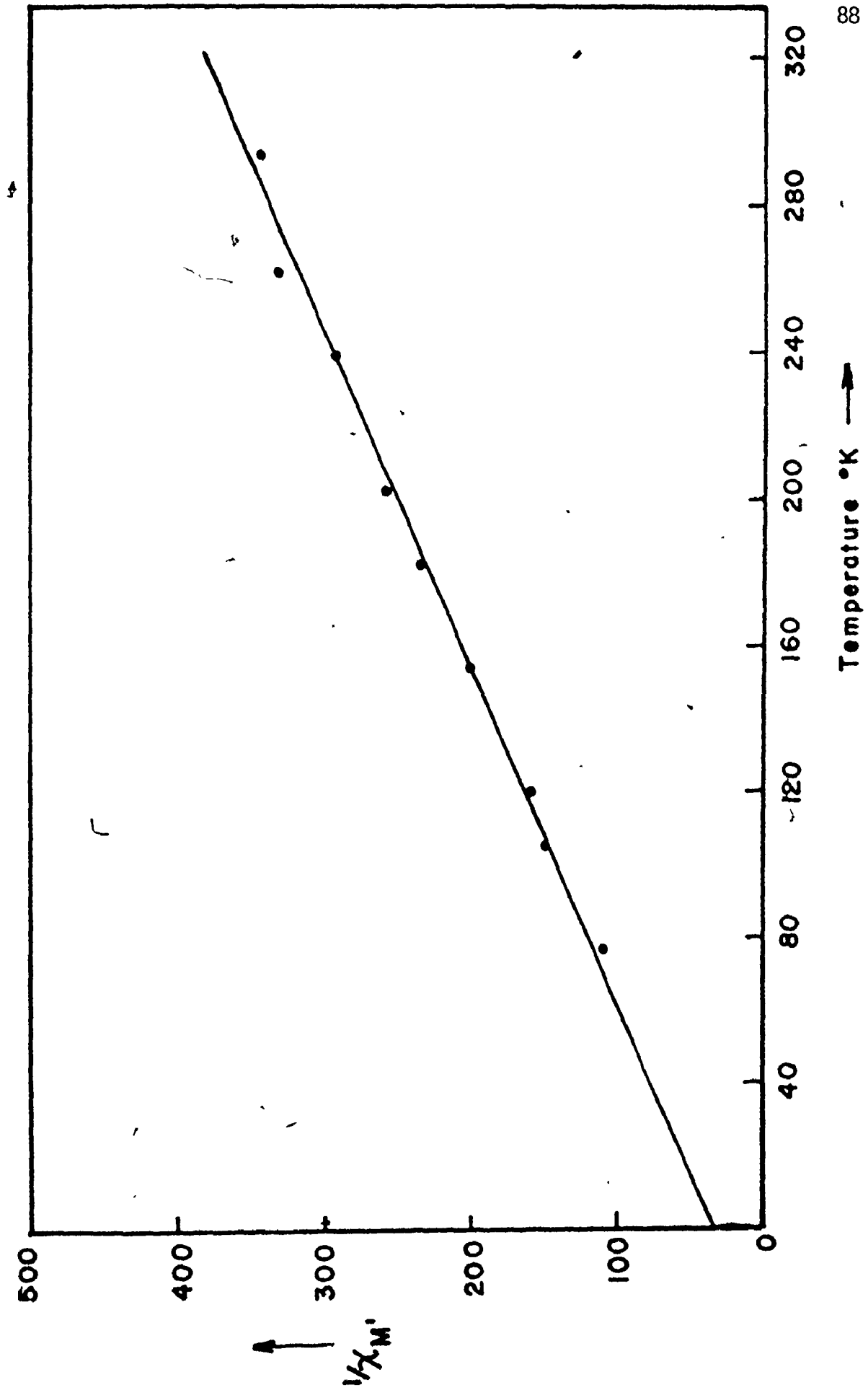
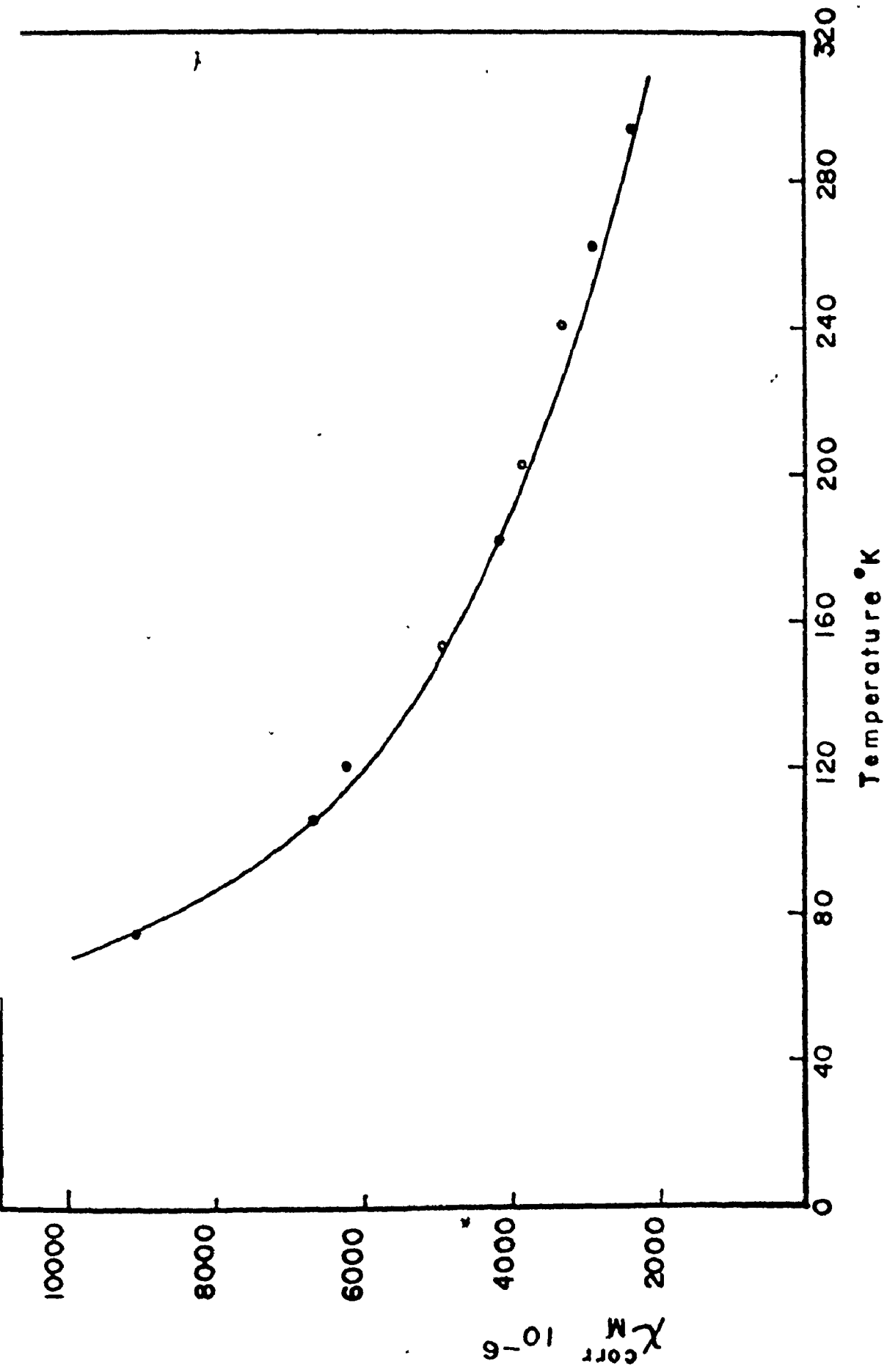


Figure 5.2. A Plot of x_M^{corr} Against T for $(\text{C}_6\text{H}_5\text{NH}_3)_3\text{Fe}(\text{S}_2\text{C}_2\text{O}_2)_3 \cdot \text{H}_2\text{O}$.



Mössbauer Parameters for Iron-Dithiooxalate Complexes

Complex	Temp. °K	Centre Shift mm/sec	Quadrupole Splitting mm/sec
$\text{Fe}(\text{dto})_3 \cdot 6\text{H}_2\text{O}$	77	0.37	0.42
	196	0.33	0.35
	298	0.27	0.31
$\text{Fe}(\text{dto})_3 \cdot \text{H}_2\text{O}$	4	0.37	1.06
	77	0.36	1.09
	298	0.26	0.68
$(\text{NH}_3)_3\text{Fe}(\text{dto})_3 \cdot 3\text{H}_2\text{O}$	77	0.40	1.68
	298	0.32	1.36
	330	0.28	1.05
$(\text{NH}_3)_3\text{Fe}(\text{dto})_3 \cdot \text{H}_2\text{O}$	4	0.40	1.27
	77	0.38	1.12
	298	0.29	0.64
$(\text{NH}_3)_3\text{Fe}(\text{dto})_3 \cdot \text{H}_2\text{O}^*$	77	0.38	1.14
	298	0.29	0.64
$(\text{C}_5\text{H}_5)_4\text{As}]_3\text{Fe}(\text{dto})_3 \cdot 3\text{CH}_3\text{NO}_2$	77	0.53	0.90
	298	0.43	0.95
$(\text{C}_5\text{H}_5)_3\text{P})_2\text{Ag}]_3\text{Fe}(\text{dto})_3$	77	0.42	0.99
	298	0.24	0.87
$(\text{C}_5\text{H}_5)_3\text{P})_2\text{Cu}]_3\text{Fe}(\text{dto})_3$	77	0.33	1.18
	298	0.24	1.17
$(\text{C}_5\text{H}_5)_4\text{N}]_2\text{Fe}(\text{dto})_2(\text{NO})$	77	0.29	1.04
$(\text{C}_9\text{H}_9)_4\text{N}]_2\text{Fe}(\text{dto})_2(\text{NO})$	4	0.29	1.05
	77	0.28	1.00
	196	0.26	1.04
	298	0.36	0.67
$(\text{C}_9\text{H}_9)_4\text{N}]_2\text{Fe}(\text{dto})_2(\text{NO})^*$	77	0.28	1.03
	298	0.35	0.68

prepared from ferrous salt.

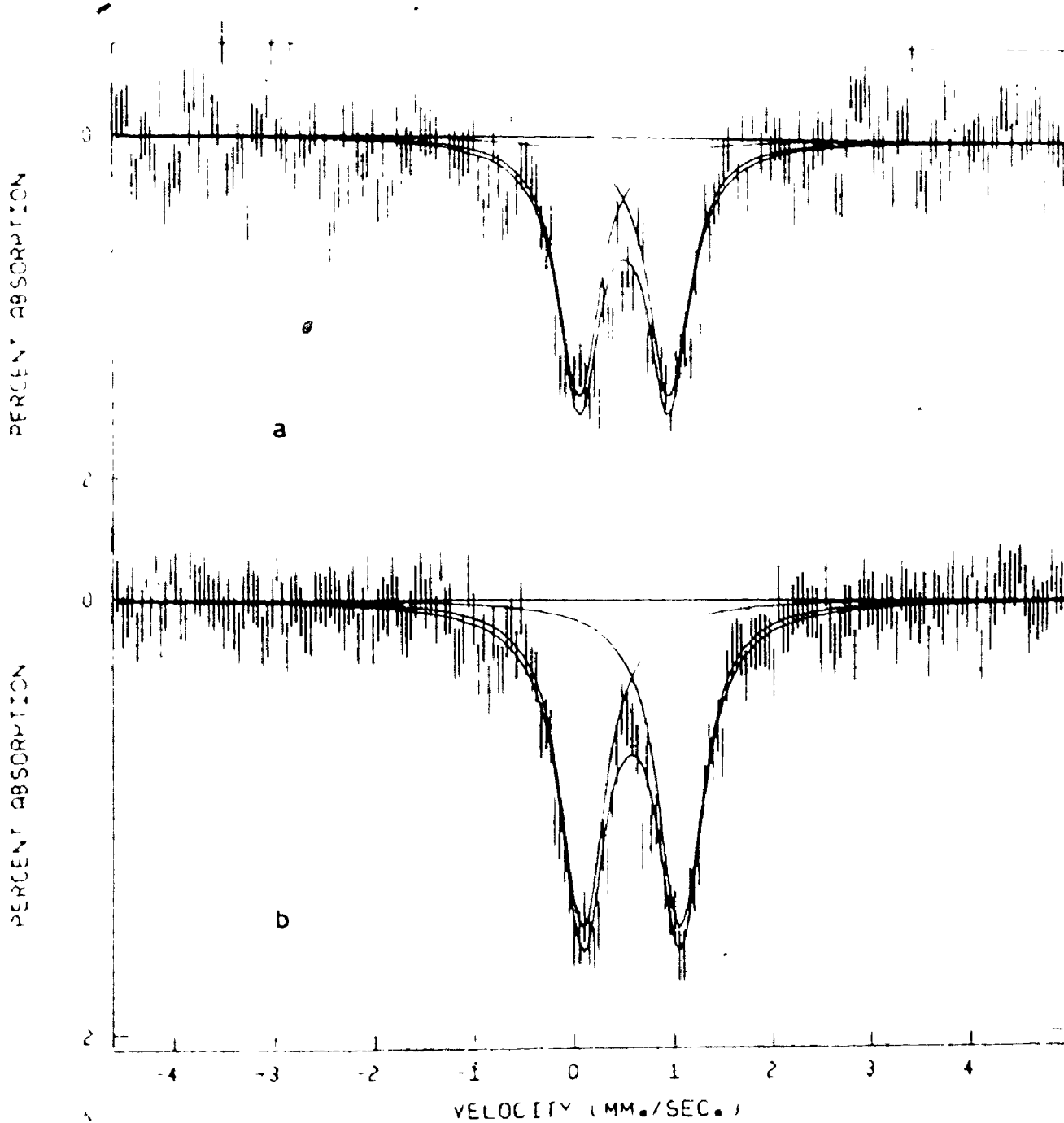
dithiooxalate

ethylenediamine

much lower than those for the dithiooxalates. An increase in the π back-donation to the ligand antibonding orbitals causes a decrease in the effective 3d population, which in turn causes a decrease in the centre shift. Thus, dithiooxalate is a weaker π -acceptor ligand than cyanide. The centre shifts of these dithiooxalates do fall in the same range as the dithiolene (36,139) and dithiocarbamate complexes (140). This indicates that the extent of electron delocalizations is about the same for all these systems, though this is contrary to the conclusions of Coucouvanis *et al.* (70). The electronic spectra and the magnetic properties of the tris(dithiooxalato) complexes of Cr(III) and Co(III) (64) reveal that dithiooxalate is not a strong ligand, in the spectrochemical sense, but it does lead to an exceptional decrease in electron-electron repulsion on the central metal ion, which in turn causes sulfur to appear as a strong field donor atom.

All of the complexes, except $[(C_4H_9)_4N]_2Fe(S_2C_2O_2)_2(NO)$, show a decrease in shift of $0.1 \pm 0.002 \text{ mm sec}^{-1}$ on raising the temperature from 77°K to 298°K, which is close to that expected from the second-order Doppler effect (87,88). The centre shift values for the tetraphenyl arsonium salt of tris(dithiooxalato)iron(III) are significantly higher than that of the other low spin complexes. Moreover, the magnetic moment of this compound at room temperature is higher than that expected for a low spin compound. This high magnetic moment could arise from the presence of a small amount of high spin Fe^{3+} impurity but this would not account for the high centre shift. The higher centre shift may indicate that the CH_3NO_2 molecules which are incorporated on crystallisation are actually coordinated to the central metal, Fig. 5.3. The

Figure 5.3. The Mossbauer Spectra of $[(C_6H_5)_4As]_3Fe(S_2C_2O_2)_3 \cdot 3CH_3NO_2$
at (a) 298°K (b) 77°K.



centre shifts of nitrosyl complexes at 77°K are smaller than those of the other complexes. This decrease is not unexpected because back-donation from the metal d orbitals into the empty antibonding orbital on the NO group will reduce the shielding of the s electrons which, in turn, increases the s electron density at the iron nucleus and decreases the centre shift.

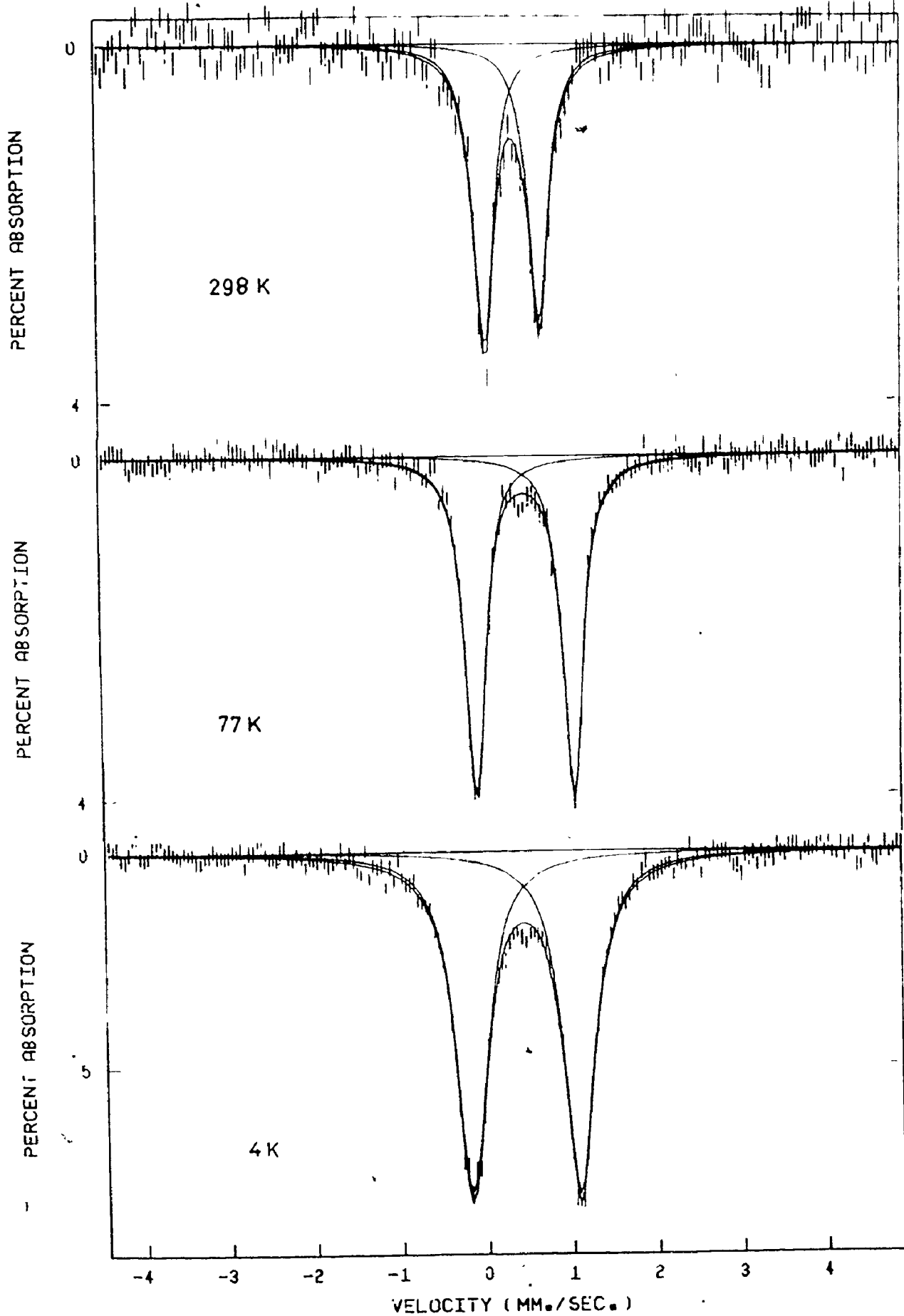
High spin Fe^{3+} has a ${}^6A_1(t_{2g}^3 e_g^2)$ electronic ground state and is spherically symmetric. Any electric field gradient will arise solely from charges external to the central atom by direct contribution or by indirect polarisation. It is unlikely that there will be any low-lying excited levels in this configuration, so that thermal alterations of the electron configuration are small and the quadrupole splitting will be essentially independent of temperature. The ${}^2T_2(t_{2g}^5)$ configuration of low spin Fe(III) signifies a single electron hole in a cubic triplet level. In a ligand field of cubic symmetry, the 3d-orbitals in such compounds retain sufficient degeneracy for there to be no electric field gradient. However, in complexes of lower symmetry such as trigonal or tetragonal further degeneracy is removed, thereby producing a non-zero electric field gradient. Thermal population of the low-lying excited states then causes a variation in the electron configuration with temperature, and since as seen in Table 2.1 different 3d-orbitals have differing contributions to the electric field gradients, there is a strong temperature dependence of the quadrupole splitting. The variation of quadrupole splitting with temperatures within a compound could either be due to this thermal equilibration between the low-lying states of d-orbitals or to the existence of a spin-crossover

equilibrium ${}^6A_1 \rightarrow {}^2T_2$.

Low-spin iron(III) complexes with an octahedral arrangement of six equivalent ligands usually exhibit only small quadrupole splittings, e.g., $K_3[Fe(CN)_6] \Delta = 0.30 \text{ mm sec}^{-1}$ (141), and the magnitude of this splitting had been interpreted as indicating that the three d-levels are close in energy and almost equally populated. The $[Fe(S_2C_2O_2)_3]^{3-}$ complexes, however, exhibit relatively large quadrupole splittings ($1.68 - 0.30 \text{ mm sec}^{-1}$) indicating a considerable distortion from cubic symmetry and a non-degenerate set of orbitals. This is consistent with the trigonal prismatic structure suggested by Gerlock et al. (142) and others (48,49) for the related trisdithiolate complexes of a number of transition metals. Molecular orbital descriptions of the bonding have been suggested for this type of complex (48,49) but because of the complexity of the calculations the ordering of the metal orbitals is not absolutely certain. The quadrupole splittings of the $[Fe(S_2C_2O_2)_3]^{3-}$ complexes vary from compound to compound (Table 5.3). It seems possible that this variation is at least partly due to the arrangement of cations and solvent molecules around the central anion as well as to the distortion of the anion from O_h symmetry. A similar variation has been noted for ferricyanides (143,144).

The temperature dependence of quadrupole splittings of some of the dithiooxalate complexes are very large (Fig. 5.4). This variation in quadrupole splitting could be either due to a ${}^6A_1 - {}^2T_2$ equilibrium or due to the thermal distribution in the t_{2g} levels. The former may be unlikely since there is no significant change in the magnetic moments with temperature and also a sharp quadrupole doublet was observed even at 4°K. Usually ${}^6A_1 - {}^2T_2$ systems show some line broadening at 4°K due to

Figure 5.4. The Mössbauer Spectra of $(C_6H_5NH_3)_3Fe(S_2C_2O_2)_3 \cdot H_2O$
at 298°K, 77°K and 4°K.



an increase in spin-lattice relaxation times (44) in $\pm \frac{3}{2}$ transition. But this was not observed. Spectra at liquid helium temperatures (4°K) were only recorded for few complexes because the magnetic data showed no significant changes at low temperatures. Data at temperatures higher than 300°K, where the 6A_1 state might be expected to be more populated, could not be obtained because of the low recoil free fractions at higher temperature and because the complexes tended to decompose on heating. In view of the relatively small changes in magnetic moment with temperature and of the nature of the changes in the Mössbauer parameters it is concluded that these compounds are not examples of 6A_1 - 2T_2 crossover systems.

The most likely explanation for the temperature variation of the quadrupole splitting parameter is the thermal equilibrium of electrons within the t_{2g} level. Golding (100) has calculated, for low spin Fe(III) systems, how the quadrupole splitting would vary with temperature for different values of δ/ζ , where δ is a distortion parameter and ζ is the spin-orbit coupling constant. Following Golding's calculation and using $\zeta = 400 \text{ cm}^{-1}$, the free ion value and $\zeta' = 270 \text{ cm}^{-1}$, estimated value from $\text{KBaFe}(\text{S}_2\text{C}_2\text{O}_2)_3 \cdot 6\text{H}_2\text{O}$ magnetic data (64), the distortion parameter δ is found to be in the range of $\sim 66 \text{ cm}^{-1}$ to 200 cm^{-1} and the splitting of the 2T_2 ground state is $\sim 200 \text{ cm}^{-1}$ to 600 cm^{-1} for these dithiooxalate complexes (Table 5.4) (Fig. 5.5).

A high spin iron(III) in a cubic environment should show zero quadrupole splitting. However, the observed quadrupole splitting for $[\text{((C}_6\text{H}_5)_3\text{P})_2\text{M}]_3\text{Fe}(\text{S}_2\text{C}_2\text{O}_2)_3$ where M = Ag or Cu, is $1 \pm 0.2 \text{ mm/sec}$. A typical spectrum is shown in Fig. 5.6. The large value of quadrupole splitting presumably arises from the distortion from cubic symmetry.

A Comparison for Calculated and Experimental Data for Some Iron-Dithiooxalate Complexes

Compound	$\frac{\delta}{\zeta}$	δ^a cm ⁻¹	$3\delta^b$ cm ⁻¹	ΔE_Q (calc)		ΔE_Q (expt)	
				4°K	77°K mm/sec	4°K	77°K mm/sec
KBaFe(dto) ₃ ·6H ₂ O	$\frac{1}{6}$	66	198	0.42	0.42	---	0.42
KSrFe(dto) ₃ ·H ₂ O	$\frac{1}{2}$	200	600	1.15	1.15	1.06	1.09
(C ₆ H ₅ NH ₂) ₃ Fe(dto) ₃ ·H ₂ O	$\frac{1}{2}$	200	600	1.15	1.15	---	1.12

a the distortion parameter

b the splitting of t_{2g} levels

Figure 5.5. A Plot of Quadrupole Splitting vs. Temperature. Solid Lines are the Theoretical Curves. The Experimental Points for $\text{KBaFe(dto)}_3 \cdot 6\text{H}_2\text{O}$ (x), $\text{KSrFe(dto)}_3 \cdot \text{H}_2\text{O}$ (o) and $(\text{C}_6\text{H}_5\text{NH}_3)_3\text{Fe(dto)}_3 \cdot \text{H}_2\text{O}$ (Δ) are shown.

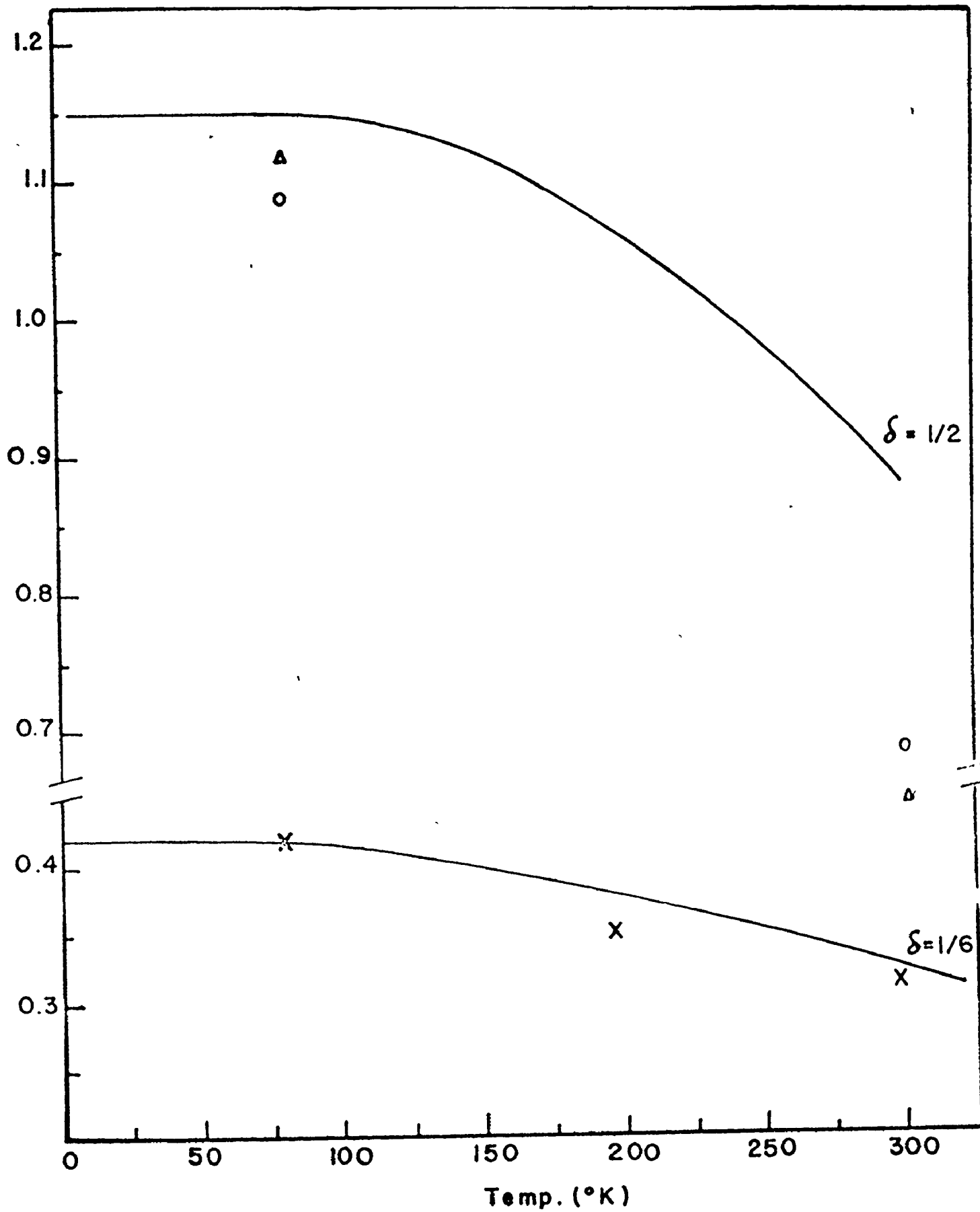
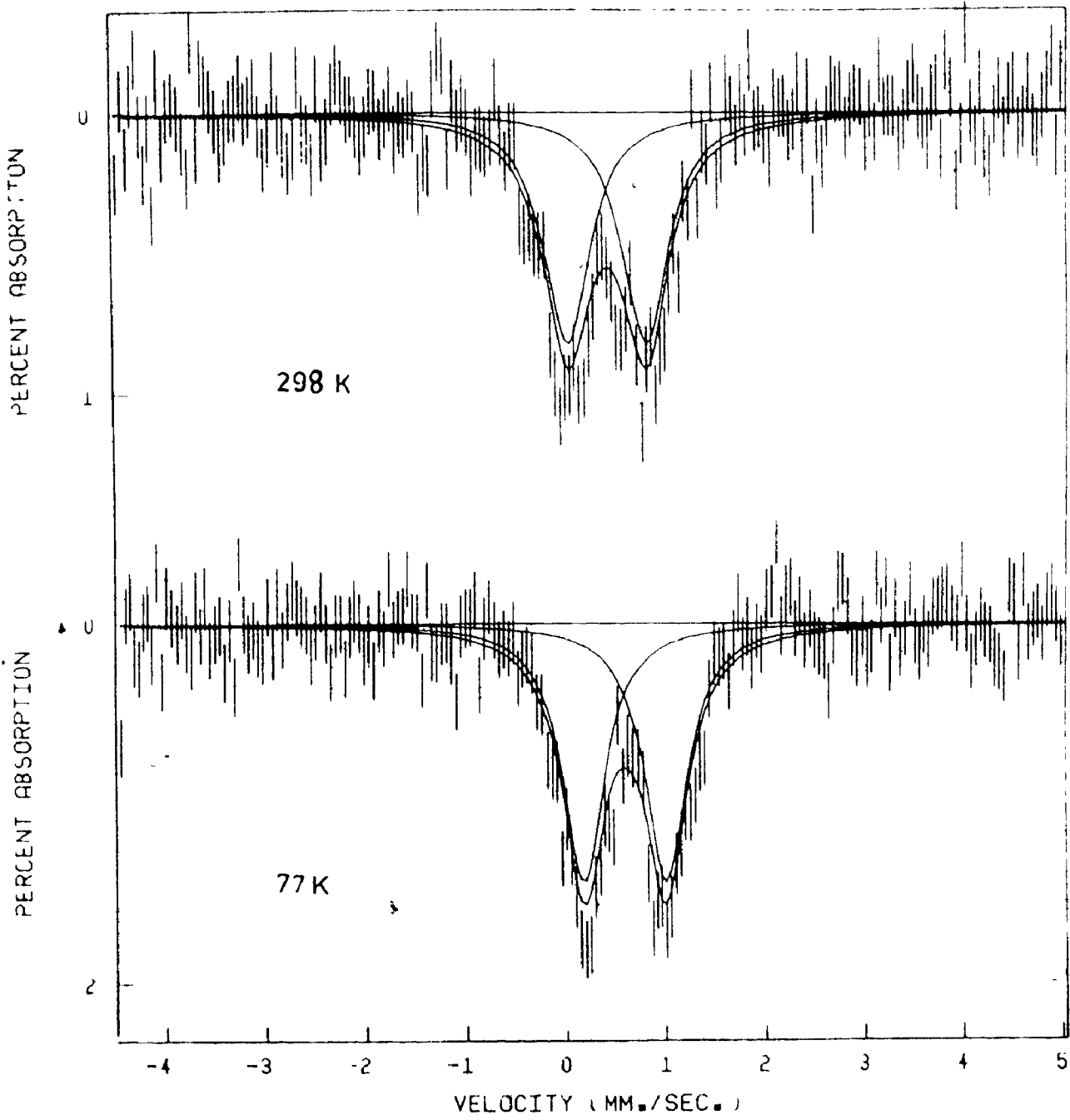


Figure 5.6. The Mössbauer Spectra of $[(\text{C}_6\text{H}_5)_3\text{P}_2\text{Cu}]_3\text{Fe}(\text{S}_2\text{C}_2\text{O}_2)_3$
at 298°K and 77°K.



The crystal structure of $[\text{Ag}(\text{P}(\text{C}_6\text{H}_5)_3)_2]_3\text{Fe}(\text{O}_2\text{C}_2\text{S}_2)_3$ (132) showed that the Fe atom is constrained to have C_3 symmetry by a movement of the $\text{O}_2\text{C}_2\text{S}_2\text{Ag}$ grouping away from the metal atom by about 0.10 \AA combined with a rotation around an axis perpendicular to the crystallographic threefold axis of the molecule. The geometry is closer to trigonal prismatic rather than regular octahedron (132). No significant variation of quadrupole splitting with temperature was expected nor observed for these high spin iron(III)-oxygen bonded dithiooxalate complexes.

(ii) Frozen Solution Studies

Trisdithiooxalatoferrate(III) complexes have been prepared by reaction of excess potassium dithiooxalate with either ferric or ferrous salts. In the previous section, a significant variation in quadrupole splitting is observed for these complexes. It was suggested that some of this variation might be due to the arrangement of cations and/or incorporated solvent molecules around the central anion. The influence of cations and solvent molecules upon the Mossbauer parameters would presumably be eliminated or reduced upon dissolution in water so that an examination of the spectra in frozen solution might help to resolve these influences. It is also of interest to determine why a ferric complex is isolated from the reaction of a ferrous salt with the potential reducing agent potassium dithiooxalate and it was thought that frozen solution studies might help in this regard.

Before discussing the results, it should be pointed out that there are difficulties involved in carrying out frozen aqueous solution Mossbauer studies. Firstly, the frozen solution has to be quenched rapidly before the solid has time to crystallise to ensure that one is indeed examining a solution. Secondly, it is possible that the solvent may coordinate to the metal atom. Thirdly, Mossbauer spectra of frozen solutions have very low absorptions and generally larger linewidths which cause larger errors than normal in the parameters obtained.

Frozen aqueous solutions of iron(III)-dithiooxalate complexes give a doublet spectrum having C.S. = 0.45 mm/sec and Q.S. = 0.92 mm/sec. The quadrupole splitting of the frozen solutions are lower than those of the solid complexes at 77°K suggesting that the effect of the cations

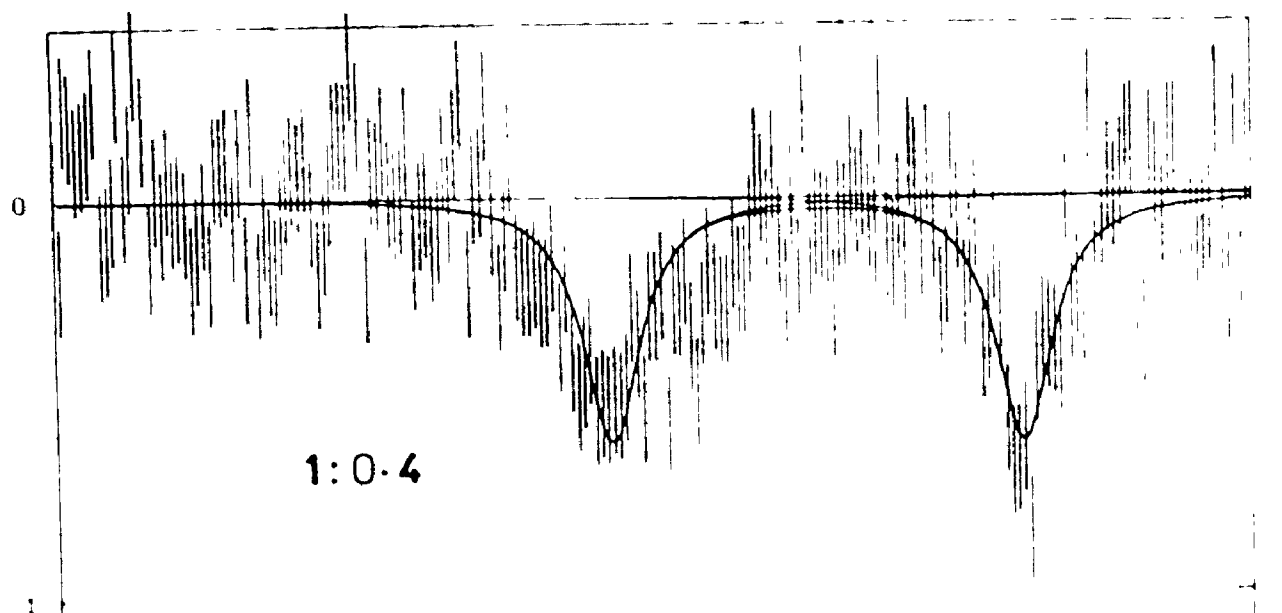
and/or the incorporated solvent is fairly large in the solid complexes

Frozen aqueous solutions of ferric nitrate and potassium dithiooxalate (K_2dto) give Mössbauer spectra which consist of two overlapping quadrupole split absorptions. It is found that the relative intensities of these absorptions vary as the ratio of ferric ion to dithiooxalate ion (dto^{2-}) is changed (Fig. 5.7). A Mossbauer spectrum of frozen aqueous ferric nitrate solutions gives a broad resonance at C.S. = 0.44 mm/sec. For ratios of $Fe^{3+}:dto^{2-}$ up to 1:2 the only iron species detectable is observed at C.S. = 1.37 ± 0.03 mm/sec with a quadrupole splitting of 3.26 ± 0.2 mm/sec. On the basis of these data this species is tentatively assigned as high spin Fe(II). As the ratio $Fe^{3+}:dto^{2-}$ is increased, another doublet (C.S. = 0.31 ± 0.03 mm/sec, Q.S. = 1.30 ± 0.07 mm/sec) attributable to $[Fe(dto)_3]^{3-}$ appears and is the predominant species at ratios of 1:6 (Table 5.5). Presumably then there are two reactions occurring in these solutions. The reduction of ferric to ferrous being dominant at the lower concentrations of dto^{2-} ligand while complex formation of $[Fe(dto)_3]^{3-}$ is more favourable at the higher ligand concentrations.

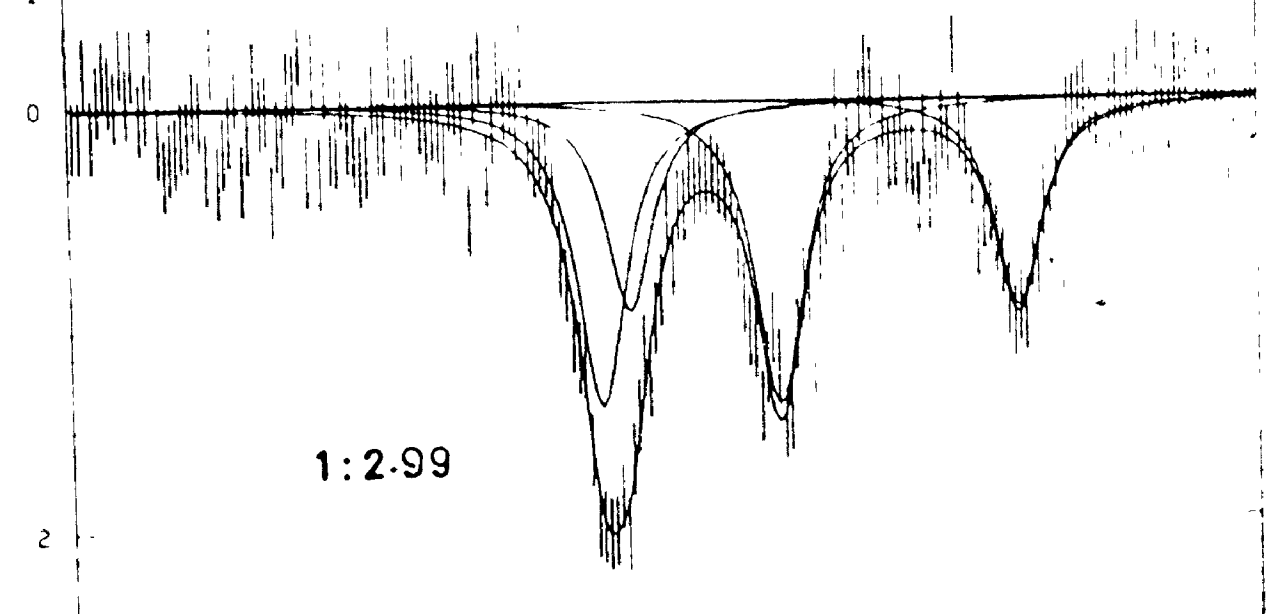
Although a reduction to ferrous ion is observed at very low concentrations of dithiooxalate ligand, there must still be unreacted ferric ion in the solution. However, this hydrated ferric ion is not detectable in these solutions since the ferric nitrate resonance is very broad and difficult to detect in the presence of other more strongly absorbing species. In order to further investigate the reactions occurring different ratios of ferric sulfate to potassium dithiooxalate were studied in aqueous solutions. Ferric sulfate was used instead of $Fe(NO_3)_3$ since it gives a Mössbauer doublet with narrow linewidths.

Figure 5.7. The Mossbauer Spectra of Frozen Aqueous Solutions of Ferric Nitrate and Potassium Dithiooxalate in the Ratios $\text{Fe}^{3+}:\text{dto}^{2-}$ of 1:0.4; 1:2.99; and 1:6.5.

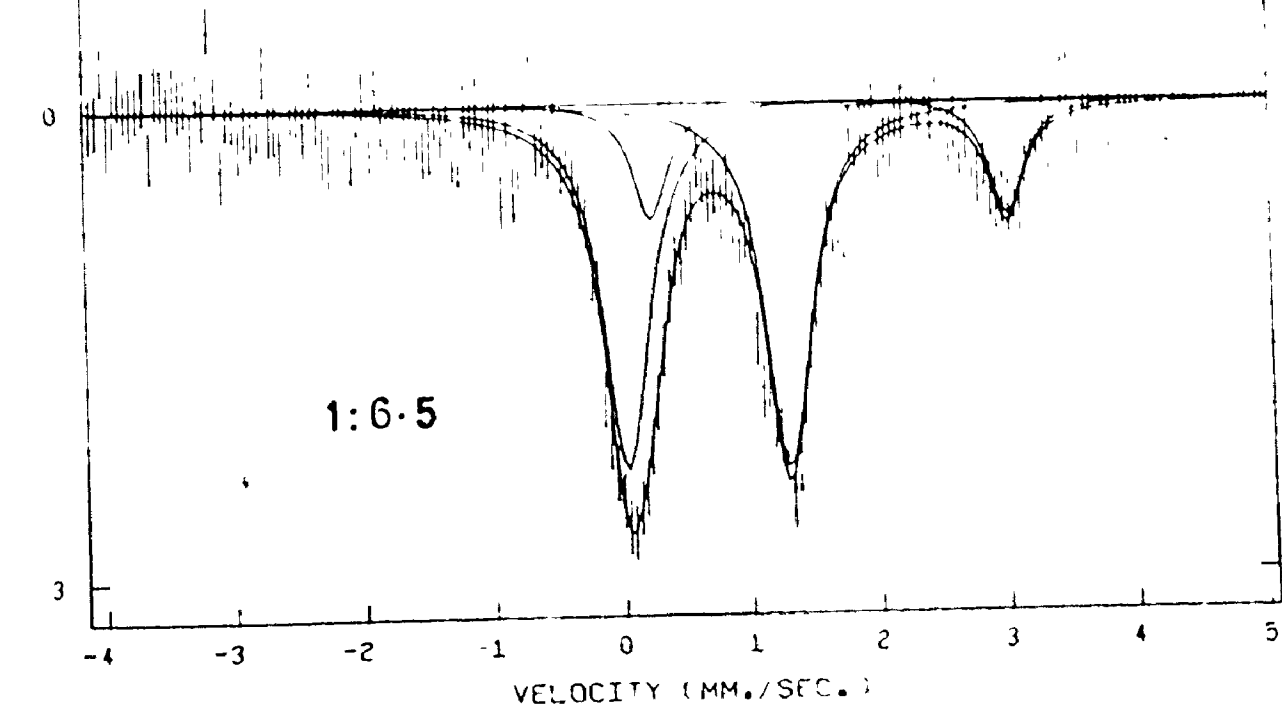
PERCENT ABSORPTION



PERCENT ABSORPTION



PERCENT ABSORPTION



VELOCITY (MM./SEC.)

TABLE 5.5

Mössbauer Data for Frozen Aqueous Solutions of Mixtures of Ferric Nitrate
and Potassium Dithiooxalate

Fe ⁺³ :dto ²⁻	Centre Shift mm/sec		Quadrupole Splitting mm/sec	
	Fe(III)	Fe(II)	Fe(III)	Fe(II)
1:0.00	~ 0.44	a broad resonance		
1:0.10		1.40		3.45
1:0.4		1.39		3.22
+ 1:1.07		1.38		3.28
1:2.04		1.33		3.09
1:2.54	0.28		1.23	
		1.39		2.91
1:2.85	0.31		1.28	
		1.29		2.90
+ 1:2.99	0.34		1.37	
		1.36		3.05
1:3.00	0.33		1.34	
		1.38		2.93
1:3.91	0.33		1.26	
		1.33		2.86
1:6.00	0.33		1.28	
		1.55		2.74
+ 1:6.50	0.35		1.25	
		1.31		2.76

+ from the same batch.

At ratios of 1:0.5 ($\text{Fe}^{+3}:\text{dto}^{2-}$) a doublet initially from $\text{Fe}_2(\text{SO}_4)_3$ in aqueous solution still appears together with the high spin Fe(II) species (Fig. 5.8, Table 5.6) confirming that the $\text{Fe(III)} \rightarrow \text{Fe(II)}$ reduction depends upon the amount of added dto^{2-} . Mössbauer spectra at ratios of 1:3 and 1:6 are essentially the same as those obtained when ferric nitrate was used.

Addition of dto^{2-} to solutions containing ferrous salts also results in the production of two iron species (Fig. 5.9, Table 5.7). For low ratios of metal to ligand ion, the predominant species has C.S. = 1.35 mm/sec and Q.S. = 3.35 mm/sec and appears to be identical to that produced from the corresponding ferric to ligand solutions discussed above; that is, it is a high spin Fe(II) species. Ratios higher than 1:1 give solutions containing species having C.S. = 1.40 mm/sec and Q.S. = 3.2 mm/sec and C.S. = 0.46 mm/sec, Q.S. = 0.60 mm/sec. The former set of parameters clearly arises from high spin Fe(II) as in systems discussed previously, but the latter set of data could arise from either low spin iron(II) or an iron(III) complex. Since the solid complexes isolated from the reaction of ferrous salt and potassium dithiooxalate are $[\text{Fe}^{\text{III}}(\text{dto})_3]^{3-}$ then this species (C.S. = 0.46 mm/sec, Q.S. = 0.60 mm/sec) must be assigned to an iron(III) complex rather than a low spin iron(II) complex. This Fe(III) complex may not necessarily be the $[\text{Fe}(\text{dto})_3]^{3-}$ ion but could be an aquo-dithiooxalatoferate(III) such as $[\text{Fe}(\text{dto})_2(\text{H}_2\text{O})_2]^-$. Thus, addition of dto^{2-} to aqueous solutions of Fe^{3+} appears to result first in the reduction of the Fe^{3+} to an iron(II) species which is then reoxidised at higher ratios of dithiooxalate. The initial reduction is perhaps not surprising since oxalates


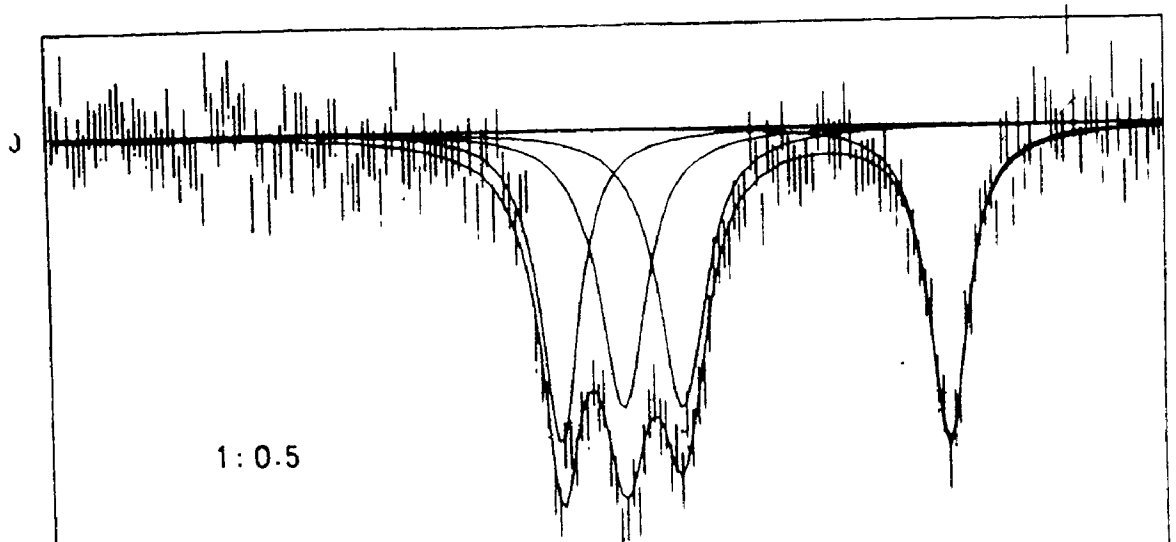
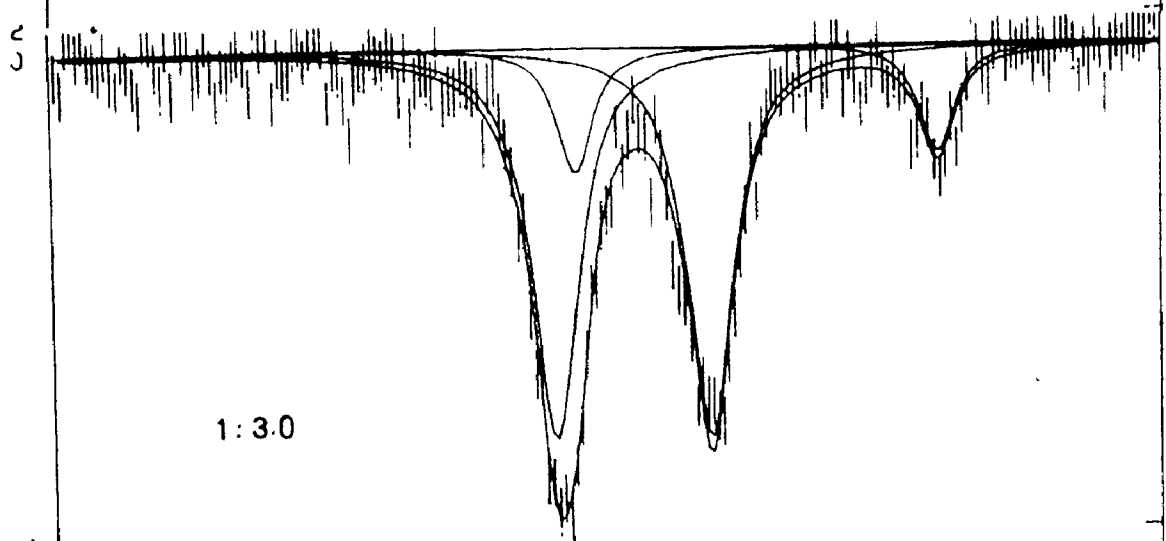


Figure 5.8. The Mössbauer Spectra of Frozen Aqueous Solutions of Ferric Sulfate and Potassium Dithiooxalate in the Ratios $\text{Fe}^{3+}:\text{dto}^{2-}$ of 1:0.5; 1:3.0; and 1:6.0.

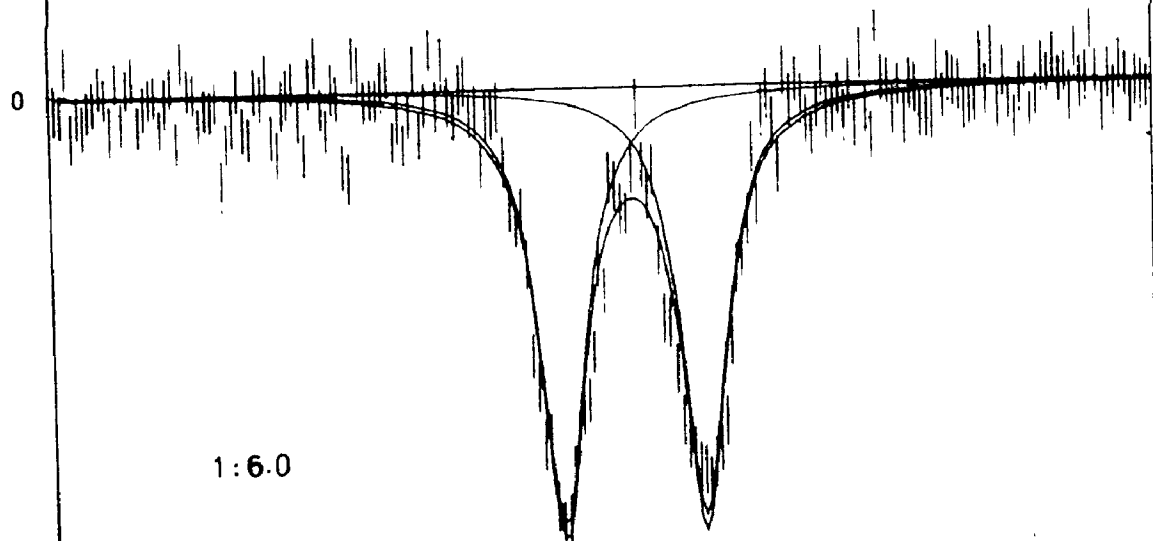
PERCENT ABSORPTION



PERCENT ABSORPTION



PERCENT ABSORPTION



VELOCITY (MM./SEC.)

TABLE 5.6

Mössbauer Data for Frozen Aqueous Solutions of Mixtures of Ferric Sulfate
and Potassium Dithiooxalate

$\text{Fe}^{3+}:\text{dto}^{2-}$	Centre Shift mm/sec		Quadrupole Splitting mm/sec	
	Fe(II)	Fe(III)	Fe(II)	Fe(III)
1:0.00		0.52		0.44
1:0.50	1.38		3.31	
		0.52		0.53
1:3.00	1.42		3.05	
		0.36		1.34
1:6.00		0.38		1.23

Figure 5.9. The Mössbauer Spectra of Frozen Aqueous Solutions of Ferrous Ammonium Sulfate and Potassium Dithiooxalate in the Ratios $\text{Fe}^{2+}:\text{dto}^{2-}$ of 1:0.49; 1:3.0; and 1:5.85.

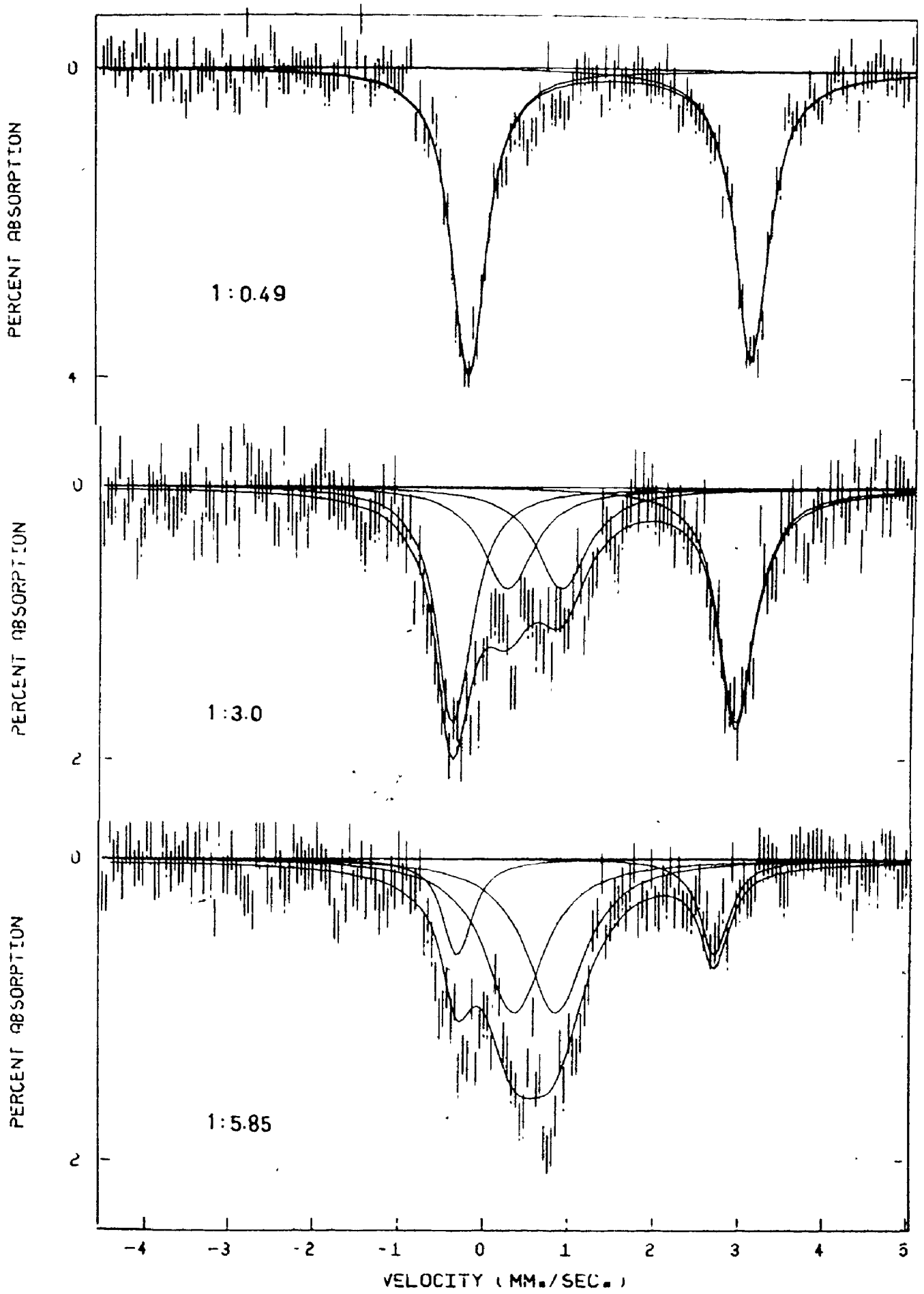


TABLE 5.7

Mössbauer Data for Frozen Aqueous Solution of Mixtures of
Ferrous Ammonium Sulfate and Potassium Dithiooxalate

$\text{Fe}^{+2}:\text{dto}^{-2}$	Centre Shift mm/sec		Quadrupole Splitting mm/sec	
	Fe(II)	Fe(III)	Fe(II)	Fe(III)
1:0.00	1.38		3.35	
1:0.49	1.36		3.30	
1:1.00	1.32		3.06	
1:1.05	1.32		3.22	
		0.44		0.94
1:3.00	1.16		3.28	
		0.45		0.60
1:5.85	1.15		3.08	
		0.52		0.45

are good reducing agents but the subsequent reoxidation was unexpected.

In order to see whether the rate of addition of dto^{2-} affected the products, specific amounts of dithiooxalate ion were successively added to the same aqueous solution of ferric salt and Mössbauer spectra were recorded after each addition. Each of these spectra is very similar to the corresponding spectrum recorded when all of the dithiooxalate was added at the same time indicating that the rate of addition does not affect the products.

The pH of the solutions are found to be different at different ratios of metal to ligand. The relevant data for the ferric nitrate-dithiooxalate system are

Ratio	pH
1:0.5	3.11
1:6.0	4.80

In order to see whether or not the reactions were pH dependent different ratios of ferric nitrate to potassium dithiooxalate solutions were buffered at $\text{pH} \sim 3.0$ where Fe(II) is the predominant species in the non-buffered solutions and Mössbauer spectra were recorded. If the oxidation-reduction was pH dependent, no ferric ion should be produced at $\text{pH} 3.0$, in the presence of excess dithiooxalate ligand. However, a quadrupole doublet assigned to the low spin Fe(III) species still appears at higher ligand concentrations. Also, solutions of ferrous ammonium sulfate and potassium dithiooxalate buffered at $\text{pH} \sim 4.8$ where Fe(III) is the main product, produce Fe(II) species together with Fe(III) species (Table 5.8). However, Mössbauer spectra for different ratios of ferric to dithiooxalate ion in 10% H_2SO_4 solutions only

TABLE 5.8

Mössbauer Data for Frozen Solutions of Mixtures of Ferric Nitrate
(or Ferrous Ammonium Sulfate) and Potassium Dithiooxalate

Fe ⁺³ :dto ⁻²	Fe ⁺² :dto ⁻²	Condition	Centre Shift mm/sec		Quadrupole Splitting mm/sec	
			Fe(II)	Fe(III)	Fe(II)	Fe(III)
1:1		pH 4.8, light	1.38		3.30	
				0.55		0.59
1:2.80		pH 3.0, dark	1.31		3.21	
				0.45		0.93
1:3.00		pH 4.8, light				
	1:2.5	pH 3.0, light	1.31		3.05	
				0.42		1.01
	1:2.5	pH 3.0, dark	1.34		3.15	
				0.44		0.85
	1:5.5		pH 3.0, light	1.15		3.21
0.47					0.46	
1:6.0		pH 4.8, light	1.09		3.03	
				0.47		0.43

give one doublet which is attributed to a Fe(II) species. No Fe(III) species was observed even at 1:6 ratios (Table 5.9). In acidic solutions oxalate ion behaves as a strong reducing agent and one might expect thiooxalate to act in a similar manner. The presence of only Fe(II) under these conditions is perhaps therefore not surprising.

The sensitivity of trisoxalatoferrates to light has been known for a long time and a photochemical oxidation of Fe(II) to Fe(III) can occur (145). The production of Fe(III) in these solutions may be feasible by an electron transfer from the metal to the ligand. It is thought that the analogous dithiooxalate complexes might have similar properties since some of the trisdithiooxalatoferrate(III) solid complexes are sensitive to light. However, Mossbauer spectra for different ferric (or ferrous) to dto^{2-} ratios, recorded from solutions prepared in the dark are identical to those from solutions prepared in daylight. Electron spin resonance is a very useful technique to study radical ions in photochemical reactions. In order to obtain further information on these iron dithiooxalate systems, e.s.r. was used. Irradiation of different ratios of ferric salt to dithiooxalate ligand in 10% sulfuric acid solutions frozen at 77°K produced radicals which were detected by their e.s.r. spectra (Fig. 5.10). After a 1 hour irradiation, an e.s.r. spectrum consisting of a doublet separated by ~ 500 gauss at $g = 1.01$, a doublet of asymmetric lines separated by ~ 130 gauss at $g = 2.002$, and a single asymmetric line at $g = 2.003$ were observed. Spectra for different ratios of Fe(+2) to dto^{2-} give the same spectral lines. These spectra are very similar to those obtained by Eaton and Stuart (146) from the irradiation of $\text{K}_3\text{Co}(\text{C}_2\text{O}_4)_3$ in 10% H_2SO_4 solutions

TABLE 5.9

Mossbauer Data for Frozen Acidic Solutions (10% H_2SO_4) of
Mixtures of Ferric Nitrate and Potassium Dithiooxalate

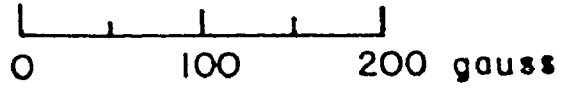
$\text{Fe}^{+3}:\text{dto}^{-2}$	Centre Shift mm/sec	Quadrupole Splitting mm/sec
1:0.5	1.40	3.39
1:2.3	1.39	3.42
1:2.8	1.40	3.41
1:4.8	1.39	3.40

Figure 5.10. E.s.r. Signals Obtained from a Solution of Ferric Nitrate
and Potassium Dithiooxalate in 10% H₂SO₄ at 77°K.

CHS°

g = 2.003

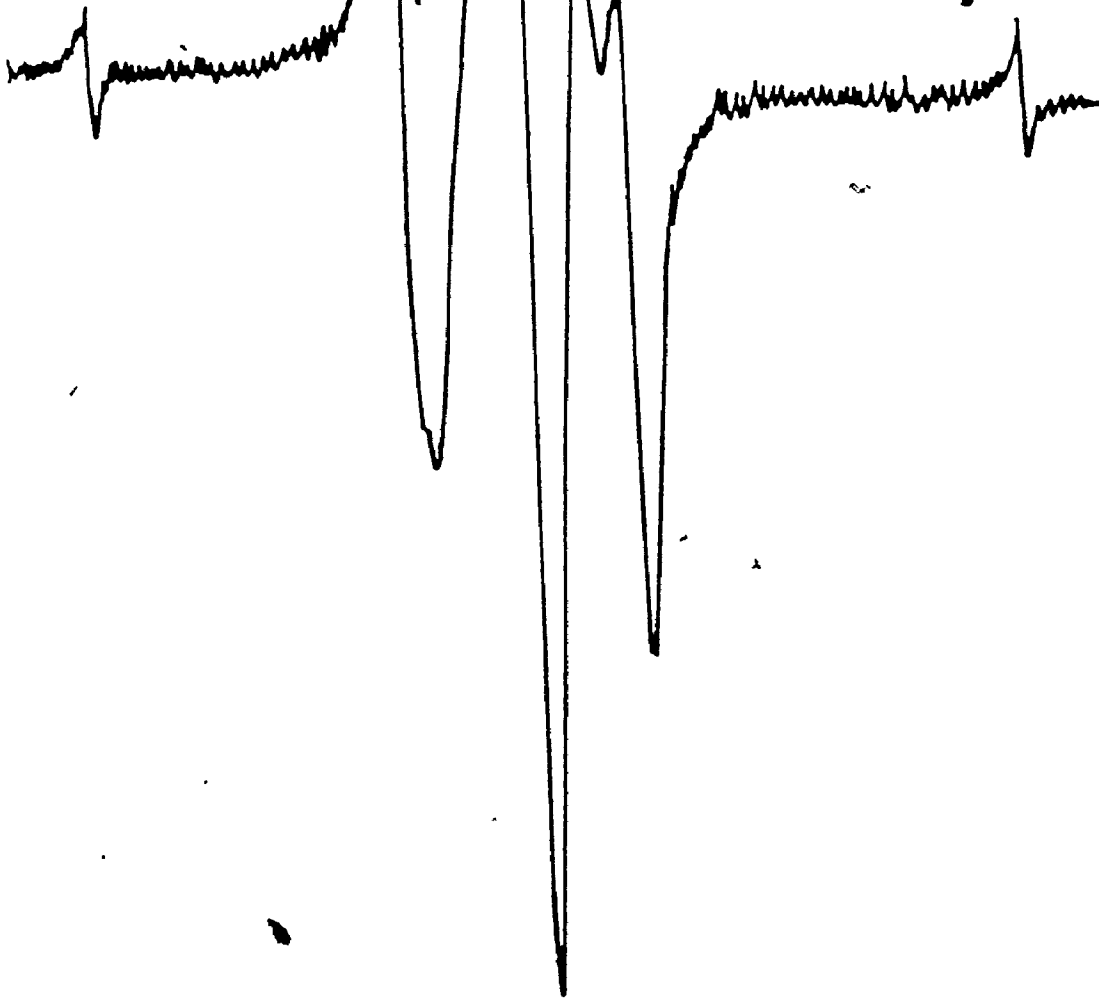
114



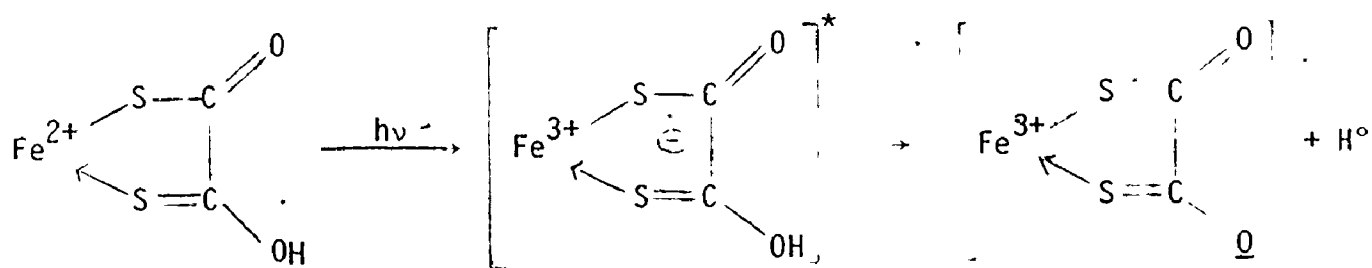
H°

CHS°
g = 2.002

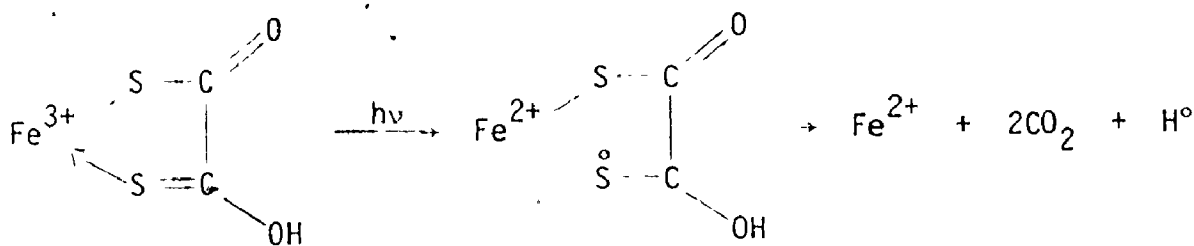
H°
g = 2.01



and an acidic solution of CoCl_2 and $\text{K}_2\text{C}_2\text{O}_4$, and the following assignments are based on their results. The two lines separated by ~ 500 gauss are assigned as hydrogen atoms, the asymmetric doublet separated by ~ 130 gauss as HCS° , and an asymmetric single line as COS° , COSH° or a complexed form of these radicals. The mechanism of the oxidation-reductions in these iron-dithiooxalate systems are assumed to be the same as those of the cobalt-oxalate systems, suggested by Eaton and Suart (146). In the case of Fe(II), an electron transfer through the thiooxalate system is required.



In the case of Fe(III), the following process is suggested.



Hydrogen atoms then react with thiooxalate ion and produce COS° or COSH° radical ion. No detectable e.s.r. signals were observed for different ferric to dtho²⁻ ratios in aqueous and buffered solutions upon irradiation so that confirmation of a radical oxidation of Fe(II) \rightarrow Fe(III) could not be obtained.

The magnetic data for these solution systems are inconclusive

since mixtures of dithiooxalate compounds which are paramagnetic, are produced in solution. Thus, the reduction in iron-dithiooxalate systems is unambiguous but the mechanism of the unexpected reoxidation is uncertain though a radical mechanism seems most likely.

CHAPTER VI
LIQUID CRYSTALS STUDIES

Liquid crystals have been used as solvents for many experimental techniques such as, n.m.r. and e.s.r., from which structural information can be obtained from ordered samples ("single crystals"). Recently, the Mössbauer effect of solute molecules in an aligned liquid crystalline system has been observed (78,104). Liquid crystals can be used as a simple method to obtain the sign of the quadrupole splitting by Mössbauer spectroscopy although there are some difficulties, such as solubility of the complex in the liquid crystal and of their stability in the high temperature phases of liquid crystals.

In order to observe the Mössbauer effect in a liquid crystal, an absorber molecule should have an extended molecular axis which will therefore be easily aligned by their liquid crystal environment. Also, the molecule should exhibit a large quadrupole splitting and should not interact with the liquid crystalline materials. If a solute molecule is aligned by its environment, then orientation dependence of the relative intensities of the quadrupole-split lines will allow a determination of the sign of the quadrupole splitting.

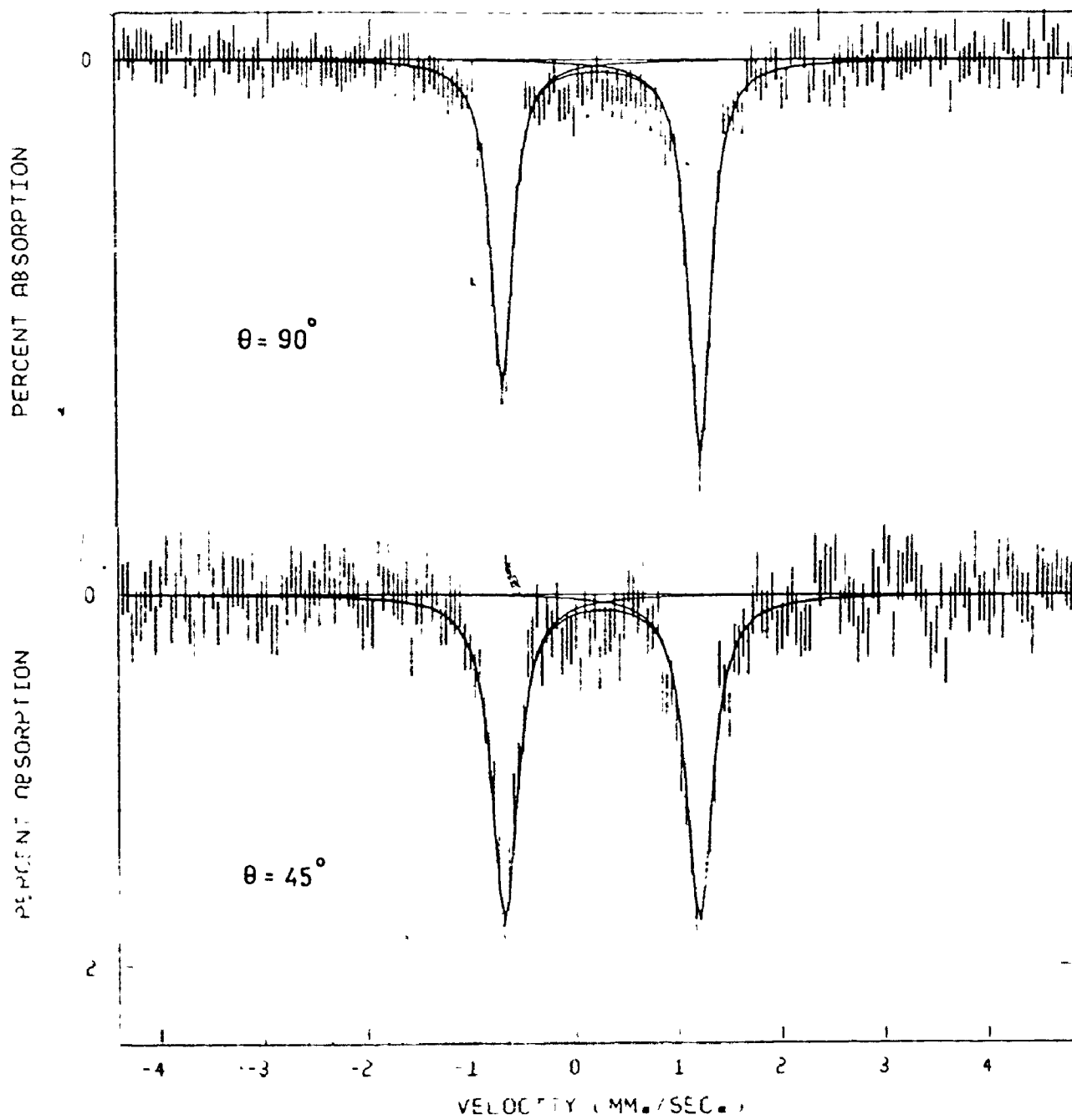
In Chapter IV, it is suggested that the sign of the quadrupole splitting of iron-nitrosyl complexes would indicate the lowest energy d-orbital of iron. In order to obtain the sign of the quadrupole splitting, liquid crystals were used to obtain a "single crystal" for iron-nitrosyl complexes. The degree of ordering of the sample by its liquid

crystal environment depends on the shape of the sample molecule and its length relative to that of liquid crystal molecule. In order to get meaningful results for iron-nitrosyl complexes in liquid crystals $[\text{C}_5\text{H}_5\text{Fe}(\text{CO})_2]_2$ and $[\text{Fe}(\text{NO})_2\text{SC}_2\text{H}_5]_2$ were used for trial experiments. These two molecules have long molecular axes so that one can assume that they can be easily aligned by their liquid crystal environment. The liquid crystals used in this study were N-(p-methoxybenzylidene-p-butylaniline), p-(p-ethoxyphenylazo)phenyl hexanoate and p-(p-ethoxyphenylazo)phenyl heptanoate.

The samples were dissolved in the liquid crystal at the nematic temperature (see Chapter III) and aligned by cooling from that temperature to room temperature in a magnetic field of ~ 9000 gauss. At room temperature, the sample was removed from the magnet, cooled to 77°K and a Mössbauer spectrum was recorded. Assuming the sample was aligned parallel to the axis of the magnetic field, the gamma ray direction is perpendicular to the sample holder; that is, θ , the angle between the molecular axis of the sample and the gamma ray beam is 90° . The angle can be adjusted by rotating the sample holder to any desired angle.

A Mössbauer spectrum of a polycrystalline powder $[\text{C}_5\text{H}_5\text{Fe}(\text{CO})_2]_2$ gives a doublet of equal intensity, having C.S. = 0.22 mm/sec and Q.S. = 1.89 mm/sec. This centre shift and quadrupole splitting remained constant when the sample was dissolved in a liquid crystal. It can therefore be assumed that the molecule did not chemically interact with the liquid crystal solvent. At an angle of 90° , the relative intensities of two lines were different (1:1.23), and approximately equal (1:1.04) at an angle of 45° (Fig. 6.1). This shows that the molecule is oriented. As

Figure 6.1. The Mössbauer Spectra of $[\text{CpFe}(\text{CO})_2]_2$ in the Liquid Crystal
(N-(p-methoxybenzylidene)(p-butylaniline) at $\theta = 90^\circ$ and 45° .



mentioned on page 26, the $\pm \frac{3}{2} \rightarrow \pm \frac{1}{2}$ transition has a less intense absorption than the $\pm \frac{1}{2} \rightarrow \pm \frac{1}{2}$ transition at 90° . Thus, for a spectrum in Fig. 6.1, the line at negative velocities is assigned as $\pm \frac{3}{2} \rightarrow \pm \frac{1}{2}$ transition and the other at positive velocities as $\pm \frac{1}{2} \rightarrow \pm \frac{1}{2}$ transition. For $\theta = 90^\circ$, if the less intense line (the $\frac{3}{2}$ line) is at negative velocities the sign of the quadrupole splitting (or the sign of the electric field gradient) is negative. Thus, V_{zz} is negative for $[\text{C}_5\text{H}_5\text{Fe}(\text{CO})_2]_2$.

The experiment with $[\text{Fe}(\text{NO})_2\text{SC}_2\text{H}_5]_2$ was not successful due to the decomposition of this sample in the liquid crystals tried.

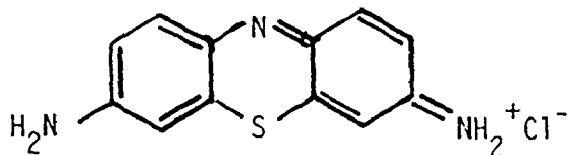
Data from these experiments show that molecules can be oriented in these liquid crystals and it therefore appeared worthwhile to try to obtain the sign of the quadrupole splitting by this method for the $\text{Fe}(\text{NO})_2\text{LX}$ molecules studied in Chapter IV.

Several attempts were made to orient the $\text{Fe}(\text{NO})_2\text{LX}$ molecules in those liquid crystals. Unfortunately, the area ratios of the quadrupole doublet were always found to be equal within experimental error. No decomposition was observed in these systems. It appears that the molecular axes of the $\text{Fe}(\text{NO})_2\text{LX}$ complexes are not long enough to allow them to be aligned by these liquid crystals. Since the $[(\text{NO})_2\text{FeX}]_2$ molecules are somewhat related to the $[\text{C}_5\text{H}_5\text{Fe}(\text{CO})_2]_2$ molecule which was successfully aligned, attempts were made to study these compounds in liquid crystals. Unfortunately, these were unsuccessful as the molecule decomposed before the liquid crystal molecules could be aligned.

APPENDIX

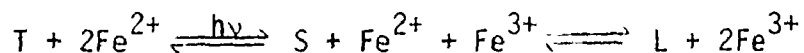
The results presented in Chapter V suggest that Mössbauer spectroscopy may be a useful tool in the study of photochemical reactions in solution. It was hoped that evidence to support this could be obtained by studying known photochemical reactions in solution.

The photochemical behaviour of solutions containing thionine



and ferrous ion has been investigated by several groups (145). When thionine solutions are irradiated in the presence of ferrous ions, a considerable bleaching is observed and the reduced dye and ferric ion are produced (147). This bleaching of the colour is observed even in sunlight. This photochemical reaction seemed to be so simple that the ferrous-thionine system was chosen to study the photochemical oxidation of Fe²⁺ to Fe³⁺ using the Mössbauer effect.

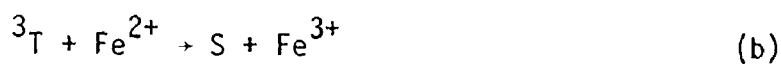
Two different mechanisms have been proposed for the ferrous-thionine system. According to Rabinowitch (148), Schlag (149), and Hardwick (150) the light acts on the equilibria



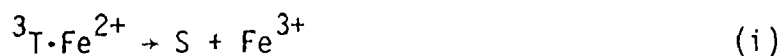
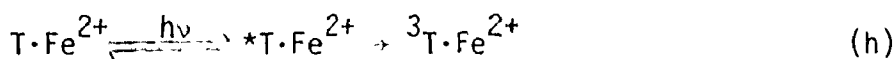
(T = thionine, S = semithionine, L = Leucothionine). They assumed that the primary one electron reduction occurred between a thionine molecule in its triplet excited state and a ferrous ion. An alternative mechanism, proposed by Havemann and coworkers (151,152) involves a

thionine-ferrous ion complex as a photosensitive species. They assumed that, upon irradiation, the intra-ligand excited state of the $T \cdot Fe^{2+}$ complex would undergo a conversion to a low-lying excited state which may also be considered as the ground state of the $S \cdot Fe^{3+}$ complex; a subsequent reaction between $S \cdot Fe^{3+}$ and Fe^{2+} would then lead to $L + 2Fe^{3+}$.

The results obtained by Ainsworth (153) suggest that both free thionine molecules and thionine- Fe^{2+} complexes are photoactive. For low Fe^{2+} concentrations ($[Fe^{2+}] \leq 10^{-3}$), the reaction takes place between ferrous ions and an excited species of thionine (3T):



At higher ferrous ion concentrations, the reaction proceeds mainly through an electron transfer within the thionine- Fe^{2+} complexes.



plus Reactions (d), (e) and (f).

Although the actual mechanism of the ferrous-thionine system

is not well defined yet, it can be assumed that this system is an intramolecular photoredox reaction involving the reduction of the ligand and the oxidation of the metal ion.

In this present work, bleaching was not observed in either Fe^{3+} -thionine solutions or the thionine solution alone. It was only observed for mixtures of thionine ($\sim 10^{-5}$ M) and Fe^{2+} ($\sim 10^{-2}$ M) in acid solution in the presence of light. Precautions were taken to exclude Fe^{3+} ion in the initial Fe^{2+} -thionine solution. The solutions were degassed before use and the irradiation was done on an evacuated tube containing the ferrous-thionine mixture. The solution was photolysed either by sunlight or photolyzing light from a quartz-iodide projection lamp. The bleached solution, after a one-hour irradiation, was injected into the Mössbauer cell which was then frozen before recording the spectrum. Mössbauer data are given in Table A.1. The Mössbauer spectra of the solutions before and after the irradiation did not seem to be different from one another (Fig. A.1). To get better resolution in order to have a better chance of detecting small amounts of Fe^{3+} , the sample was enriched in ^{57}Fe . Fig. A.2 shows spectra obtained for this system. Before irradiation, a doublet was observed. This doublet is characteristic of an Fe^{2+} species. After irradiation, another doublet with very low intensity appears in between the doublet attributable to Fe^{2+} , indicating the presence of another species in the ferrous-thionine system. This system was analyzed for a one doublet and a two doublet fit. χ^2 for these fits were 452 with 388 degrees of freedom and 415 with 382 degrees of freedom for the one and two doublet fits, respectively. Although the χ^2 values are not very different, a two doublet fit seems to be

TABLE A.1

Mössbauer Data for Acid Solutions of a Mixture of Ferrous Ammonium Sulfate and Thionine

Condition	C.S. mm/sec		Q.S. mm/sec		Intensity ratios of Fe ²⁺ :Fe ³⁺
	Fe(II)	Fe(III)	Fe(II)	Fe(III)	
Before Irradiation	1.37		3.31		
After Irradiation	1.37		3.35		
† Before Irradiation	1.37		3.38		
† After Irradiation	1.40		3.36		25:1
		0.42		0.64	

† Using enriched ⁵⁷Fe.

Figure A.1. The Mössbauer Spectra of Frozen Solution of Ferrous Ammonium Sulfate and Thionine in 0.1M H₂SO₄
(a) Before and
(b) After Irradiation.

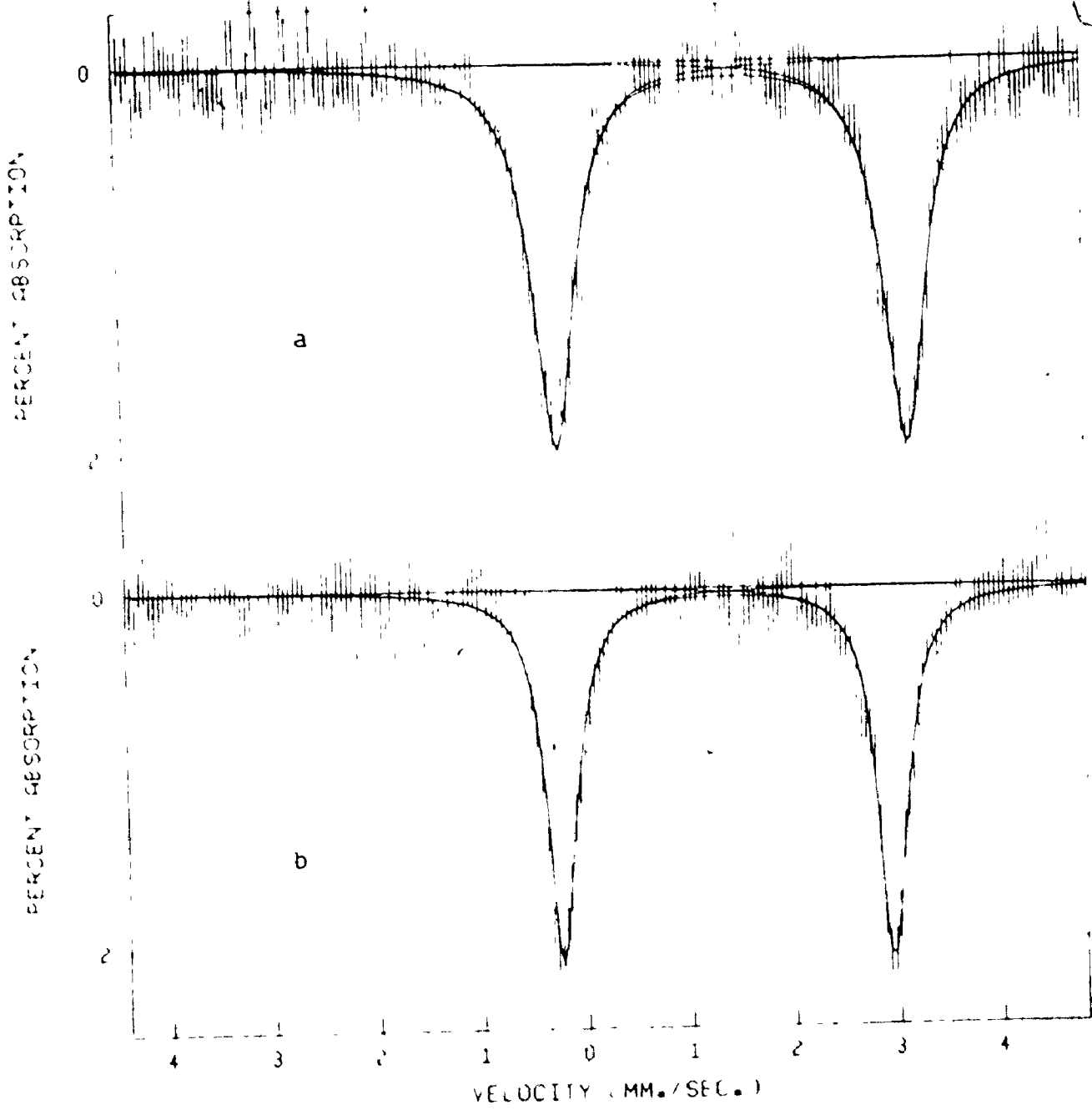
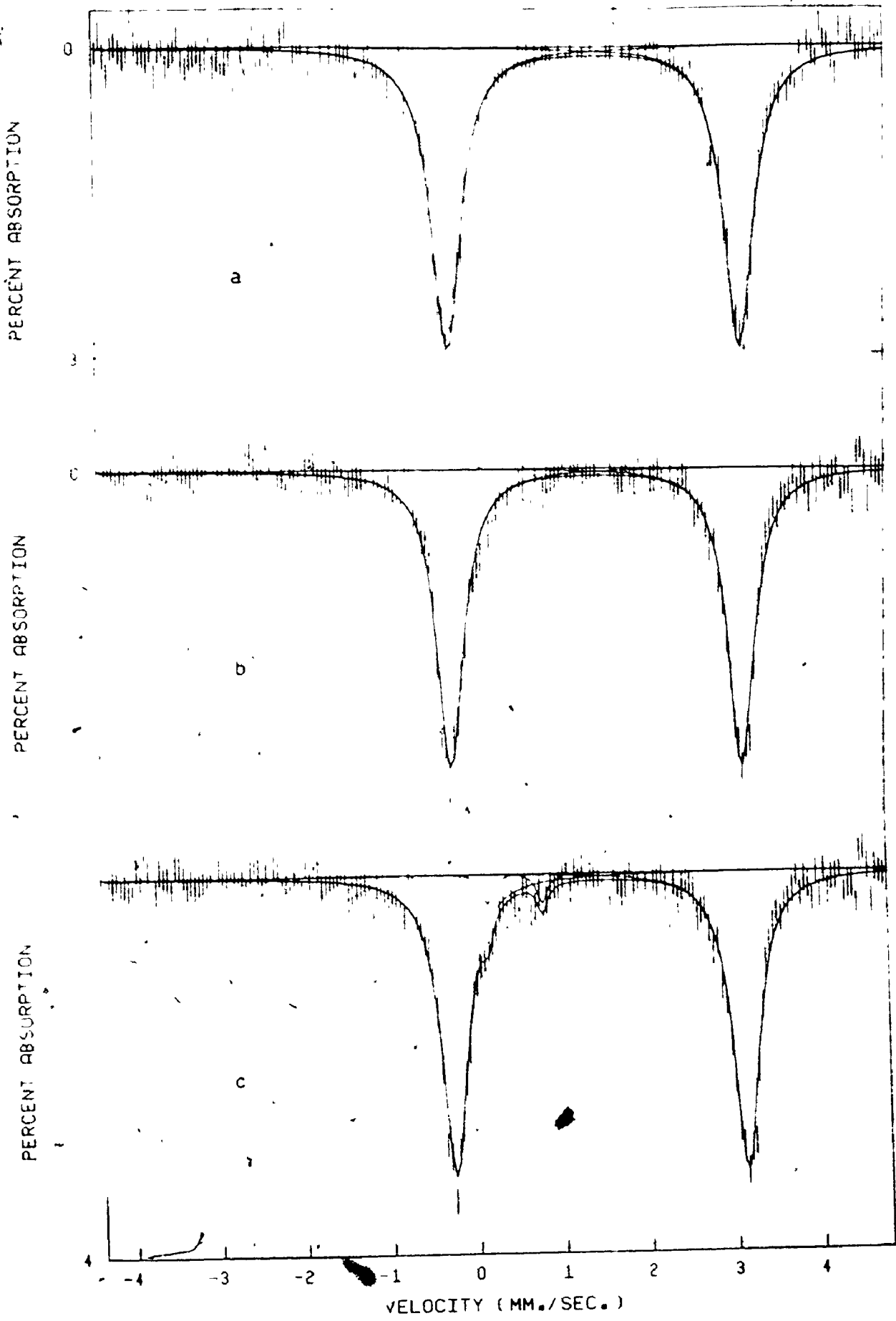


Figure A.2. The Mossbauer Spectra of Frozen Solution of a Mixture of Fe^{2+} (enriched in ^{57}Fe) and Thionine in 0.1M H_2SO_4

(a) Before Irradiation

(b) After Irradiation with a One Doublet Fit and

(c) After Irradiation with a Two Doublet Fit.



better than a one doublet fit. The centre shift (0.42 mm/sec) and the quadrupole splitting (0.64 mm/sec) of this new doublet is characteristic of ferric ion. This data confirms that photochemical oxidation reactions do occur in the ferrous-thionine solutions although the amount of Fe^{3+} is not very large.

It is therefore concluded that it would be possible to study photochemical reactions in solution by Mössbauer spectroscopy though longer irradiation may be necessary in order to build up sufficient quantities of the oxidized species to allow its detection. It may also be necessary to carry out the photolysis on the frozen solutions in order to trap the oxidized species and perhaps prevent the reverse reaction from having any significant effect.

REFERENCES

1. B. F. G. Johnson and J. A. McCleverty, *Prog. Inorg. Chem.*, 7, 277 (1966).
2. W. P. Griffith, *Advan. Organometal. Chem.*, 7, 211 (1968).
3. I. Bernal and S. E. Harrison, *J. Chem. Phys.*, 34, 102 (1961).
4. E. F. Hocking and I. Bernal, *J. Chem. Soc.*, 5029 (1964).
5. P. T. Manoharan and H. B. Gray, *Inorg. Chem.*, 5, 823 (1966); *J. Amer. Chem. Soc.*, 87, 3340 (1965).
6. F. A. Cotton and G. Wilkinson, "Advanced Inorganic Chemistry", 3rd Edition, Interscience Publishers, New York, 1972.
7. J. Lewis, R. J. Irving and G. Wilkinson, *J. Inorg. Nucl. Chem.*, 7, 32 (1958).
8. W. P. Griffith, J. Lewis and G. Wilkinson, *J. Inorg. Nucl. Chem.*, 7, 38 (1958).
9. R. D. Feltham, W. Silverthorn and G. McPherson, *Inorg. Chem.*, 8, 344 (1969).
10. C. A. Reed and W. R. Roper, *Chem. Comm.*, 155 (1969).
11. J. P. Collman, W. N. Hoffman and D. E. Moores, *J. Amer. Chem. Soc.*, 91, 5659 (1969).
12. D. J. Hodgson and J. A. Ibers, *Inorg. Chem.*, 7, 2345 (1968); *ibid.*, 8, 1282 (1969).
13. D. J. Hodgson, N. C. Payne, J. A. McGinnety, R. G. Pearson and J. A. Ibers, *J. Amer. Chem. Soc.*, 90, 4486 (1968).
14. D. A. Snyder and D. L. Weaver, *Inorg. Chem.*, 9, 2760 (1970).
15. C. G. Pierpont, D. G. van Derveer, W. Durland and R. Eisenberg, *J. Amer. Chem. Soc.*, 92, 4760 (1970).
16. C. S. Pratt, B. A. Coyle and J. A. Ibers, *J. Chem. Soc. (A)*, 2146 (1971).
17. Ya I. Azhpa, L. P. Kayushin and Ye. I. Nikishin, *Biofizika*, 11, 710 (1966).
18. J. C. Woolum, E. Tiezzi and B. Commoner, *Biochim. Biophys. Acta.*, 160, 311 (1968).

19. W. Gordy and H. N. Rexroad, in "Free Radicals in Biological Systems", M. S. Blois, Jr., H. W. Brown, R. M. Lemmon, R. O. Lindblom and M. Weissbluth, Eds., Academic Press, New York, New York, 1961, pp. 268-273.
20. A. F. Vanim, *Biochem. (U.S.S.R.)*, 32, 228 (1966).
21. N. V. Sidgwick, "Chemical Elements and Their Compounds", Clarendon Press, Oxford, 1950.
22. W. P. Griffith, J. Lewis and G. Wilkinson, *J. Chem. Soc.*, 3993 (1958).
23. W. Hieber and J. S. Anderson, *Z. Anorg. Allgem. Chem.*, 211, 132 (1933).
24. W. Hieber and R. Nast, *Z. Anorg. Allgem. Chem.*, 244, 23 (1940).
25. W. Hieber and W. Beck, *Z. Naturforsch.*, 13b, 194 (1958).
26. A. Jahn, *Z. Anorg. Allgem. Chem.*, 301, 301 (1959).
27. J. T. Thomas, J. H. Robertson and E. G. Cox, *Acta. Cryst.*, 11, 599 (1958).
28. L. F. Dahl, E. R. de Gil and R. D. Feltham, *J. Amer. Chem. Soc.*, 91, 1653 (1969).
29. C. C. McDonald, W. P. Phillips and M. F. Mower, *J. Amer. Chem. Soc.*, 87, 3319 (1965).
30. L. Burlamacchi, G. Martini and E. Tiezzi, *Inorg. Chem.*, 8, 2021 (1969).
31. G. Martini and E. Tiezzi, *Trans. Farad. Soc.*, 67, 2538 (1971).
32. J. P. Crow, W. R. Cullen, F. G. Herring, J. R. Sams and R. L. Tapping, *Inorg. Chem.*, 10, 1616 (1971).
33. R. E. Dessy, J. C. Charkoudian and A. L. Rheingold, *J. Amer. Chem. Soc.*, 94, 738 (1972).
34. V. I. Goldanskii and R. H. Herber, Eds., "Chemical Applications of Mössbauer Spectroscopy", Academic Press, New York, New York, 1968, p. 159.
35. R. A. Mazak and R. L. Collins, *J. Chem. Phys.*, 51, 3220 (1969).
36. T. Birchall and N. N. Greenwood, *J. Chem. Soc. (A)*, 286 (1969).

37. C. F. Johnson, R. Richards and H. A. O. Hill, *J. Chem. Phys.*, 50, 2594 (1969).
38. W. Hieber and K. Kaiser, *Z. Anorg. Allgem. Chem.*, 358, 271 (1968).
39. A. Yamagouchi, R. Penland, S. Mizushima, J. Lane, C. Curan and J. Quagliano, *J. Amer. Chem. Soc.*, 80, 527 (1958).
40. K. Swaminathan and H. M. N. H. Irving, *J. Inorg. Nucl. Chem.*, 26, 1291 (1964).
41. C. D. Flint and M. Goodgame, *J. Chem. Soc. (A)*, 750 (1968).
42. T. J. Lane, A. Yamagouchi, J. V. Quagliano, J. A. Ryan and S. Mizushima, *J. Amer. Chem. Soc.*, 81, 3824 (1959).
43. R. Rivest, *Can. J. Chem.*, 40, 2234 (1962).
44. N. N. Greenwood and T. C. Gibb, "Mössbauer Spectroscopy", Chapman and Hall, Ltd., London, 1971.
45. J. A. McCleverty, *Prog. Inorg. Chem.*, 10, 49 (1968).
46. S. I. Shupack, E. Billig, R. J. H. Clark, R. Williams and H. B. Gray, *J. Amer. Chem. Soc.*, 86, 4594 (1964).
47. C. K. Jørgensen, *Inorg. Chim. Acta, Rev.*, 2, 65 (1968).
48. G. N. Schrauzer and V. P. Mayweg, *J. Amer. Chem. Soc.*, 88, 3235 (1966).
49. E. I. Stiefel, R. Eisenberg, R. C. Rosenberg and H. B. Gray, *J. Amer. Chem. Soc.*, 88, 2956 (1966).
50. A. Davison, N. Edelstein, E. H. Holm and A. H. Maki, *J. Amer. Chem. Soc.*, 86, 2799 (1964).
51. E. Frank and C. R. Abeledo, *Inorg. Chem.*, 5, 1453 (1966).
52. R. M. Golding and H. J. Whitfield, *Trans. Farad. Soc.*, 62, 1713 (1966).
53. R. Rickards, C. E. Johnson and H. A. O. Hill, *J. Chem. Phys.*, 48, 5231 (1968).
54. T. Birchall, N. N. Greenwood and J. A. McCleverty, *Nature*, 215, 625 (1967).
55. B. B. Buchanan, *Structure Bonding*, 1, 109 (1966).
56. R. Malkin and J. C. Robinowitz, *Ann. Rev. Biochem.*, 36, 113 (1967).

57. D. Coucouvanis, *Prog. Inorg. Chem.*, 11, 233 (1968).
58. D. Coucouvanis, S. J. Lippard and J. A. Zubieta, *J. Amer. Chem. Soc.*, 90, 3281 (1968), and references therein.
59. A. L. Balch, *J. Amer. Chem. Soc.*, 91, 6962 (1969).
60. L. H. Pignolet and R. H. Holm, *J. Amer. Chem. Soc.*, 92, 1791 (1970).
61. H. O. Jones and H. S. Tasker, *Proc. Chem. Soc.*, 25, 247 (1910); *J. Chem. Soc.*, 95, 1904 (1910).
62. E. G. Cox, W. Wardlaw and K. C. Webster, *J. Chem. Soc.*, 1475 (1935).
63. F. P. Dwyer and A. M. Sargeson, *J. Amer. Chem. Soc.*, 81, 2335 (1959).
64. R. L. Carlin and F. Canziani, *J. Chem. Phys.*, 40, 371 (1964).
65. C. E. Schäffer and C. K. Jørgensen, *J. Inorg. Nucl. Chem.*, 8, 143 (1958).
66. C. K. Jørgensen, *Prog. Inorg. Chem.*, 4, 73 (1962).
67. A. R. Latham, V. C. Hascall and H. B. Gray, *Inorg. Chem.*, 4, 788 (1965).
68. J. J. Morrison and W. A. Baker, *Inorg. Chim. Acta*, 3, 463 (1969).
69. D. Coucouvanis, *J. Amer. Chem. Soc.*, 92, 707 (1970).
70. D. Coucouvanis, R. E. Coffman and D. Piltingsrud, *J. Amer. Chem. Soc.*, 92, 5004 (1970).
71. D. Coucouvanis, *J. Amer. Chem. Soc.*, 93, 1786 (1971).
72. R. L. Martin and A. H. White in "Transition Metal Chemistry", R. L. Carlin, Ed., Vol. 4, Marcel Dekker, Inc., New York, New York, 1968, p. 113.
73. I. Dezsi, B. Molnar, T. Tarnoczi and K. Tompa, *J. Inorg. Nucl. Chem.*, 29, 2486 (1967).
74. G. A. Renovitch and W. A. Baker, Jr., *J. Amer. Chem. Soc.*, 89, 6377 (1967).
75. G. W. Gray, "Molecular Structure and the Properties of Liquid Crystals", Academic Press, New York, New York, 1962.
76. G. H. Brown, J. W. Doane and V. D. Neff, "Structure and Physical Properties

- of Liquid Crystals", D. E. Schuele and R. W. Hoffman, Eds., CRC Critical Reviews of Solid State Sciences, 1970, pp. 303-379.
77. A. Saupe, *Angew. Chem. Intern. Edit.*, 7, 97 (1968).
78. D. L. Uhrich, R. E. Detjen and J. M. Wilson, "Mössbauer Effect Methodology", Vol. 8, I. J. Gruverman and C. W. Seidal, Eds., Plenum Press, New York, New York, 1973.
79. J. M. Wilson and D. L. Uhrich, *Mol. Cryst., Liquid Cryst.*, 13, 85 (1971).
80. M. J. Potasek, E. Münck, J. L. Groves and P. G. Debrunner, *Chem. Phys. Lett.*, 15, 55 (1972).
81. R. L. Mössbauer, *A. Physik.*, 151, 124 (1958).
82. R. L. Mössbauer, *Naturwiss.*, 45, 538 (1958); *Z. Naturforsch.*, 14a, 211 (1959).
83. C. Kittel, "Introduction to Solid State Physics", Wiley, New York, 1956, Ch. 5 and 6.
84. G. K. Wertheim, "Mössbauer Effect: Principles and Applications", Academic Press, New York, 1964.
85. S. De Benedetti, G. Lang and R. Ingalls, *Phys. Rev. Lett.*, 6, 60 (1961).
86. L. R. Walker, G. K. Wertheim and V. Jaccarino, *Phys. Rev. Lett.*, 6, 98 (1961).
87. R. V. Pound and G. A. Rebka, Jr., *Phys. Rev. Lett.*, 4, 274 (1960).
88. B. D. Josephson, *Phys. Rev. Lett.*, 4, 342 (1960).
89. R. L. Collins and J. C. Travis in "Mössbauer Effect Methodology", Vol. 3, I. J. Gruverman, Ed., Plenum Press, New York, 1967.
90. A. J. F. Boyle and H. E. Hall, *Rept. Progr. Phys.*, 25, 441 (1962).
91. G. M. Bancroft, M. J. Mays and B. E. Prater, *J. Chem. Soc. (A)*, 956 (1970).
92. R. R. Berret and B. W. Fitzsimmons, *J. Chem. Soc. (A)*, 525 (1967).
93. B. W. Fitzsimmons, N. J. Steeley and A. W. Smith, *J. Chem. Soc. (A)*, 143 (1969).

94. R. V. Parish and R. H. Platt, *J. Chem. Soc. (A)*, 2145 (1969).
95. R. Ingalls, *Phys. Rev.*, 128, 1155 (1962).
96. R. Ingalls, *Phys. Rev.*, 133A, 787 (1964).
97. C. E. Johnson, *Proc. Phys. Soc.*, 88, 943 (1966).
98. R. Sternheimer, *Phys. Rev.*, 130, 1423 (1963).
99. G. M. Bancroft, "Mössbauer Spectroscopy", McGraw Hill Book Co. Ltd., England, 1973.
100. R. M. Golding, *Mol. Phys.*, 12, 13 (1967).
101. R. M. Golding, F. Jackson and E. Sinn, *Theor. Chim. Acta.*, 15, 123 (1969).
102. P. Zory, *Phys. Rev.*, 140A, 1401 (1965).
103. R. L. Collins, *J. Chem. Phys.*, 42, 1072 (1965).
104. D. L. Uhrich, J. M. Wilson and W. A. Resch, *Phys. Rev. Lett.*, 24, 355 (1970).
105. T. C. Gibb, R. Greatrex and N. N. Greenwood, *J. Chem. Soc. (A)*, 890 (1968).
106. V. I. Goldanskii, E. F. Makarov and V. V. Khrapov, *Phys. Lett.*, 3, 344 (1963).
107. V. I. Goldanskii, E. F. Makarov and V. V. Khrapov, *Soviet Phys. JETP*, 17, 508 (1963).
108. S. V. Karyagin, *Doklady Akad. Nauk S.S.S.R.*, 148, 1102 (1963).
109. M. Blume, *Phys. Rev. Lett.*, 14, 96 (1965).
110. A. J. Stone, appendix to G. M. Bancroft, W. K. Ong, A. J. Maddock, R. H. Price and A. J. Stone, *J. Chem. Soc. (A)*, 1966 (1967).
111. A. Guest, Ph.D. Thesis, Department of Chemistry, McMaster University, Hamilton, Ontario, September, 1968.
112. D. F. Evans, *J. Chem. Soc.*, 2003 (1959).
113. W. Hieber and R. Marin, *Z. Anorg. Allgem. Chem.*, 240, 241 (1939).
114. A. I. Vogel, "A Textbook of Quantitative Inorganic Analysis", Third Ed., Longman Group Limited, London, 1961.

115. T. Birchall and M. F. Morris, *Can. J. Chem.*, 50, 211 (1972).
116. K. Nakamoto, "Infrared Spectra of Inorganic and Coordination Compounds", Second Ed., Wiley-Interscience, 1970.
117. R. J. H. Clark and C. S. Williams, *Inorg. Chem.*, 4, 350 (1965).
118. H. Soling and R. W. Asmussen, *Acta. Chem. Scand.*, 11, 1534 (1957).
119. J. F. Gibson, *Nature*, 196, 64 (1962).
120. B. W. Dale, R. J. P. Williams, P. R. Edwards and C. E. Johnson, *Trans. Farad. Soc.*, 64, 620 (1968).
121. T. C. Gibb, R. Greatrex, N. N. Greenwood and D. T. Thompson, *J. Chem. Soc. (A)*, 1663 (1967).
122. I. H. Sabherwal and A. B. Burg, *Chem. Comm.*, 1001 (1970).
123. R. V. Parish and R. H. Platt, *Inorg. Chim. Acta*, 4, 65 (1970).
124. S. L. Ruby and P. A. Flinn, *Rev. Mod. Phys.*, 36, 351 (1964).
125. P. T. Manoharan and W. C. Hamilton, *Inorg. Chem.*, 2, 1043 (1963).
126. S. E. Livingstone, *Quart. Rev.*, 19, 386 (1965).
127. D. Coucouvanis and D. Piltingsrud, *J. Amer. Chem. Soc.*, 95, 5556 (1973).
128. C. S. Robinson and H. O. Jones, *J. Chem. Soc.*, 62 (1912).
129. K. R. Butler and M. R. Snow, *Inorg. Nucl. Chem. Lett.*, 8, 541 (1972).
130. J. Fujita, A. E. Martell and K. Nakamoto, *J. Chem. Phys.*, 36, 324, 331 (1962).
131. D. Coucouvanis, N. C. Baenziger and S. M. Johnson, *J. Amer. Chem. Soc.*, 95, 3875 (1973).
132. F. J. Hollander and D. Coucouvanis, *Inorg. Chem.*, 13, 2381 (1974).
133. G. R. Davies, R. H. B. Mais and P. G. Owston, *Chem. Comm.*, 81 (1968).
134. M. Colapietro, A. Domenicano, L. Scaramuzza, A. Vaciago and L. Zambonelli, *Chem. Comm.*, 583 (1967).
135. B. N. Figgis, *Trans. Farad. Soc.*, 57, 198, 204 (1961).

136. K. Stevens, Proc. Roy. Soc. (A), 219, 542 (1953).
137. A. H. Ewald and E. Sinn, Aust. J. Chem., 21, 927 (1968).
138. P. R. Brady, J. F. Duncan and K. F. Mok, Proc. Roy. Soc. (A), 287, 343 (1965).
139. T. Birchall, Can. J. Chem., 47, 4563 (1969).
140. E. Cervone, F. D. Camessei, M. L. Luciani and C. Furlani, J. Inorg. Nucl. Chem., 31, 1101 (1969).
141. N. L. Costa, J. Danon and R. M. Zavier, J. Phys. and Chem. Solids, 23, 1783 (1962).
142. M. Gerloch, S. F. A. Kettle, J. Locke and J. A. McCleverty, Chem. Comm., 30 (1966).
143. W. Kerler, Z. Phys., 167, 176 (1962).
144. E. Fluck, W. Kerler and W. Neuwirth, Angew. Chem. Intern. Edn., 2, 277 (1963).
145. V. Balzani and V. Carassiti, "Photochemistry of Coordination Compounds", Academic Press, 1970, p. 145.
146. D. R. Eaton and S. R. Suart, J. Phys. Chem., 72, 400 (1968).
147. J. J. Weiss, Nature, 136, 794 (1935).
148. E. Rabinowitch, J. Chem. Phys., 8, 551 (1940).
149. J. Schlag, Z. Physik., Chem. Frankfurt, 20, 53 (1959).
150. R. Hardwick, J. Amer. Chem. Soc., 80, 5667 (1958).
151. R. Havemann and H. Pietsch, Z. Physik. Chem. Leipzig, 208, 98 (1957).
152. R. Havemann and K. G. Reimer, Z. Physik. Chem. Leipzig, 216, 334 (1961).
153. S. Ainsworth, J. Phys. Chem., 64, 715 (1960).